BRNO UNIVERSITY OF TECHNOLOGY

VYSOKÉ UČENÍ TECHNICKÉ V BRNĚ

FACULTY OF ELECTRICAL ENGINEERING AND COMMUNICATION

FAKULTA ELEKTROTECHNIKY
A KOMUNIKAČNÍCH TECHNOLOGIÍ

DEPARTMENT OF PHYSICS

ÚSTAV FYZIKY

ALTERNATIVE APPROACHES FOR PREPARATION OF ALN NANOLAYERS BY ATOMIC LAYER DEPOSITION

ALTERNATIVNÍ PŘÍSTUPY PŘÍPRAVY TENKÉ VRSTVY NITRIDU HLINÍKU POMOCÍ METODY DEPOZICE ATOMÁRNÍCH VRSTEV

DOCTORAL THESIS
DIZERTAČNÍ PRÁCE

AUTHOR
AUTOR PRÁCE
Mgr. et Mgr. Rashid Dallaev

SUPERVISOR
ŠKOLITEL
doc. Ing. Petr Sedlák, Ph.D.

BRNO 2021

Abstract

Aluminum nitride (AlN) is a promising semi-conductive material with a wide band gap. Thin films of AlN find implementation in a variety of electronic and optoelectronic devices. First and foremost, the aim of the research presented within the scope of this dissertation is to introduce new precursors into ALD process for deposition of AlN thin films. The proposed precursors are superior to traditional ones either in cost-efficiency or reactivity. A part of the dissertation is devoted to enhancement of the understanding of chemical processes which take place during and after deposition. In this regard, a working solution to improving the chemical composition of the resulting films, as well as ameliorating deficiencies, for instance, oxidization, has been proposed. Another important aspect of this study has to do with a thorough analysis of hydrogen phenomenon in AlN ALD thin films. Hydrogen impurities have been investigated with the use of accurate and advanced techniques belonging to ion-beam analysis (IBA) groups.

Keywords

Thin films, semiconductor materials, aluminum nitride, atomic layer deposition, chemical composition analysis, ion-beam analysis, silicon substrates, hydrogen impurities, high-temperature annealing, surface characterization

Bibliographic citation

DALLAEV, R. *Alternative approaches for preparation of AlN nanolayers by atomic layer deposition*. Brno: Brno University of Technology, Faculty of Electrical Engineering and Communication, 2021, 107 p., Supervisor: associate prof. Ing. Petr Sedlák, Ph.D.

Abstrakt

Nitrid hliníku (AlN) je slibný polovodivý materiál s velkou mezerou v pásu. Tenké filmy AlN nacházejí uplatnění v různých elektronických a optoelektronických zařízeních. V první řadě je cílem výzkumu prezentovaného v rámci této disertační práce představit nové prekurzory do procesu ALD pro depozici tenkých vrstev AlN. Navrhované prekurzory jsou lepší než tradiční prekurzory buď v nákladové efektivnosti nebo reaktivitě. Část disertační práce je věnována prohloubení porozumění chemickým procesům, které probíhají během a po depozici. V tomto ohledu bylo navrženo pracovní řešení ke zlepšení chemického složení výsledných filmů a ke zmírnění nedostatků, například oxidace. Dalším důležitým aspektem této studie je důkladná analýza fenoménu vodíku v tenkých vrstvách AlN ALD. Vodíkové nečistoty byly zkoumány pomocí přesných a pokročilých technik patřících do skupin analýzy iontovým paprskem (IBA).

Klíčová slova

Tenké vrstvy, polovodičové materiály, nitrid hliníku, depozice atomové vrstvy, analýza chemického složení, analýza iontovým paprskem, silikonové substráty, vodíkové nečistoty, vysokoteplotní žíhání, charakterizace povrchu

Bibliografická citace

DALLAEV, R. *Alternativní přístupy přípravy tenké vrstvy nitridu hliníku pomocí metody depozice atomárních vrstev.* Brno: Vysoké učení technické v Brně, Fakulta elektrotechniky a komunikačních technologií, 2021, 107 s. Vedoucí dizertační práce: doc. Ing. Petr Sedlák, Ph.D.

Declaration

I declare that my thesis on the topic of "Alternative approaches for preparation of AlN nanolayers by atomic layer deposition" was created by myself under the professional leadership of my supervisor and on the basis of the technical literature and other informational sources completely cited in the References section.

Brno, May 28, 2021 ....

Rashid Dallaev

Acknowledgments

Hereby I would like to express my gratitude to my supervisor Doc. Petr Sedlák, PhD for his valuable advice and willingness to provide guidance at any stage of the given research.

I also want to emphasize the role of my current employer, Brno University of Technology for providing the necessary resources which made this research possible.

Last but not least my thanks go to my family and friends for their emotional support.

Research described in this dissertation was financially supported by the Ministry of Education, Youth and Sports of the Czech Republic under the project CEITEC 2020 (LQ1601), by the National Sustainability Program under grant LO1401 and by Internal Grant Agency of Brno University of Technology, grant No. FEKT-S-20-6352. The research infrastructure of the SIX Center was used in this work. CzechNanoLab project LM2018110 funded by MEYS CR is gratefully acknowledged for the financial support of the measurements/sample fabrication at CEITEC Nano Research Infrastructure.

The author also acknowledges the Tandem laboratory at Uppsala University (VR-RFI contract #2017-00646_9, as well as the Swedish Foundation for Strategic Research SSF under contract RIF14-0053) for granting access to perform ion beam experiments.

Table of Contents

Introduction 8
1 State of the art 11
1.1 Atomic layer deposition 11
1.2 Aluminum nitride thin films 13
2 Aims of the dissertation 15
3 Investigation of the effect of temperature treatment with the following etching on Si substrates 17
3.1 Motivation of the article 17
3.2 Conclusion on the article 17
3.3 Contribution 17
3.4 Article 1 17
4 AlN thin films deposited by thermal ALD using and hydrazine and ammonia as precursors 33
4.1 Motivation of the article 33
4.2 Conclusion on the article 33
4.3 Contribution 33
4.4 Article 2 33
5 AlN thin films deposited by thermal ALD using Hydrazinium Chloride and Triisobutylaluminum as precursors 47
5.1 Motivation of the article 47
5.2 Conclusion on the article 47
5.3 Contribution 47
5.4 Article 3 47
6 Study of the chemical composition of AlN layers obtained by PE-ALD 62
6.1 Motivation of the article 62
6.2 Conclusion on the article 62
6.3 Contribution 62
6.4 Article 4 62
7 Analysis of AlN layers deposited on the surface of HOPG by PE-ALD 69
7.1 Motivation of the article 69
7.2 Conclusion on the article 69
7.3 Contribution 69
7.4 Article 5 69

8 Investigation of hydrogen content in AlN nanolayers deposited by PE-ALD 76
8.1 Motivation of the study 76
8.2 Relevance of the study 76
8.3 Sample preparation 78
8.4 Characterization methods 81
8.5 Atomic force microscopy results 82
8.6 Secondary-ion mass spectrometry results 83
8.7 Nuclear reaction analysis results 84
8.8 Elastic recoil detection analysis results 86
8.9 Conclusion of the study 89
Conclusion 91
References 95
Author’s publications 102
List of abbreviations 105
List of figures 106
Curriculum vitae 107

Introduction

The origin of atomic layer deposition (ALD) method dates back to 1970s, when it was yet referred to as atomic layer epitaxy (ALE). ALE was considered to be a subtype of chemical vapor deposition (CVD) group of methods in which chemical reaction between the precursor and the substrate are performed in an alternate manner and separated by purging stages. The first utilization of ALE is reported to be for the deposition of zinc sulfide (ZnS), which is a material that was employed in electroluminescent displays fabrication process. Almost 50 years has passed since then and through this time ALD has established itself as a reliable, and in many scenarios, indispensable technique for deposition of highly conformal thin layers of a wide range of different materials [1, 2].

The reason for this is that ALD method has a number of advantages over its competitors. For example, it allows coverage of very large areas, offers a great degree of control over the growth process, provides precision up to angstrom level, ensures superior chemical purity and results in the films having better surface characteristics. The results of ALD process are also easily reproducible. In Figure 1, a general scheme of an ALD process is given. As can be seen, the introduction of the first precursor is followed by purging stage. During this stage, unreacted components are being removed from the chamber by some inert gas (e.g. nitrogen or argon). Then comes the introduction of the second precursor which is also followed by purging and then the cycle repeats itself. One such cycle is considered to be one atomic layer of a deposited material. It is also worth mentioning, that reactions in ALD are self-limiting, and upon occupation of all the active sites on the substrate, no more chemical interaction between the surface and the substrate is possible. Thus, this cyclic nature of ALD is supposed to ensure better degree of purity of the films [3-6].

ALD also has some variation, such as photo-assisted ALD, metal ALD, particle ALD etc. One of the most prominent and the most relevant to the content of this dissertation is plasma-enhanced atomic layer deposition variation (PE-ALD). As the name implies it involves the usage of a plasma source. Plasma facilitates dissociation of the precursor, thereby improving its reactivity. At the same time, it allows conducting depositions at lower temperatures in comparison with regular/thermal ALD, and in ALD world, lower deposition temperatures oftentimes translate into better general quality of the resulting films [7, 8].

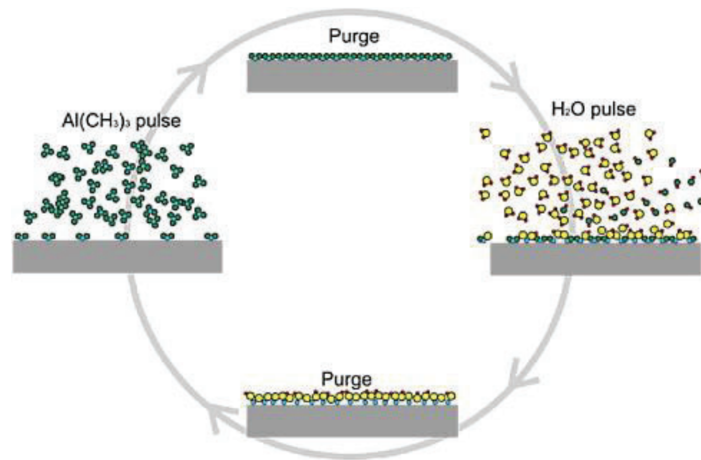

Figure 1. Scheme of an ALD process [9]

Aluminum nitride (AlN) is a semiconductive compound with a wide band gap (6.2 eV). Aside from wide-band gap, the following advantages and remarkabe properties are usually ascribed to AlN: chemcal resistance; ability to retain its properties under high temperatures; excellent thermal conductivity (285 W/m·K); mechanical robustness; low dielectric constant; thermal expansion coefficient (CTE) similar to that of silicon; high potential for piezoelecticity, large refractive index (~2.0), high breakdown voltage [10-14].

Due to the vast list of advantages provided by incorporation of AlN, this material is attracting ever increasing interest from a great amount of researchers and specialists in the field of both electronic and optoelectronics. Thus, applications of AlN include but not limited to: micro-electromechanical systems (MEMS), energy harvesters, ultrasonic transducers, sensors, ultraviolet diodes, actuators, laser diodes, acoustic wave devices, fingerprint detectors etc. Additionally, AlN demonstrates excellent compatibility with complementary metal-oxide semiconductor (CMOS) manufacturing process, whereas its competitors, such as zinc oxide (ZnO) and lead zirconate titanate (PZT), pose certain contamination risks [15-19].

Nowadays, one of the major modern applications of AlN thin films lies in fabrication process of micro electro mechanical systems (MEMS). This term includes all sort of actuators and sensors which undergo microfabrication, in the way similar to integrated circuits (ICs). Conventionally, they are fabricated on silicon wafers. Initially, MEMS utilized zinc oxide (ZnO) due to the lack of deposition techniques that could ensure reliable and repeatable results in depositions of other materials. In recent days, a great amount of MEMS devices is refabricated on a large scale with the intention to incorporate AlN, thereby enhancing durability and overall performance. The actual list of these devices is quite extensive, here

are some of them: resonators, chemical sensors, accelerometers, microphones, energy harvesters and various switches etc. [20]

AlN has three different type of crystal structure: wurtzite, zenc-blende and rocksalt. Among these, the wurzite structure is known to be the most stable under normal conditions. This structure is hexagonal and demonstrates piezoelectric properties. Figure 2 represents the wurtzite structure of AlN in different crystal planes.

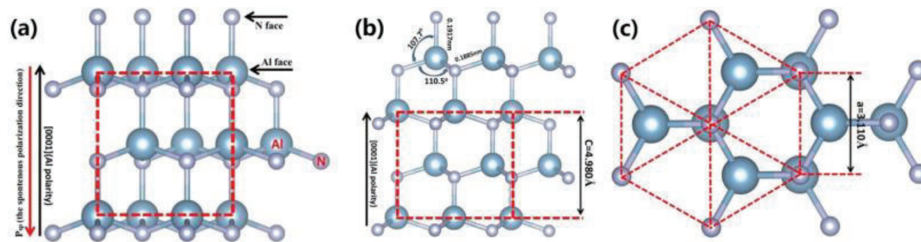

Figure 2. Illustration of the AlN wurtzite structure, where the (a) m plane, (b) a plane, and (c) c plane [18].

1 State of the art

1.1. Atomic layer deposition

There is no shortage of studies reporting on ALD being utilized for various purposes and the amount of the records in literature featuring ALD is increasing each year. Among devices that profit from the utilization of ALD technology are various chemical sensors. Chemical sensors, nowadays, are becoming increasingly sophisticated and their characteristics, such as sensitivity and durability, are ever improving, while the overall cost is decreasing. This progress in the industry is made possible by incorporation of various 2D nanomaterials as well as their heterostructures. This has to do with the fact most of these materials have unique structure and demonstrate superb potential for ultra-high carriers mobility under normal conditions. The list of such materials include a variety of thin (1-10nm) 2D oxide layers, which along with widely known graphene, are also employed as sensing electrodes (SE) in the sensors [21, 22]. These thin layers can boast large surface area, high concentration of carriers mobility, and remarkable thermal conductivity. Extensive surface area results in larger area of interaction of SE material and the measured analyte [23]. ALD, in this regard, has all the necessary requirements to ensure that surface area up to 450 m^2/g can be attained, and given the precise control over the growth process, makes possible to deposit layers as thin as only a few atomic layers. This combination of large surface area and ultra-thin nature of the SE layers is frequently sough-after when it comes to chemicals sensors for both liquids and gases alike [24-26]. It has been reported in the literature [27, 28] that other techniques used in SE fabrication, namely, various sputtering technique, are not quite up to the challenge when 2D large surface areas layers are concerned. Moreover, the resulted layers produced by those methods usually show a plethora of various defects, for instance notorious pin-holes, whereas ALD is capable of yielding defect-free uniform nanolayers [29].

Since the industry of semiconductive materials is continuously making steps toward miniaturization, the ability to control the film growth on the atomic level is becoming increasingly relevant. ALD has no rivals in terms of producing films with high levels of conformity and defect-free nature (pin-holes). Aside from the area of semiconductors, ALD finds its application in the areas that pose a great demand for conformity, for instance: coatings that serve as a diffusion barrier, providing low values of gas permeability [30].

Applications of ALN, however, are not limited only to electronics. For instance, Sarah Hashemi Astaneh et al. report in their review article [31] on benefits of using ALD for

modification of dental materials. Specifics of ALD described earlier, such as self-limiting reaction, ability to cover large areas in uniform manner and ultimate growth control, make it the go-to method for coating materials with complex shapes and coarse surfaces. Since the dental industry often employs 3D materials with porous surfaces, ALD stands once again as a perfect option for the task when necessity for surface modification or functionalization of these materials arises.

Much for the same reasons that were described for dental materials, ALD is also widely reported to be an excellent choice for coating and functionalization of various nanoparticles (NP). NP also come in intricate shapes and have extremely large surface area, which makes their functionalization a cumbersome task for methods lacking the advantages of ALD [32].

Ever increasing demand for miniaturization in electronics is constantly forcing the industry to search for alternative structure designs. For example, there is so-called tri-gate into production structure introduced by Intel [33]. This is an alternative stucture for metal–oxide–semiconductor field-effect transistor (MOSFET), in which instead of implementing conventional planar channel (Figure 3a), incorporation of fin-like Si slabs protruding out of the bulk crystal is suggested (Figure 3b). Such design results in a lot of surface area that needs to covered with a thick layer of a gate oxide in a uniform and conformal manner. Taking into account aforementioned advantages of ALD, it is needless to say that there is no other technique more sutiable for such a task. In fact, it can be argued that designs like this one might not have been introduced if ALD had not been already an established method for growing high aspect ratio confromal layers [34].

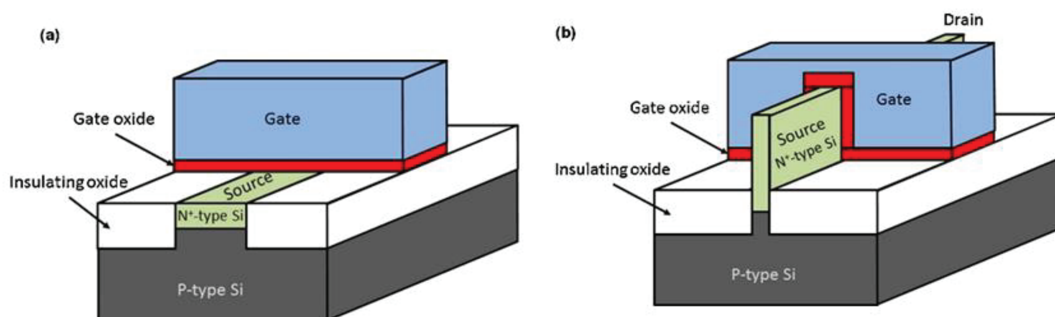

Figure 3. Schematic illustration of MOSFET structure with (a) the conventional planar design; (b) the tri-gate design [34]

1.2 Aluminum nitride thin films

As can be seen the applications of ALD are truly versatile, and it can be altogether safely assumed, that as technology is becoming increasingly sophisticated and the world of electronics is continuously striving towards downscaling, the demand for ALD and its variations is expected to keep growing.

However, as this dissertation is particularly aimed at ALD of AlN thin films, it is important to examine the state-of-the-art in regard to commonly used methods for deposition of AlN, as well established ALD recipes. Thin films have physical properties that differ significantly from those of bulk samples of the same material. The choice of substrate is an important stage in the process of film synthesis, because the surfaces and interfaces between the film and the substrate "control" the nucleation method and play a decisive role in the initial stage of film growth. Even by adjusting the temperature of the substrate, it is possible to achieve the optimum layer for the formation of the crystal lattice of the resulting layer.

Currently, the literate on this topic is rather abundant. Aside from ALD, there is a plethora of PVD methods that are widely used for deposition of AlN thin films. Among those methods are: magnetron sputtering (MS) [35-39]; molecular beam epitaxy (MBE) [40-43]; ion beam assisted deposition (IBAD) [44-46]; pulsed laser deposition (PLD) [47-49]. Traditional chemical vapour deposition (CVD) method and its variation, in general seems to be utilized less often in modern days, nevertheless, a good amount of records can still be found [50-53]. It can be explained by the fact that PVD methods, while being less affordable due their sophistication and rather expensive parts, provide superior quality of the layers. This conclusion can be made from the record provided above.

Even though technically ALD is also a variant of CVD, as chemical interaction take place during the deposition, its concept is fundamentally different. Cyclic nature of ALD makes a huge difference and that is the reason why its popularity continues to rise.

There is no shortage of records where researchers attempted ALD of AlN with the use of various precursors and deposition parameters with varied success. It appears that currently the most successful recipe involves the usage of PE-ALD with $Al(CH_3)_3$ and N_2H_2 gas mixture as aluminum and nitrogen precursors respectively [54, 55]. There are many studies in which authors used aluminum chlorine ($AlCl_3$) as an aluminum precursor $AlCl_3$ [56, 57]. The downside of aluminum chloride is that there is always a certain amount of chlorine

detected in the resulting films. While chlorine is unambiguously an impurity and its presence in the final product is undesired, the bigger concern, however, consists in the risk of chamber contamination [58]. If chlorine is detected in the layer, there is a decent chance that it has also impregnated itself in the chamber's inner structure. Hence, a thorough cleaning procedure would be required after the usage of chlorine containing precursors, as its incorporation into the chamber can jeopardize the further experiments. Which is why, chlorine containing aluminum precursors are gradually supplanted by metalorganic ones. Unlike chlorine, organic ligands require less energy to dissociate from the metal and do not pose any harm to the equipment.

It needs to be stated, however, that regardless of the precursors choice, chosen parameters and type of ALD, overwhelming percentage of the relevant studies report on some sort of contaminations, which vary from minor to rather considerable. A good amount of contamination, such as carbon and hydrogen, can be minimized through correctly chosen deposition parameters which ensure the proper completion of all the chemical processes and removal of the residual by-products. An important part of these parameters is the deposition temperature. For this reason, a term known as 'ALD window' exists, which is effectively a temperature range at which films with the best quality are grown. This window varies for different precursors and ALD variants (e.g. PE-ALD) [1].

The most notorious and persistent issue in terms of contamination, however, is the proneness of AlN to intense oxidization upon exposure to air. In fact, even high-quality AlN deposited by PVD methods are not immune to oxidization issue [42, 46, 47]. Therefore, this problem calls for appropriate post-processing solutions, which can include deposition of a passivating layer or high-temperature annealing.

2 Aims of the dissertation

The purpose of this dissertation is to bring contribution into optimization of ALD technology for deposition of AlN thin films by proposing alternative solutions to the established recipes. A decent part of this work is dedicated to fundamental research on AlN chemical composition and following treatment of impurities as a part of post-processing procedure. The research presented within this work is aimed at providing insight into benefits of alternative ways for deposition of AlN by ALD and bridging possible gaps in understanding of AlN ALD process as such.

There are several crucial parameters that influence the quality of a resulting film, such as: the type of precursor, the type of substrate and its preliminary treatment, deposition temperature and exposure time of a certain precursor are the most important of them. Atomic layer deposition process can also be enhanced by using plasma module allowing for deposition at lower temperatures which in its turn expands the choice of precursors. By choosing parameters of the deposition process, the content of the structure of resulting film is controlled. Optimization of the deposition regimes of aluminum nitride thin films and the preparation of samples followed by further comprehensive analysis of their properties using various analytical techniques are the results of this study.

Thus, the following stages constitute the general aim of this dissertation:

1) Investigation of alternatives to the well-established recipes, this step includes but not limited to:

a) The choice of a precursor: N_2H_4, N_2H_5Cl, N_2/H_2 plasma etc.

b) The choice of a substrate: silicon, silicon carbide, LSAT, highly oriented pyrolytic graphite (HOPG) etc. and its preliminary treatment

c) The choice of deposition parameters such as: temperature, exposure time of precursors, thickness of the resulting layer, power of plasma etc.

2) A thorough characterization of the obtained films:

a) surface topography and morphology (atomic form microscopy, scanning electron microscopy)

b) chemical composition (X-ray photoelectron spectrometry, Secondary ion mass spectrometry, Fourier-transform infrared spectroscopy, Energy-dispersive X-ray spectroscopy, Nuclear reaction analysis, Elastic recoil detection analysis ERDA)

c) optical properties (X-ray diffractometry, spectroscopic ellipsometry)

3) Analysis of impurities in the resulted films (oxygen, hydrogen, carbon)

4) Suggestion of a viable method for eliminating, or at least minimizing the impurities of the resulted films

5) Conclusion and justification of the results

This dissertation is presented in a form of author's published papers prefaced by a short discussion on motivation and conclusion. These papers are effectively a series of experiments in which AlN thin films were deposited at different parameters, on different substrates and with the use of different precursors. The experiments were followed by a thorough analysis in order to reveal benefits and drawbacks of each approach, provide insight into chemical processes during the deposition and suggest solutions for ameliorating incidental inadequacies. It is also worth emphasizing that characterization of the AlN layers within the given papers is mostly focused at (but not limited to) chemical composition analysis and the conclusions are made based on the degree of chemical purity which a certain approach delivers. The focus at chemical composition is justified by the fact that quality of the films and therefore performance of an end-product is greatly determined by the degree of its chemical purity. Hence, it is essential to eliminate/minimize the amount of contamination before any further steps can be considered.

3 Investigation of the effect of temperature treatment with the following etching on Si substrates

3.1 Motivation of the article

The study described in the following article comprises a thorough and comprehensive analysis of chemical composition and surface morphology of Si substrates undergone temperature treatment with following etching by Ar atoms. Si substrates are ones of the most often used substrates for thin film deposition in various chemical and physical vapour deposition methods, not less so in ALD. It is general knowledge that the surface condition of a substrate affects the consequent growth of the deposited layer. Even within the scope of the research described in the given dissertation, Si substrates were employed most frequently for deposition of AlN thin films. Which is why, the study of the changes on the surface induced by etching and temperature processing is not only an important and justified task but also has a direct relation to the topic of this dissertation.

3.2 Conclusion on the article

The result of this study suggest that there was a native oxide layer as well as small carbon impregnations on the surface of Si wafers, annealing seems to result in thickening of this native oxide layer, the longer the wafer is exposed to temperature treatment the thicker the oxide layer grows. Etching by Ar atoms completely removed the presence of carbon contamination and significantly reduced the oxidization of the wafers.

Stereometric analysis provided a thorough picture of how the morphology and topography of Si wafers were affected by comparing them before and after the processing. Considering that Si wafers are probably the most convention substrates, data provided within the scope of this study can be crucial not only during atomic layer deposition of AlN layers but practically in any PVD or CVD method.

3.3 Contribution

My contribution lies in the processing of the samples, acquisition and interpretation of the XPS spectra, acquisition and interpretation of the AFM images, data curation and visualisation. I have also written the major part of the manuscript.

3.4 Article 1

The article **Stereometric Analysis of Effects of Heat Stressing on Micromorphology of Si Single Crystals** was published in **Silicon** journal (ISSN: 1876-990X; 2021 IF: 1.499).

Silicon
https://doi.org/10.1007/s12633-019-0085-4

ORIGINAL PAPER

Stereometric Analysis of Effects of Heat Stressing on Micromorphology of Si Single Crystals

Dallaev Rashid[1] · Sebastian Stach[2] · Ştefan Ţălu[3] · Dinara Sobola[1] · Alia Méndez-Albores[4] · Gabriel Trejo Córdova[5] · Lubomír Grmela[1]

Received: 21 September 2018 / Accepted: 17 January 2019
© Springer Nature B.V. 2019

Abstract

The purpose of this work is study of silicon single crystal wafer thermal stability in correlation with three-dimensional (3D) surface characterization using atomic force microscopy (AFM). The samples were heated up to 500 °C for the period of 2 and 4 h. Then the surfaces of wafers were processed by ion beam. The difference in surface structure of processed and reference samples was investigated. Structural and compositional studies are provided by X-ray photoelectron spectroscopy. Stereometric analysis was carried out on the basis of AFM-data, for stressed and unstressed samples. The results of stereometric analysis show the correlation of statistical characteristics of surface topography and structure of surface and near-surface area. Characterization techniques in combination with data processing methodology are essential for description of the surface condition. All the extracted topographic parameters and texture features have demonstrated a deeper analysis that can be used for new micro-topography models.

Keywords Atomic force microscopy · Si single crystal wafers · Stereometric analysis · Topography · X-ray photoelectron spectroscopy

1 Introduction

Exploration on fundamental aspects of nanostructures that exhibit functionality, including the various physical, chemical and hybrid methods of nanomaterial synthesis and nanofabrication, is the key to nanotechnology [1–4].

Silicon wafers play a huge role in nowadays electronics such as solar cells, micro- and nano-electromechanical systems (MEMS/NEMS), due to its great optical and electrical properties. They also are widely used as substrates for various techniques of thin films preparation (ALD [5], CVD [6], magnetron sputtering [7], spin coating [8], etc). Despite the fact that it is a very common and widespread material there is still a problem of insufficient experimental data concerning its behavior in harsh environments, for example - continuous temperature stress. Furthermore, sometime the preliminary processing of the substrates by heating or annealing is required [9, 10]. Which is why, it is still relevant to conduct studies on silicon wafers exposed to various outer influences [11]. The main goal of this work is to provide analytical data on changes in topography and chemical composition of Si wafers under different periods of stress heating and following etching procedure. This data might prove to be helpful in choosing the right processing procedure of substrate during heterostructures and thin films fabrication processes.

The studies of temperatures stresses recently have attracted a lot of attention owing to their large isothermal entropy achieved in commercially nanomaterials [1, 3]. The effects of temperature process influence non-

✉ Dallaev Rashid
xdalla03@vutbr.cz

1 Faculty of Electrical Engineering and Communication, Physics Department, Brno University of Technology, Technická 8, 616 00 Brno, Czech Republic

2 Faculty of Computer Science and Materials Science, Institute of Informatics, Department of Biomedical Computer Systems, University of Silesia, Będzińska 39, 41-205 Sosnowiec, Poland

3 The Directorate of Research, Development and Innovation Management (DMCDI), The Technical University of Cluj-Napoca, Constantin Daicoviciu Street, no. 15, 400020 Cluj-Napoca, Cluj county, Romania

4 Centro de Química-ICUAP Benemérita Universidad Autónoma de Puebla, Ciudad Universitaria Puebla, 72530 Puebla, Mexico

5 Center of Research and Technological Development in Electrochemistry (CIDETEQ), Parque Tecnológico Sanfandila, Pedro Escobedo, Querétaro, A.P. 064., C.P, 76703 Querétaro, Mexico

Published online: 26 January 2019

Table 1 Details and ID of prepared samples

ID	Technical specifications
#1	Silicon wafer without thermal processing before argon sputtering
#2	Silicon wafer without thermal processing after argon sputtering
#3	Silicon wafer at first thermal processing before argon sputtering
#4	Silicon wafer at first thermal processing after argon sputtering
#5	Silicon wafer at second thermal processing before argon sputtering
#6	Silicon wafer at second thermal processing after argon sputtering

irreversible atomic processes, structural phase transitions, chemical and physical properties of materials [12–16]. According to several sources the optimal temperature for thermal processing of silicon wafers is below 1050 °C. Values higher than 1050 °C often produce slip generation or dislocation movements [17–19]. Any values below 1050 °C will not cause any structural changes to a silicon wafer. The changes will take place in the chemical composition on the surface of a wafer, in our particular case in the thickness of the oxide layer, as demonstrated in the corresponding section of this work.

There are several researches in which authors attempted to study behavior of Si wafers under influence of high temperatures [20–22]. For example, Suzuki T. has reported in his study how high-temperature annealing affects generation of oxidation-induced stacking faults (OSF) in a silicon wafer [23]. D. Gräf et al. have reported that the temperature stress in oxygen atmosphere considerably improves the electric properties of Si wafers [24].

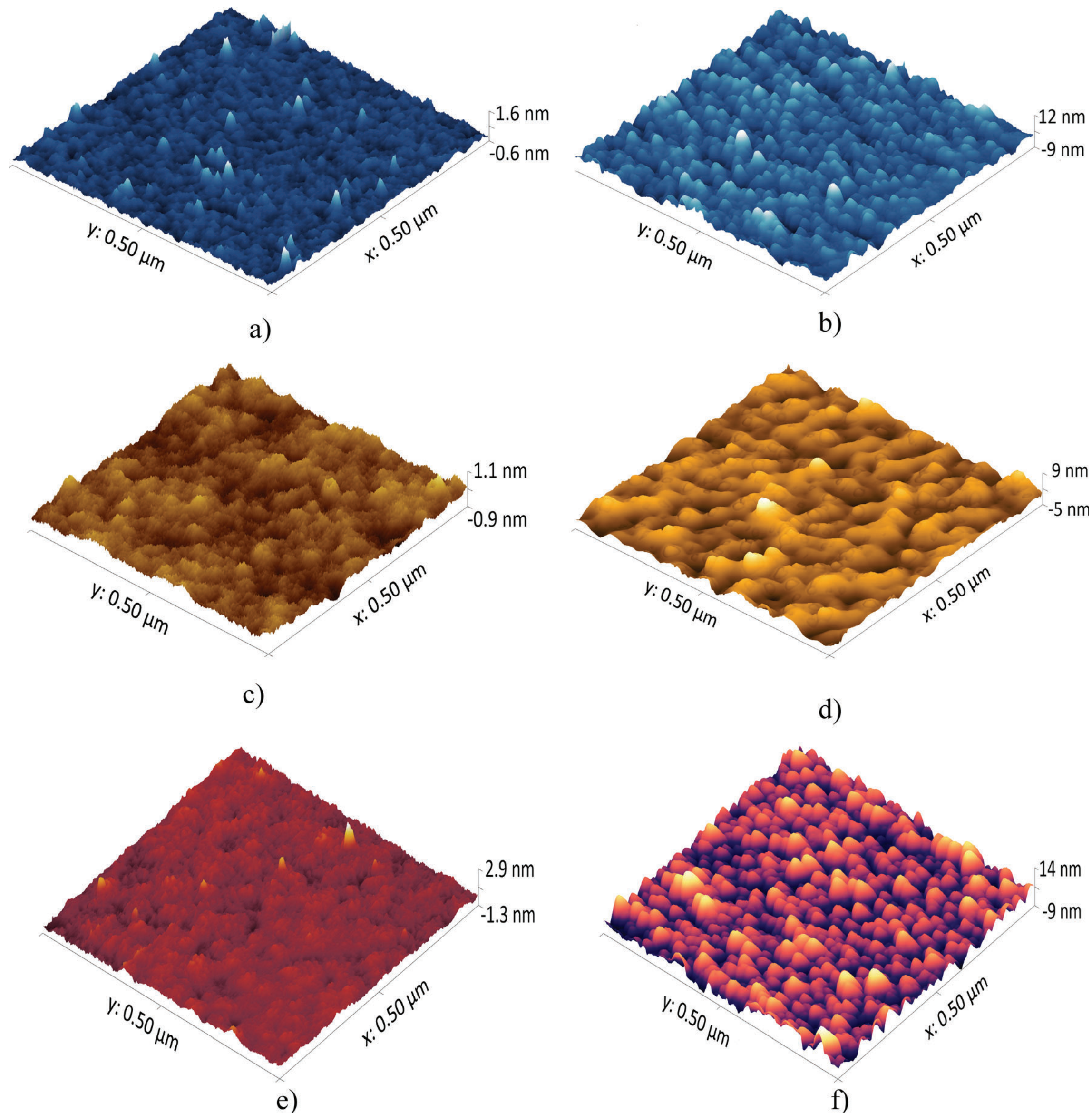

Fig. 1 AFM images for samples: **a**) #1; **b**)#2; **c**) #3; **d**) #4; **e**) #5; **f**) #6

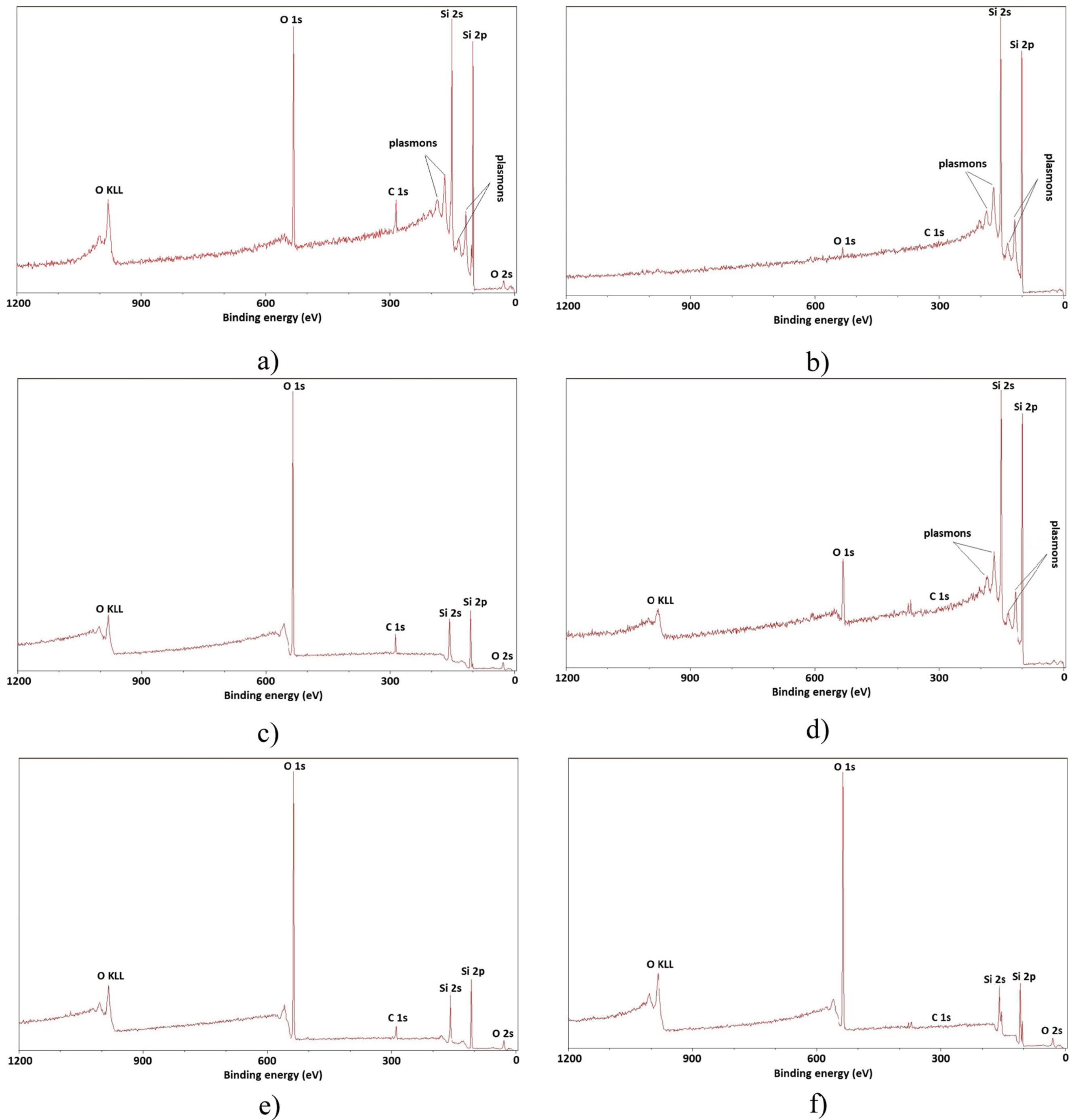

Fig. 2 XPS wide spectra for samples: **a**) #1; **b**) #2; **c**) #3; **d**) #4; **e**) #5; **f**) #6

Table 2 Chemical composition of the samples given in percentage ratio

Concentration at%	O1s	C1s	Si2s	Si2p
#1) no etching	30,3	4,7	31,7	33,3
#2) after etching	2,3	0,6	48,3	48,8
#3) 2 h, no etching	69,2	4,95	10,8	15,0
#4) 2 h, after etching	12,0	0,45	41,2	46,6
#5) 4 h, no etching	68,1	3,13	11,2	17,5
#6) 4 h, after etching	65,9	0,31	13,7	20,1

In our paper we focus on surface modifications of Si wafers by thermal annealing and argon ion etching with conditions which have never been tried before. We investigate the changes of chemical composition, crystallographic properties and stereometric analysis of modified surface of Si crystal before and after temperature stressing. For this purposes, X-ray Photoemission spectroscopy (XPS) and stereometric analysis of surface measured by Atomic force microscopy (AFM) were carried out.

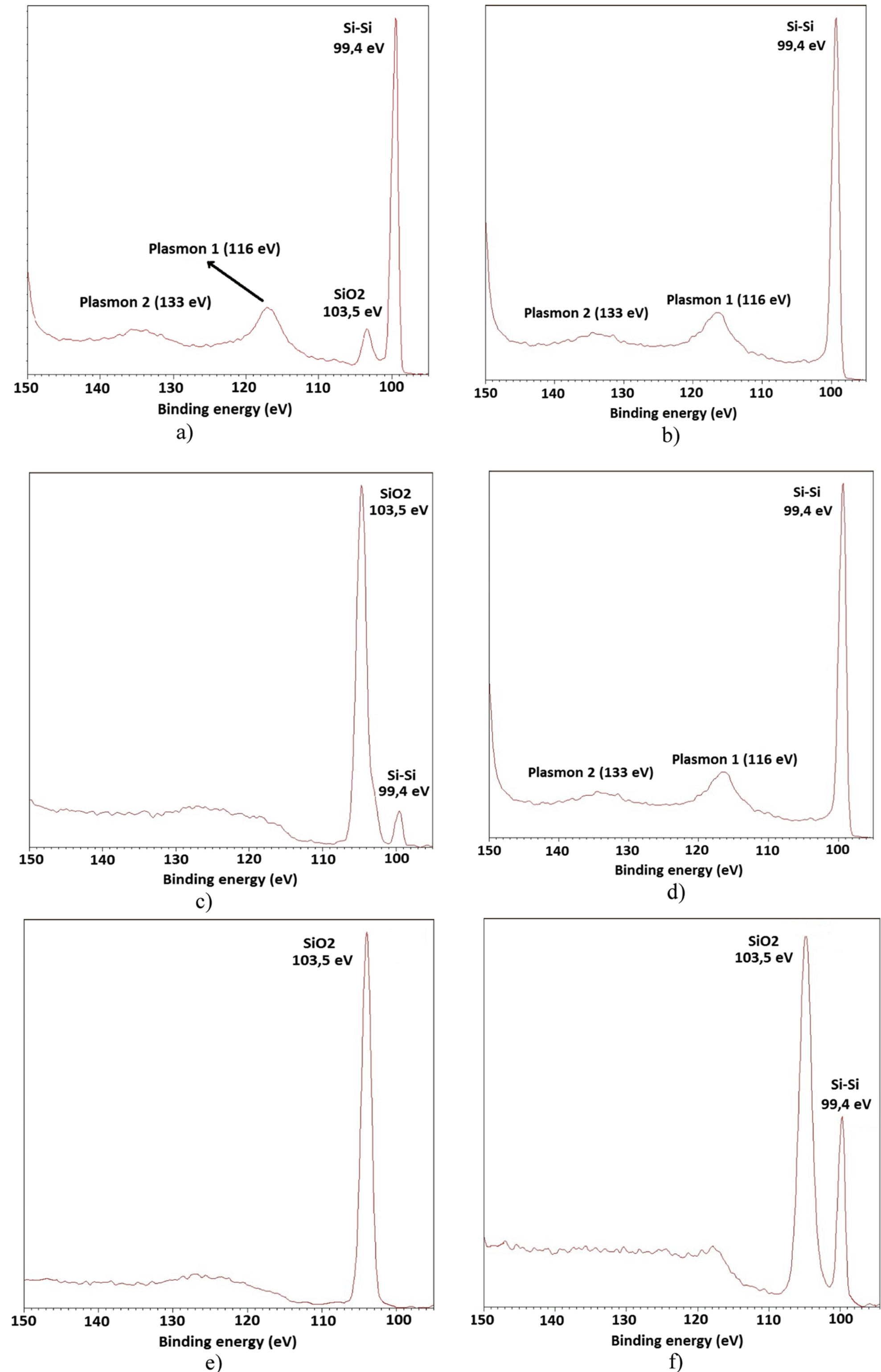

Fig. 3 Comparison of high resolution Si2p peaks of: **a**) #1; **b**) #2; **c**) #3; **d**) #4; **e**) #5; **f**) #6

AFM represents an outstanding imaging tool for the research and analysis of nanostructures and surfaces, especially in thin films [25–29].

The comprehensive description of the surface micromorphology of these materials [30–32] correlated with fractal/multifractal analysis [33–38] is an important challenge necessary for the understanding of their properties and their potential technological exploitation.

In the present work, the study of temperature stability of Si thermal stability have been investigated in

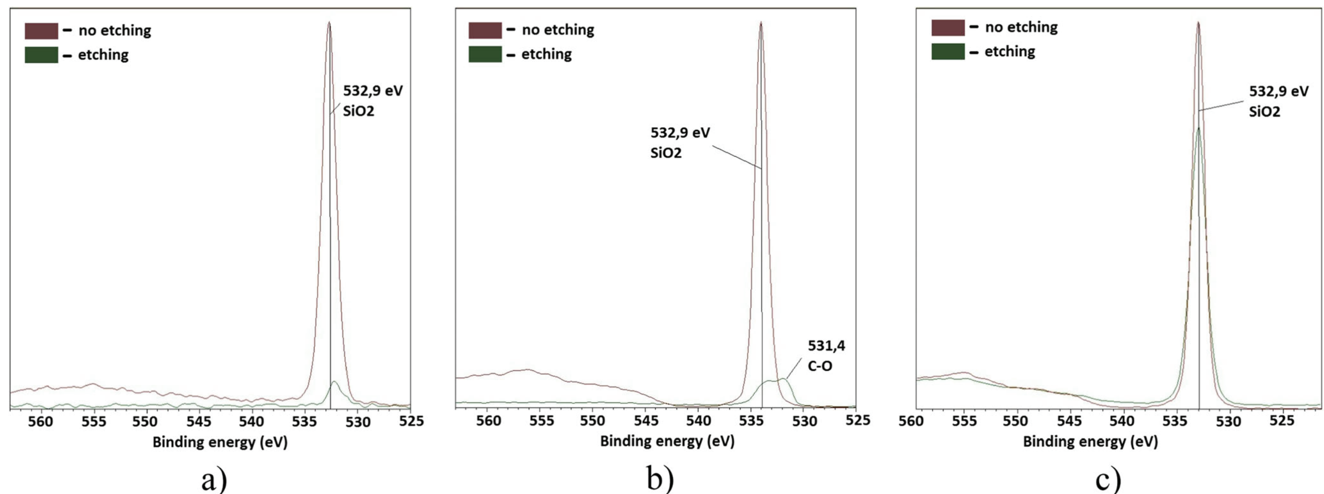

Fig. 4 Comparison of high resolution O1s peaks of: **a**) #1, #2; **b**) #3, #4; **c**) #5, #6

correlation with three-dimensional (3D) surface characterization by AFM imaging, and a fractal approach has been performed in the analysis of the obtained 3D AFM images.

2 Materials and Methods

2.1 Materials

Silicon wafers 4 in., thickness 525 ± 25 um (100), 1-side polished, p-type (Borron) of MicroChemicals production were used. Different wafers were heated up to 500 °C and annealed for two different time periods (i.e. 2 h and 4 h). Heating of the samples from room temperature to 500 °C was carried out uniformly during 30 min in air. The measurements of surface composition by XPS were carried out after cooling of the samples to room temperature. XPS spectra were done in vacuum at following parameters: 15 mA emission current, slot collimation mode, hybrid lens mode and 20 eV resolution of pass energy.

Depth profiling was done inside XPS chamber by Ar ions using Minibeam 6 Gas Cluster Ion Source with following parameters: 20keVAr500+; etch size square 1.9 × 1.9 mm2; pre etch time 5 s; post etch time 5 s, duration of etching was 5 min.

AFM images were obtained after extracting the samples from vacuum chamber. Details and ID of prepared samples are given in Table 1.

2.2 Imaging Techniques

Atomic force microscopy characterizations were carried out for the quantitative analysis of specific microstructural characteristics of samples using taping AFM mode.

All AFM measurements were done at room temperature and normal humidity. Scan rate was 0.580 Hz and probe RTESPA-150 was used. All 512 × 512 pixel images were obtained by scanning square areas of 0.5 μm × 0.5 μm (Fig. 1).

2.3 Structure Investigation

In order to investigate how chemical composition of wafers changes with annealing and etching processes we have conducted high resolution XPS analysis. The wide spectra for each sample are given in Fig. 2.

According to Fig. 2 we can assume that there was a native oxide film on the surface of Si wafers and some carbon impurities. The etching process significantly reduces the amount of oxygen and practically eliminates the presence of carbon in all scenarios. The Auger peak of oxygen as well as the small peak at 26 eV usually assigned to O2s electrons also disappear [39].

However, annealing in air results in thickening of the oxide layer which is why the effect of etching becomes less considerable [40]. After 4 h of annealing (e, f) the amount of oxygen on XPS spectra remains practically unchanged.

The atomic percent ratio is given in Table 2.

We have also provided high resolution images of Si2p peak, to demonstrate in more detail how annealing and etching affect the behavior of Si bonds, which is the most important aspect in this work (Fig. 3).

It can be seen from images a) and b) that there are two peaks of Si2p: one is of Si-O bond at ~103,5 eV resulting from the oxide layer on the surface and another at ~99,4 eV ascribed to Si-Si bond in the bulk of the wafer. After etching the Si-O peak disappears leaving a sole Si-Si peak. There are also two plasmon peaks can be noticed at 116 and 133 eV in Si2p

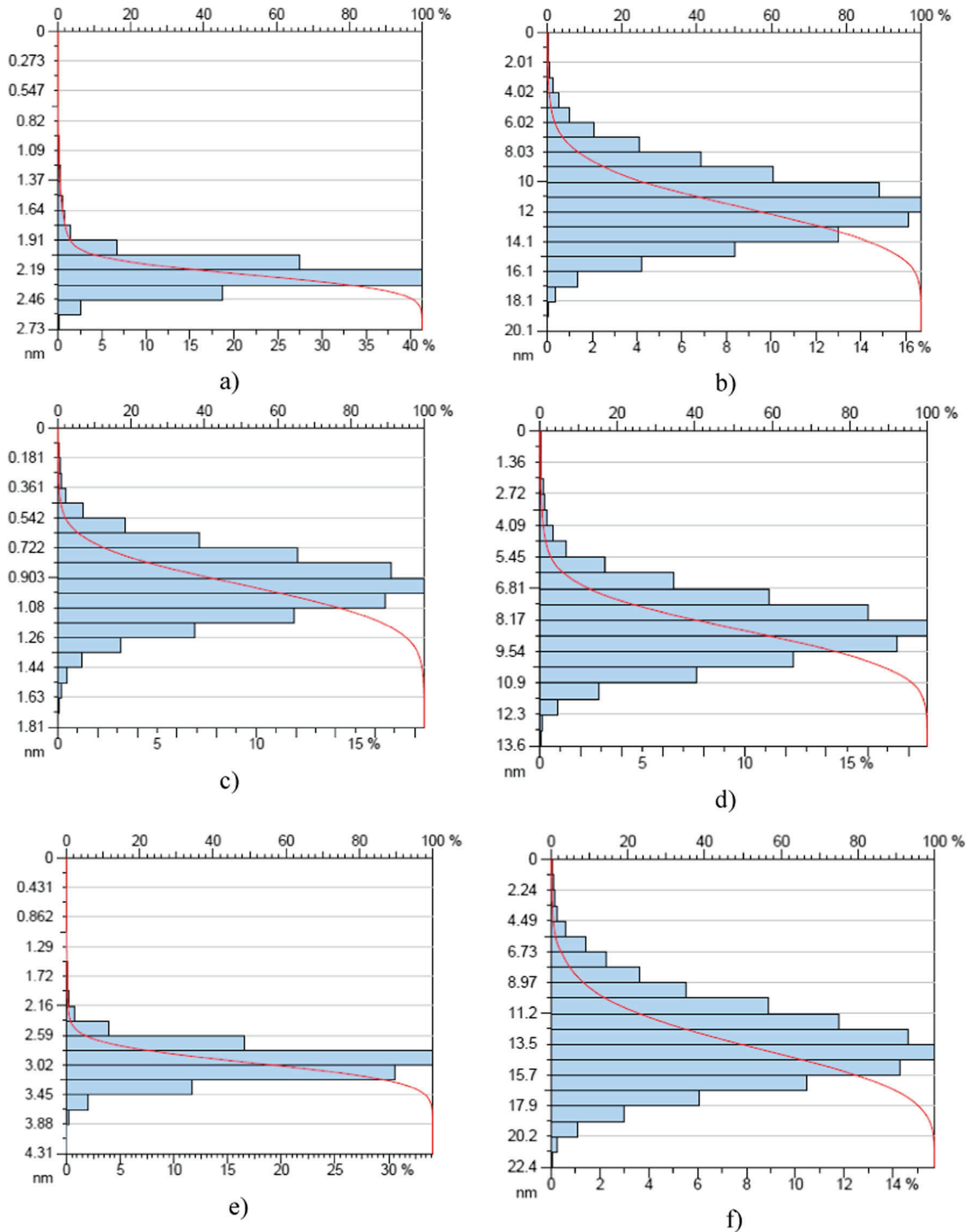

Fig. 5 The depth histograms of the samples: for samples: **a)** #1; **b)** #2; **c)** #3; **d)** #4; **e)** #5; **f)** #6. The horizontal axis represents the bearing ratio [%], and the vertical axis represents the depths (measurement unit)

multiplet [41]. Images c), d), e) and f) display the same tendency however in the latter two the effect is not that drastic due to higher thickness of the oxide layer. We can observe the occurrence of Si-Si bond although Si-O is still being prevalent.

Analysis of O1s peaks occurring at ~ 532,9 eV also confirms the presence of silicon oxide on the surface. Apart from that, after 2 h of etching (b) a doublet of O1s can be observed. The subpeak at energy of 531,4 eV usually ascribed to C-O bond (Fig. 4) [42].

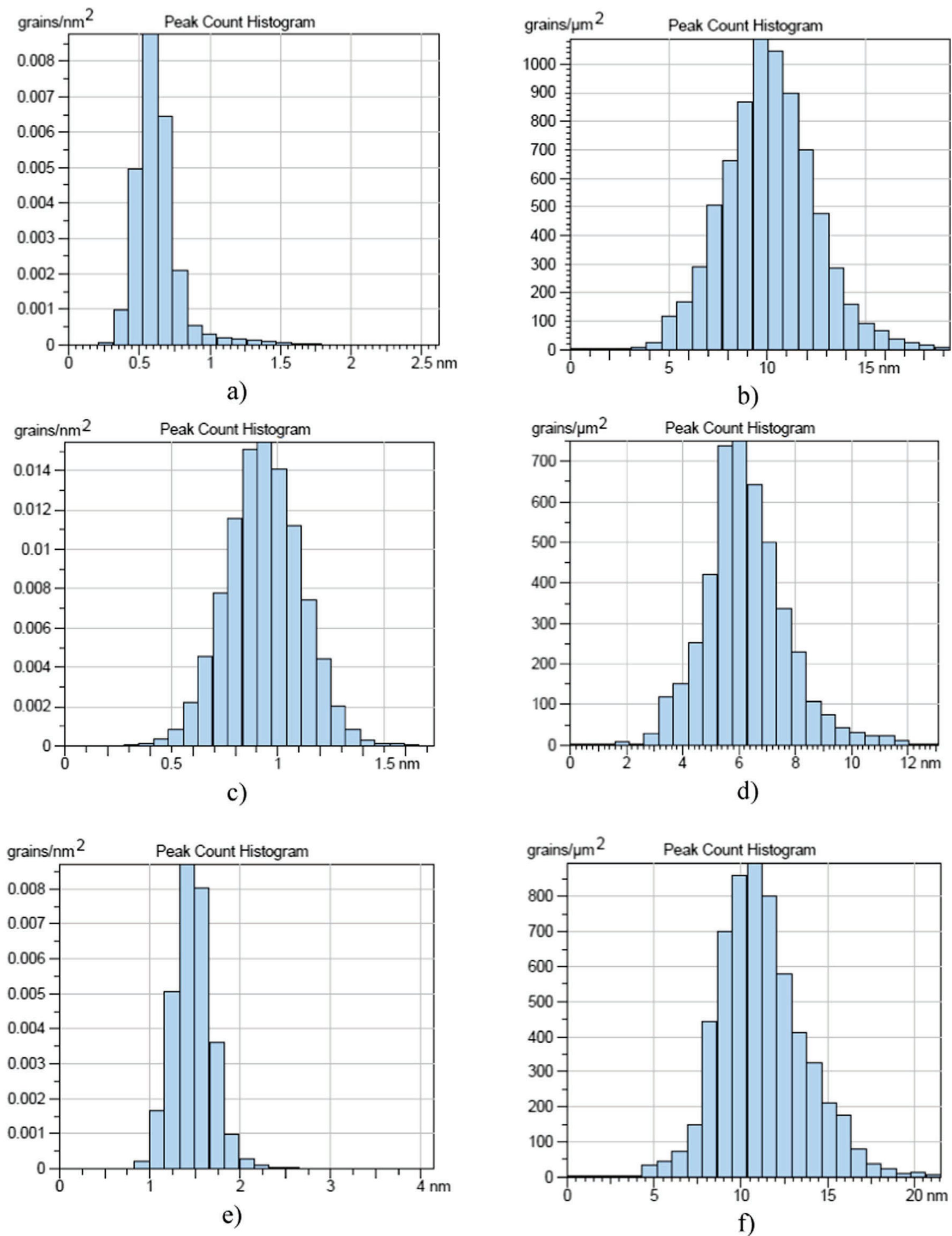

Fig. 6 The peak count histograms of the samples: for samples: **a**) #1; **b**) #2; **c**) #3; **d**) #4; **e**) #5; **f**) #6

3 Results and Discussion

Study of topography was carried out by scanning probe microscpe ICON (Bruker). The AFM surface micrographs were analysed by Mountains Map® 7 Software [43], according to ISO 25178-2:2012 [44].

The experiments of this study characterize the structure of Si crystals before and after temperature stress. Every applied method of the sample characterization shows the presence of changes of surface and near-surface area. XPS techniques represent changes of surface structure after temperature processing and explain the origin of differences of surface condition.

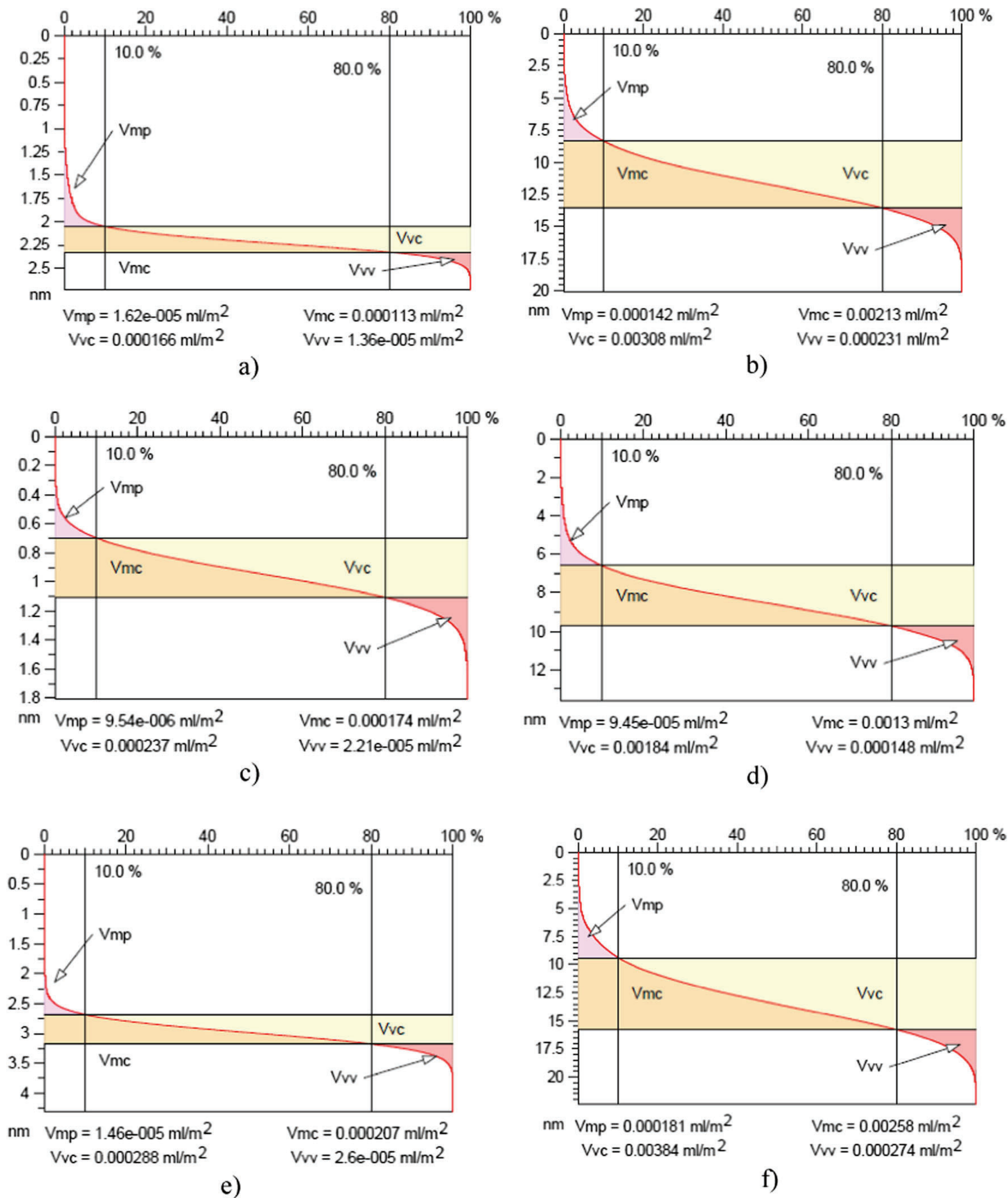

Fig. 7 Graphical study of volume parameters (surface): *Vmp*, *Vvc*, *Vmc* & *Vvv* parameters based upon the Abbott curve calculated for the samples: **a**) #1; **b**) #2; **c**) #3; **d**) #4; **e**) #5; **f**) #6. Two bearing ratio thresholds are defined (using the vertical bars that are drawn with dotted lines). By default, these thresholds are set at bearing ratios of 10% and 80%. The first threshold, *p1* (default: 10%), is used to define the cut level *c1* (and *p2* defines *c2*, respectively)

The stereometric analysis was carrying out on the basis of AFM data, because it gives real 3D information about surface texture. The surface topography was described in chosen terms of stereometric analysis.

In Fig. 5 are shown the depth histograms associated with the analyzed samples from Fig. 1. The Abbott-Firestone curve is overlaid in red. This curve represents the bearing ratio curve; it means that for a specific depth, the percentage of the material traversed in relation to the area covered.

The peak count histograms associated with the analyzed samples from Fig. 1. are shown in Fig. 6.

The graphical study of volume parameters (surface): *Vmp*, *Vvc*, *Vmc* & *Vvv* parameters based upon the Abbott curve calculated on the surface associated with the analyzed samples from Fig. 1, are shown in Fig. 7.

The graphical study of Sk parameters associated with the analyzed samples from Fig. 1, are shown in Fig. 8.

For these surfaces we applied the morphological envelopes method for fractal analysis. The graph of the calculated volume for surfaces is drawn as a function of the scale (size of the structuring elements). The fractal dimension is calculated from the slope of that one of the two regression lines that corresponds best (i.e. the one out of the two regression lines whose correlation coefficient is nearer to 1 for a profile and nearer to 2 for a surface) [43].

It Table 3 are given a summary of the fractal dimensions D_f values for analyzed samples from Fig. 1.

A summary of the statistical parameters results is shown in Tables 4 and 5.

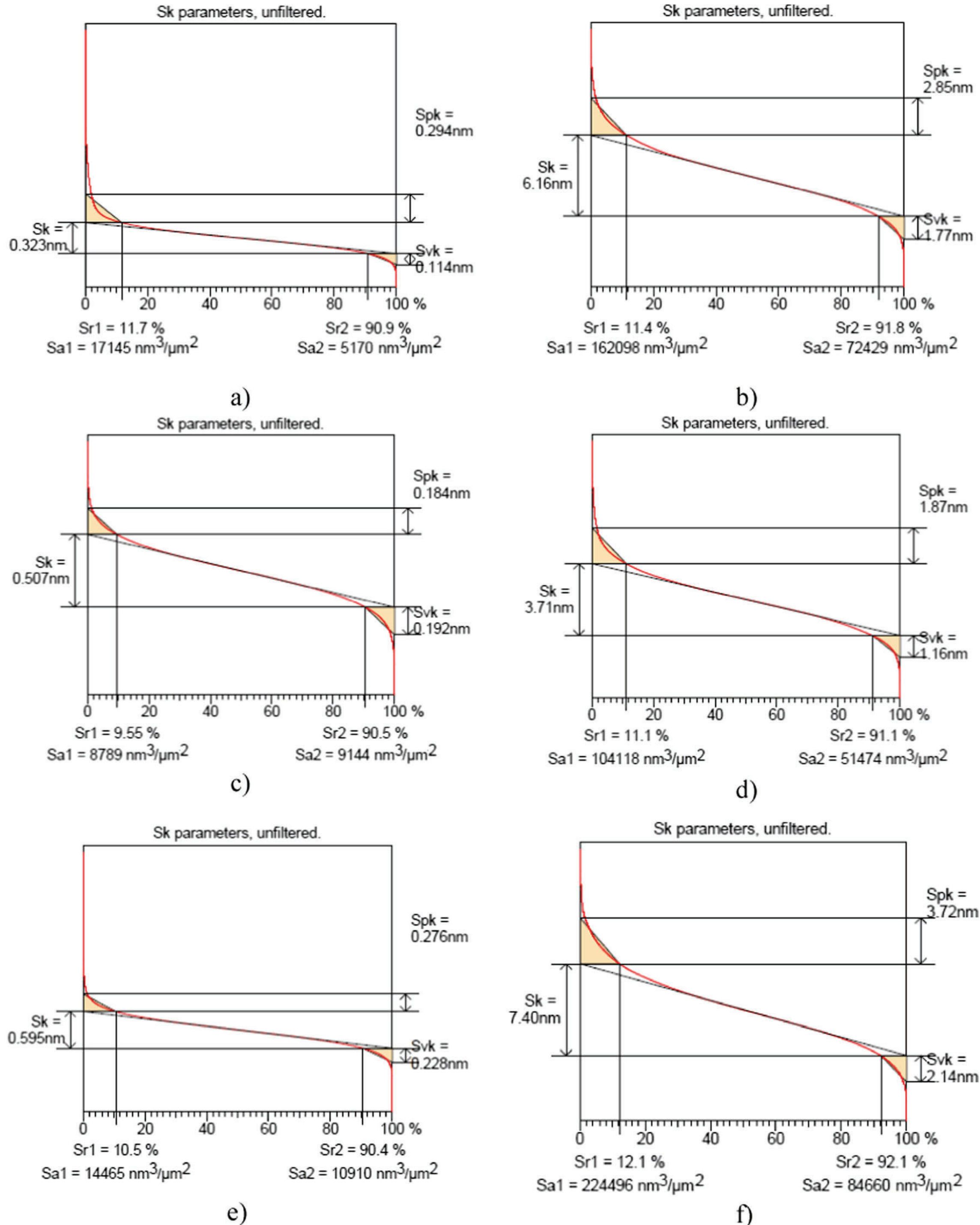

Fig. 8 Graphical study of Sk parameters of the samples: **a**) #1; **b**) #2; **c**) #3; **d**) #4; **e**) #5; **f**) #6

Table 3 The fractal dimensions D_f values, for scanning square areas of $0.5 \times 0.5\ \mu m^2$, for samples: a) #1; b) #2; c) #3; d) #4; e) #5; f) #6

Sample no.	Fractal dimension D_f	Correlation coefficient R^2
# 1	2.48 ± 0.01	0.997
# 2	2.66 ± 0.01	0.998
# 3	2.54 ± 0.01	0.998
# 4	2.58 ± 0.01	0.997
# 5	2.55 ± 0.01	0.997
# 6	2.26 ± 0.01	0.998

*Statistically significant difference: $P < 0.05$

Statistical surface parameters and data obtained from AFM records by using MountainsMap® premium software typically revealed different spatial surface patterns (Fig. 1).

In Fig. 5 the shapes of the histograms reveal information about the nanoscale patterns, having a single peak that indicates a unimodal distribution.

The peak count histograms also indicate displacement of the dominant peak which means changing of texture in Z-direction (Fig. 6).

The graphical study of volume parameters (surface) (Fig. 7) and Sk parameters (Fig. 8) highlighted the quantitative values of these parameters.

The fractal surface geometry is revealed by fractal dimension of AFM images (Table 3). The highest value of fractal dimension was obtained for sample #2 ($D_f = 2.66 \pm 0.01$), and the lowest value was found for sample #6 ($D_f = 2.26 \pm 0.01$). Also, it can be seen that the values of fractal dimension increase for no processing samples (for samples #1, #3, #5), whereas the values of fractal dimension decrease for processing samples (for samples #2, #4, #6),

Tables 4 & 5 summarizes results of stereometric analyses of images shown in Fig. 1.

As can be seen, height parameters of no processing samples (for samples #1, #3, #5) including Sq, Sa, and Sv explained in the appendix, all are increased by increasing thermal processing.

Table 4 The statistical parameters for the analyzed samples: a) #1, b) #2, and c) #3, according to ISO 25178-2: 2012

The statistical parameters	Symbol	#1 Values	#2 Values	#3 Values
Height Parameters				
Root mean square height	Sq [nm]	0.163	2.42	0.195
Skewness	Ssk [−]	2.22	0.410	0.0331
Kurtosis	Sku [−]	15.8	3.40	3.23
Maximum peak height	Sp [nm]	2.21	11.5	0.945
Maximum pit height	Sv [nm]	0.520	8.56	0.861
Maximum height	Sz [nm]	2.73	20.1	1.81
Arithmetic mean height	Sa [nm]	0.112	1.91	0.155
Functional Parameters				
Areal material ratio	Smr [%]	100	100	100
Inverse areal material ratio	Smc [nm]	0.163	3.17	0.249
Extreme peak height	Sxp [nm]	0.235	4.15	0.380
Spatial Parameters				
Auto-correlation length	Sal [μm]	0.0103	0.0126	0.0226
Texture-aspect ratio	Str [−]	0.819	0.410	0.859
Texture direction	Std [°]	0.363°	0.346°	0.607°
Hybrid Parameters				
Root mean square gradient	Sdq [−]	0.0727	0.583	0.120
Developed interfacial area ratio	Sdr [%]	0.263	13.8	0.707
Functional Parameters (Volume)				
Material volume	Vm [$\mu m^3/\mu m^2$]	1.62e-005	0.000142	9.54e-006
Void volume	Vv [$\mu m^3/\mu m^2$]	0.000179	0.00332	0.000259
Peak material volume	Vmp [$\mu m^3/\mu m^2$]	1.62e-005	0.000142	9.54e-006
Core material volume	Vmc [$\mu m^3/\mu m^2$]	0.000113	0.00213	0.000174
Core void volume	Vvc [$\mu m^3/\mu m^2$]	0.000166	0.00308	0.000237
Pit void volume	Vvv [$\mu m^3/\mu m^2$]	1.36e-005	0.000231	2.21e-005
Feature Parameters				
Density of peaks	Spd [$1/\mu m^2$]	1377	1329	12,276
Arithmetic mean peak curvature	Spc [1/μm]	147	340	268
Ten point height	S10z [nm]	1.60	12.7	0.723
Five point peak height	S5p [nm]	1.23	8.09	0.320
Five point pit height	S5v [nm]	0.370	4.60	0.403
Mean dale area	Sda [μm^2]	0.000907	0.00133	9.11e-005
Mean hill area	Sha [μm^2]	0.000716	0.000723	7.91e-005
Mean dale volume	Sdv [μm^3]	1.58e-008	2.31e-007	7.69e-010
Mean hill volume	Shv [μm^3]	2.03e-008	2.99e-007	6.95e-010

*Statistically significant difference: $P < 0.05$

Table 5 The statistical parameters for the analyzed samples: a) #4, b) #5, and c) #6, according to ISO 25178-2: 2012

The statistical parameters	Symbol	#4 Values	#5 Values	#6 Values
Height Parameters				
Root mean square height	Sq [nm]	1.50	0.245	2.97
Skewness	Ssk [−]	0.502	0.663	0.458
Kurtosis	Sku [−]	4.12	7.37	3.34
Maximum peak height	Sp [nm]	8.48	2.98	13.3
Maximum pit height	Sv [nm]	5.15	1.33	9.14
Maximum height	Sz [nm]	13.6	4.31	22.4
Arithmetic mean height	Sa [nm]	1.17	0.188	2.34
Functional Parameters				
Areal material ratio	Smr [%]	100	100	100
Inverse areal material ratio	Smc [nm]	1.89	0.299	3.93
Extreme peak height	Sxp [nm]	2.61	0.448	4.99
Spatial Parameters				
Auto-correlation length	Sal [μm]	0.0163	0.0148	0.0118
Texture-aspect ratio	Str [−]	0.568	0.795	0.592
Texture direction	Std [°]	141°	0.485°	141°
Hybrid Parameters				
Root mean square gradient	Sdq [−]	0.309	0.141	0.643
Developed interfacial area ratio	Sdr [%]	4.24	0.981	17.2
Functional Parameters (Volume)				
Material volume	Vm [$\mu m^3/\mu m^2$]	9.45e-005	1.46e-005	0.000181
Void volume	Vv [$\mu m^3/\mu m^2$]	0.00199	0.000314	0.00411
Peak material volume	Vmp [$\mu m^3/\mu m^2$]	9.45e-005	1.46e-005	0.000181
Core material volume	Vmc [$\mu m^3/\mu m^2$]	0.0013	0.000207	0.00258
Core void volume	Vvc [$\mu m^3/\mu m^2$]	0.00184	0.000288	0.00384
Pit void volume	Vvv [$\mu m^3/\mu m^2$]	0.000148	2.60e-005	0.000274
Feature Parameters				
Density of peaks	Spd [$1/\mu m^2$]	550	2020	1064
Arithmetic mean peak curvature	Spc [1/μm]	408	271	312
Ten point height	S10z [nm]	7.48	1.96	16.6
Five point peak height	S5p [nm]	4.38	1.29	10.7
Five point pit height	S5v [nm]	3.10	0.664	5.91
Mean dale area	Sda [μm^2]	0.00084	0.000499	0.000945
Mean hill area	Sha [μm^2]	0.00157	0.000464	0.000933
Mean dale volume	Sdv [μm^3]	8.66e-008	1.08e-008	1.70e-007
Mean hill volume	Shv [μm^3]	2.82e-007	1.33e-008	6.33e-007

*Statistically significant difference: $P < 0.05$

The surface skewness (Ssk) of all samples is positive (Ssk > 0) which confirm the dominance of peaks on their surface with the smallest value in #3 (0.0331) and the highest value in #1 (2.22).

Since the surface kurtosis (Sku) of all samples is above 3, there exist spiky surfaces with the highest value in #1 (15.8) and the lowest value in #3 (3.23).

Furthermore, by comparing: functional, hybrid, functional (volume) and feature parameters for no processing samples (for samples #1, #3, #5) in Tables 4 and 5, it is concluded that, functional parameters (Smc and Sxp), hybrid parameters (Sdq and Sdr), functional parameters (volume) (Vv, Vmc, Vvc, Vvv) and feature parameters (Spc, S5v) are increased by increasing thermal processing.

4 Conclusions

In this study, the temperature stability of Si wafers thermal stability in correlation with three-dimensional (3D) surface

characterization using atomic force microscopy was analyzed. The samples were studied by different characterization techniques that proved changes of surface structure.

After analyzing the XPS data, it became clear that on the surface of the silicon wafers there were small impregnations of carbon and an oxide film that thickens during the annealing process. Etching eliminates the presence of carbon and partially removes the oxide layer from the surface. However, a longer etching time will be required to completely remove the oxide layer in the samples subjected to 2 and 4 h annealing.

AFM in combination with stereometric analysis characterize changes in the spatial distribution of thin films and correlate the locations of each component with changes in film morphology and topography that occur at the micrometer- and nanometer-scale. SEM-imaging support obtained data and demonstrate more difference in morphology of the stressed sample.

This is in the center of interest for surface passivation with low defect concentration. Furthermore, the condition of surface determines physical and chemical properties of materials, because some parameters directly depend on topography: hydrophobicity, optical properties, free surface, etc. The described parameters can be concern for "fingerprints" of the surface which changed after thermal processing.

Acknowledgements Research described in the paper was financially supported by the Ministry of Education, Youth and Sports of the Czech Republic under the project CEITEC 2020 (LQ1601), by the National Sustainability Program under grant LO1401 and by Internal Grant Agency of Brno University of Technology, grant No. FEKT-S-17-4626. For the research, infrastructure of the SIX Center was used. Part of the work was carried out with the support of CEITEC Nano Research Infrastructure (ID LM2015041, MEYS CR, 2016–2019), CEITEC Brno University of Technology.

Compliance with Ethical Standards

Conflicts of Interest The authors declare that they have no competing interests.

Appendix

The statistical parameters of 3D surface roughness, according to ISO 25178-2:2012 are defined as following [44].

a) Height parameters are a class of surface finish parameters that quantify the Z-axis perpendicular to the surface.

(Sq) – root mean square height is the standard deviation of the height distribution, or RMS surface roughness.
(Ssk) – Skewness is the third statistical moment, qualifying the symmetry of the height distribution. Negative skew indicates a predominance of valleys, while positive skew is seen on surfaces with peaks.
(Sku) – Kurtosis is the fourth statistical moment, qualifying the flatness of the height distribution. For spiky surfaces, $Sku > 3$; for bumpy surfaces, $Sku < 3$; perfectly random surfaces have kurtosis of 3.
(Sp) - Maximum peak height is the height between the highest peak and the mean plane.
(Sv) - Maximum pit height is the depth between the mean plane and the deepest valley.
(Sz) - Maximum height is the height between the highest peak and the deepest valley.
(Sa) - Arithmetical mean height is the mean surface roughness.

b) Functional parameters are calculated from the Abbott-Firestone curve obtained by the integration of height distribution on the whole surface.

(Smr) - Areal material ratio is the bearing area ratio at a given height. Ratio of the area of the material at a specified height *c* (cut level) to the evaluation area. The Smr(c) is expressed as a percentage. For the Smr parameter, the height *c* is counted by default from the mean plane.
(Smc) - Inverse areal material ratio is the height c at which a given areal material ratio p is satisfied. The height is calculated from the mean plane.
(Sxp) - Extreme peak height is the difference in height between q% and p% material ratio. This parameter must be configured with two thresholds entered in %.

c) Spatial parameters describe topographic characteristics based upon spectral analysis. They quantify the lateral information present on the X- and Y-axes of the surface.

(Sal) - Auto-correlation length is the horizontal distance of the autocorrelation function (tx, ty) which has the fastest decay to a specified value s, with $0 < s < 1$. The default value for s in the software is 0.2. This parameter expresses the content in wavelength of the surface. A high value indicates that the surface has mainly high wavelengths (low frequencies).
(Str) - Texture-aspect ratio is the ratio of the shortest decrease length at 0.2 from the autocorrelation, on the greatest length. This parameter has a result between 0 and 1. If the value is near 1, we can say that the surface is isotropic, i.e. has the same characteristics in all directions. If the value is near 0, the surface is anisotropic, i.e. has an oriented and/or periodical structure.
(Std) - Texture direction calculates the main angle for the texture of the surface, given by the maximum of the polar spectrum. This parameter has a meaning if Str is lower than 0.5.

d) Hybrid parameters are a class of surface finish parameters that quantify the information present on the X-, Y- and Z-axes of the surface, i.e. those criteria that depend both on the amplitude and the spacing, such as slopes, curvatures, etc.

(Sdq) - Root mean square gradient is the root-mean-square slope of the surface.
(Sdr) - Developed interfacial area ratio is the ratio of the increment of the interfacial area of the scale limited surface within the definition area over the definition area. The developed surface indicates the complexity of the surface thanks to the comparison of the curvilinear surface and the support surface. A completely flat surface will have a Sdr near 0%. A complex surface will have a Sdr of some percents.

e) Functional volume parameters are typically used in tribological studies. They are calculated using the Abbott-Firestone curve (areal material ratio curve) calculated on the surface.

Vm(p) - Material volume is the volume of the material at a material ratio p (in %).
Vv(p) - Void volume is the volume of the voids at a material ratio p (in %).
Vmp - Peak material volume of the scale limited surface is the volume of material in the peaks, between 0% material ratio and a material ratio p (in %), calculated in the zone above c1. Vmp = Vm(p)
Vmc - Core material volume of the scale limited surface is the volume of material in the core or kernel, between two material ratios p and q (in %), calculated in the zone between c1 and c2. Vmc = Vm(q) - Vm(p)
Vvc - Core void volume of the scale limited surface is the volume of void in the core or kernel, between two material ratios p and q (in %), calculated in the zone between c1 and c2. Vvc = Vv(p) - Vv(q)
Vvv - Pit void volume of the scale limited surface is the volume of void in the valleys, between a material ratio p (in %) and 100% material ratio, calculated in the zone below c2. Vvv = Vv(p)

f) Feature parameters are derived from the segmentation of a surface into motifs (hills and dales). Segmentation is carried out in accordance with the watersheds algorithm.

Spd - Density of peaks is the number of peaks per unit area.
Spc - Arithmetic mean peak curvature is the arithmetic mean of the principle curvatures of peaks within a definition area.
S10z - Ten point height is the average value of the heights of the five peaks with the largest global peak height added to the average value of the heights of the five pits with the largest global pit height, within the definition area. S10z = S5p + S5v
S5p - Five point peak height is the average value of the heights of the five peaks with the largest global peak height, within the definition area.
S5v - Five point pit height is the average value of the heights of the five pits with the largest global pit height, within the definition area.
Sda - Closed dale area is the average area of dales connected to the edge at height c.
Sha - Closed hill area is the average area of hills connected to the edge at height c.
Sdv - Closed dale volume is the average volume of dales connected to the edge at height c.
Shv - Closed hill volume is the average volume of hills connected to the edge at height c.

Publisher's Note Springer Nature remains neutral with regard to jurisdictional claims in published maps and institutional affiliations.

References

1. Sengupta A, Sarkar CK (eds) (2015) Introduction to Nano: Basics to Nanoscience and Nanotechnology. Springer. https://doi.org/10.1007/978-3-662-47314-6
2. Ţălu Ş (2015) Micro and nanoscale characterization of three dimensional surfaces. Basics and applications, Napoca Star Publishing House, Cluj-Napoca
3. Šesták J, Simon P (2012) Thermal analysis of micro, Nano- and non-crystalline materials: transformation, crystallization, kinetics and thermodynamics. Springer Science & Business Media. https://doi.org/10.1007/978-90-481-3150-1.
4. Méndez A, Reyes Y, Trejo G, Stępień K, Ţălu Ş (2015) Micromorphological characterization of zinc/silver particle composite coatings. Microsc Res Tech 78:1082–1089. https://doi.org/10.1002/jemt.22588
5. Abdulagatov AI, Ramazanov SM, Dallaev RS, Murliev EK, Palchaev DK, Rabadanov MK, Abdulagatov IM (2018) Atomic layer deposition of aluminum nitride using Tris(diethylamido)aluminum and hydrazine or ammonia. Russ Microelectron 47(2):118–130. https://doi.org/10.1134/S1063739718020026
6. Mazzocchi, V., Sennikov, P. G., Bulanov, A. D., Churbanov, M. F., Bertrand, B., Hutin, L., … Sanquer, M. 99.992% 28Si CVD-grown epilayer on 300 mm substrates for large scale integration of silicon spin qubits. J Cryst Growth (2018). https://doi.org/10.1007/s00125-017-4462-5
7. Sun X, Gao K, Pang X, Sun Q, Li J (2018) Thermodynamic energy variation diagram to speculate preferred growth orientation of magnetron sputtered PbSe thin films on monocrystalline silicon substrates. Appl Surf Sci 452:1–10. https://doi.org/10.1016/j.apsusc.2018.04.200
8. Gotoh K, Cui M, Takahashi I, Kurokawa Y, Usami N (2017) Development of spin-coated copper iodide on silicon for use in

hole-selective contacts. Energy Procedia 124:598–603. https://doi.org/10.1016/j.egypro.2017.09.081
9. Alford, T. L., Tang, T., Thompson, D. C., Bhagat, S., & Mayer, J. W. Influence of microwave annealing on direct bonded silicon wafers. Thin Solid Films (2008). https://doi.org/10.1016/j.tsf.2007.06.118
10. Fung, T. H., Chan, C. E., Hallam, B. J., Payne, D. N. R., Abbott, M. D., & Wenham, S. R. (2017). Impact of annealing on the formation and mitigation of carrier-induced defects in multi-crystalline silicon. In Energy Procedia https://doi.org/10.1016/j.egypro.2017.09.087
11. Amanov A, Kwon HG, Pyun YS (2017) The possibility of reducing the reflectance and improving the tribological behavior of Si wafer by UNSM technique. Tribol Int 105:175–184. https://doi.org/10.1016/j.triboint.2016.09.042
12. Shikhgasan R, Ţălu Ş, Dinara S, Sebastian S, Guseyn R (2015) Epitaxy of silicon carbide on silicon: micromorphological analysis of growth surface evolution. Superlattice Microst 86:395–402. https://doi.org/10.1016/j.spmi.2015.08.007.
13. N. Naseri, S. Solaymani, A. Ghaderi, M. Bramowicz, S. Kulesza, Ş. Ţălu, M. Pourreza, S. Ghasemi, Microstructure, morphology and electrochemical properties of co nanoflake water oxidation electrocatalyst at micro- and nanoscale. RSC Adv, 7(21) (2017) 12923–12930. https://doi.org/10.1039/C6RA28795F.
14. Ţălu Ş, Bramowicz M, Kulesza S, Solaymani S, Shafikhani A, Ghaderi A, Ahmadirad M (2016) Gold nanoparticles embedded in carbon film: micromorphology analysis. J Ind Eng Chem 35:158–166. https://doi.org/10.1016/j.jiec.2015.12.029
15. Dallaeva D, Ţălu Ş, Stach S, Škarvada P, Tomanek P, Grmela L (2014) AFM imaging and fractal analysis of surface roughness of AlN epilayers on sapphire substrates. Appl Surf Sci 312:81–86. https://doi.org/10.1016/j.apsusc.2014.05.086
16. S. Stach, D. Dallaeva, Ş. Ţălu, P. Kaspar, P. Tománek, S. Giovanzana, L. Grmela, Morphological features in aluminum nitride epilayers prepared by magnetron sputtering, Mater Sci Pol 33(1) (2015) 175–184. https://doi.org/10.1515/msp-2015-0036.
17. Rachow T, Reber S, Janz S, Knapp M, Milenkovic N (2016) Degradation of silicon wafers at high temperatures for epitaxial deposition. Energy Science and Engineering 4(5):344–351. https://doi.org/10.1002/ese3.130
18. Rabus, M., Fiory, A. T., Ravindra, N. M., Frisella, P., Agarwal, A., Sorsch, T., … Mansfield, W. (2006). Rapid thermal processing of silicon wafers with emissivity patterns. J Electron Mater, 35(5), 877–891. https://doi.org/10.1007/BF02692543
19. Yoo WS, Fukada T, Yokoyama I, Kang K, Takahashi N (2002) Thermal behavior of large-diameter silicon wafers during high-temperature rapid thermal processing in single wafer furnace. Japanese journal of applied physics. Part 1: Regular Papers and Short Notes and Review Papers 41(7 A):4442–4449. https://doi.org/10.1143/JJAP.41.4442
20. Doi T, Koguchi M (2016) Investigation of Si(001) stable surfaces in alternating current heating. Surf Sci 653:226–236. https://doi.org/10.1016/j.susc.2016.06.015
21. Gupta P, Kulkarni MS (2006) Simulation of slip during high-temperature annealing of silicon wafers in vertical furnaces. ECS Trans 3(October):211–223. https://doi.org/10.1149/1.2355758
22. Shiraki, H., Profiler, P., Kanda, T., Hourai, M., Tomokage, H., Spectroscopy, P., … Suzuki, T. (1974). Related content silicon wafer annealing effect in loop defect generation.
23. Suzuki, T. Effect of annealing a silicon wafer in argon with a very low oxygen partial pressure. J Appl Phys (2000). https://doi.org/10.1063/1.1323512
24. Gräf D, Lambert U, Brohl M, Ehlert A, Wahlich R, Wagner P (1995) Improvement of Czochralski silicon wafers by high-temperature annealing. J Electrochem Soc 142(9):3189–3192. https://doi.org/10.1149/1.2048711
25. Elenkova D, Zaharieva J, Getsova M, Manolov I, Milanova M, Stach S, Ţălu Ş (2015) Morphology and optical properties of SiO_2-based composite thin films with immobilized terbium(III) complex with a Biscoumarin derivative. Int J Polym Anal Charact 20(1):42–56. https://doi.org/10.1080/1023666X.2014.955400
26. Ţălu Ş, Stach S, Mahajan A, Pathak D, Wagner T, Kumar A, Bedi RK (2014) Multifractal analysis of drop-casted copper (II) tetrasulfophthalocyanine film surfaces on the indium tin oxide substrates. Surf Interface Anal 46(6):393–398. https://doi.org/10.1002/sia.5492
27. A. Arman, Ş. Ţălu, C. Luna, A. Ahmadpourian, M. Naseri, M. Molamohammadi, Micromorphology characterization of copper thin films by AFM and fractal analysis, J Mater Sci Mater Electron 26 (2015) 9630–9639. https://doi.org/10.1007/s10854-015-3628-5.
28. Ş. Ţălu, S. Stach, S. Valedbagi, S.M. Elahi, R. Bavadi, Surface morphology of titanium nitride thin films synthesised by DC reactive magnetron sputtering. Mater. Sci.- Poland, 33 (2015), 137–143. https://doi.org/10.1515/msp-2015-0010
29. Knápek A, Sobola D, Tománek P, Pokorná Z, Urbánek M (2017) Field emission from the surface of highly ordered pyrolytic graphite. Appl Surf Sci 395. https://doi.org/10.1016/j.apsusc.2016.05.002
30. Ţălu Ş, Stach S, Zaharieva J, Milanova M, Todorovsky D, Giovanzana S (2014) Surface roughness characterization of poly(methylmethacrylate) films with immobilized Eu(III) -Diketonates by fractal analysis. Int J Polym Anal Charact 19: 404–421. https://doi.org/10.1080/1023666X.2014.904149
31. Y. Reyes-Vidal, R. Suarez-Rojas, C. Ruiz, J. Torres, Ş. Ţălu, A. Méndez, G. Trejo, Electrodeposition, characterization, and antibacterial activity of zinc/silver particle composite coatings. Appl Surf Sci 342 (2015), 34–41. https://doi.org/10.1016/j.apsusc.2015.03.037.
32. Sobola D, Ţălu Ş, Solaymani S, Grmela L (2017) Influence of scanning rate on quality of AFM image: study of surface statistical metrics. Microsc Res Tech 80:1328–1336. https://doi.org/10.1002/jemt.22945.
33. Ţălu Ş, Solaymani S, Bramowicz M, Kulesza S, Ghaderi A, Shahpouri S, Elahi SM (2016) Effect of electric field direction and substrate roughness on three-dimensional self-assembly growth of copper oxide nanowires. J Mater Sci Mater Electron 27:9272–9277. https://doi.org/10.1007/s10854-016-4965-8
34. Yadav RP, Kumar M, Mittal AK, Pandey AC (2015) Fractal and multifractal characteristics of swift heavy ion induced self-affine nanostructured BaF_2 thin film surfaces. Chaos 25(8) 083115
35. Ţălu Ş, Bramowicz M, Kulesza S, Ghaderi A, Dalouji V, Solaymani S, Fathi Kenari M, Ghoranneviss M (2016) Fractal features and surface micromorphology of diamond nanocrystals. J Microsc 264:143–152. https://doi.org/10.1111/jmi.12422
36. Stach S, Sapota W, Ţălu Ş, Ahmadpourian A, Luna C, Ghobadi N, Arman A, Ganji M (2017) 3D surface stereometry studies of sputtered TiN thin films obtained at different substrate temperatures. J Mater Sci Mater Electron 28(2):2113–2122. https://doi.org/10.1007/s10854-016-5774-9
37. Ţălu Ş, Stach S, Mendez A, Trejo G, Talu M (2013) Multifractal characterization of nanostructure surfaces of electrodeposited Ni-P coatings. J Electrochem Soc 161:D44–D47. https://doi.org/10.1149/2.039401jes
38. Ţălu Ş, Yadav RP, Šik O, Sobola D, Dallaev R, Solaymani S, Man O (2018) How topographical surface parameters are correlated with CdTe monocrystal surface oxidation. Mater Sci Semicond Process. https://doi.org/10.1016/j.mssp.2018.05.030
39. Connor MW, Colmenares C (1996) X-ray photoelectron characterization of SiO_2 aerogel. J Non-Cryst Solids 201:76–80. https://doi.org/10.1016/0022-3093(95)00622-2

40. Suzuki T (2000) Effect of annealing a silicon wafer in argon with a very low oxygen partial pressure. J Appl Phys 88:6881. https://doi.org/10.1063/1.1323512
41. Bekkay T, Piyakis K, Diawara Y, Sacher E, Yelon A, Currie JF (1991) Band bending and Fermi level shifts in phosphorus-doped hydrogenated amorphous silicon studied by X-ray photoelectron spectroscopy. Surf Sci 258:190–196. https://doi.org/10.1016/0039-6028(91)90913-D
42. Motamedi P, Cadien K (2014) XPS analysis of AlN thin films deposited by plasma enhanced atomic layer deposition. Appl Surf Sci 315:104–109. https://doi.org/10.1016/j.apsusc.2014.07.105
43. Mountains Map® 7 Software (Digital Surf, Besançon, France). Available from: http://www.digitalsurf.fr (last Accessed September 10th, 2018).
44. ISO 25178-2: 2012, Geometrical product specifications (GPS) - Surface texture: Areal - Part 2: Terms, definitions and surface texture parameters Available from: http://www.iso.org (last Accessed September 10th, 2018).

4 AlN thin films deposited by thermal ALD using and hydrazine and ammonia as precursors

4.1 Motivation of the article

This research was the first in the series of attempts which belong directly to the optimization of the ALD technology for deposition of AlN by introducing new approaches. The motivation of the study was to look into the expediency of utilization of rather unconventional precursors: tris(diethylamido)aluminum (TDEAA) for aluminum and hydrazine (N_2H_4) for nitrogen, as well as to provide a comparison with a more traditional precursor – ammonia (NH_3).

4.2 Conclusion on the article

As a result of this study it was found out that hydrazine (N_2H_4) indeed has an advantage over ammonia (NH_3), this advantage being the better reactivity with tris(diethylamido)aluminum (TDEAA), which results in increased density of the films. Another benefit of hydrazine usage lies in the fact that it has lower dissociation energy than ammonia, therefore allowing for lower temperatures during the deposition process. However, it was also discovered that usage of both of these precursors has a drawback which manifests in a rather significant presence of hydrogen within the resulted layers (22-26 at.%). The occurrence of the hydrogen is most likely a product of incomplete dissociation of NH_3 and N_2H_4 molecules, which resulted in a presence of various amine (N-H) or/and amide (C-N) groups, which are a part of so-called ALD defects.

4.3 Contribution

This article was written in collaboration with the colleagues from Russia and the United States (the first author). Most of the analyses were performed in the United States by the first author. My contribution as a co-author lies in preparation of the samples, interpretation of the obtained data, partial writing of the manuscript and visualisation.

4.4 Article 2

The paper **Atomic Layer Deposition of Aluminum Nitride Using Tris(diethylamido)aluminum and Hydrazine or Ammonia** was published in the year of 2018 in **Russian Microelectronics** journal (ISSN: 1608-3415).

*Note: The **Russian Microelectronics** journal at the time of publishing was indexed in WoS and had impact factor of ~0.4. Nowadays (for the unknown reason), it can be found only on Scopus. The paper itself received a fair amount of attention and by now (April, 2021) has ~15citations.*

ISSN 1063-7397, Russian Microelectronics, 2018, Vol. 47, No. 2, pp. 118–130. © Pleiades Publishing, Ltd., 2018.
Original Russian Text © A.I. Abdulagatov, Sh.M. Ramazanov, R.S. Dallaev, E.K. Murliev, D.K. Palchaev, M.Kh. Rabadanov, I.M. Abdulagatov, 2018, published in Mikroelektronika, 2018, Vol. 47, No. 2.

Atomic Layer Deposition of Aluminum Nitride Using Tris(diethylamido)aluminum and Hydrazine or Ammonia

A. I. Abdulagatov, Sh. M. Ramazanov, R. S. Dallaev, E. K. Murliev, D. K. Palchaev, M. Kh. Rabadanov, and I. M. Abdulagatov*

Dagestan State University, Makhachkala, The Republic of Dagestan, 367002 Russia
**e-mail: ilmutdina@gmail.com*

Received August 14, 2017

Abstract—Aluminum nitride (AlN_x) films were obtained by atomic layer deposition (ALD) using tris(diethylamido)aluminum(III) (TDEAA) and hydrazine (N_2H_4) or ammonia (NH_3). The quartz crystal microbalance (QCM) data showed that the surface reactions of TDEAA and N_2H_4 (or NH_3) at temperatures from 150 to 225°C were self-limiting. The rates of deposition of the nitride film at 200°C for systems with N_2H_4 and NH_3 coincided: ~1.1 Å/cycle. The ALD AlN films obtained at 200°C using hydrazine had higher density (2.36 g/cm^3, 72.4% of bulk density) than those obtained with ammonia (2.22 g/cm^3, 68%). The elemental analysis of the film deposited using TDEAA/N_2H_4 at 200°C showed the presence of carbon (~1.4 at %), oxygen (~3.2 at %), and hydrogen (22.6 at %) impurities. The N/Al atomic concentration ratio was ~1.3. The residual impurity content in the case of N_2H_4 was lower than for NH_3. In general, it was confirmed that hydrazine has a more preferable surface thermochemistry than ammonia.

DOI: 10.1134/S1063739718020026

INTRODUCTION

Aluminum nitride is a wide-gap semiconductor (~6.2 eV) with high thermal conductivity (2.85 W/cm K at 300 K), melting point (2750°C), electric resistance (10^{13} Ohm cm), and refraction index (~2.0), but low absorption coefficient ($<10^{-3}$) [1–5]. Due to these properties, AlN is promising for wide range of applications in power engineering and micro- and optoelectronics. Thin AlN films were successfully used for passivation of GaN, GaAs, SiC, InGaAs, and H–C (diamond) devices [6–9] and also for excitation of surface acoustic waves [10]. AlN epitaxial layers are also used as buffer layers when growing high-quality GaN films and nanowires by molecular beam epitaxy (MBE) [11, 12].

The AlN films mainly obtained by chemical vapor deposition (CVD) [13–16], physical vapor deposition (PVD) [10, 17, 18], molecular beam epitaxy [11, 19, 20], etc. In comparison with these methods, ALD has a number of advantages [21]: relatively low deposition temperatures, control of film thickness at the atomic level, and highly conformal coating of micro/nano structures and nanoparticles. In the ALD method, the films grow as a result of repeated surface reactions performed away from the thermodynamic equilibrium. The first studies on the thermal atomic layer deposition of AlN were performed using ammonia (NH_3) as a nitrogen precursor in combination with trimethylaluminum (TMA) [22–26] or aluminum chloride ($AlCl_3$) [27], which require high deposition temperatures of 325–500°C. At the same time, the films obtained from TMA/NH_3 usually contain 4–7 at % carbon impurities [22, 25] and a significant amount of hydrogen [28]. This is due to the thermal decomposition of TMA and low reactivity of ammonia [24, 29].

For full applicability of nitrides of the third group elements, compounds and heterostructures on their basis should be grown at temperatures below 300°C [30]. Therefore, considerable attention has been paid to plasma-enhanced atomic layer deposition (PE-ALD). Previously, the possibility of obtaining AlN films by PE-ALD from various precursors was demonstrated: $AlCl_3$ and NH_3/H_2 [31]; NH_3/H_2/Ar gas mixture [32] (at 350°C); and TMA and NH_3 [33–35] or N_2/H_2 [34, 36–38] (at 100–500°C). The use of plasma offers better possibilities in choosing the properties of materials, substrate temperature, precursors, and processing conditions, but has some drawbacks: lower film conformity and risk of its damage by plasma [39].

Previously, low-temperature ALD was performed at 200–250°C using tris(dimethylamido)aluminum ($Al_2(N(CH_3)_2)_6$) and NH_3 [40]. The AlN films obtained in [40] contained less than 1 at % carbon and oxygen impurities. However, the deposition conditions, the optimization process, etc. were not described in detail in [40]. A more detailed description of the conditions of ALD of AlN films from tris(dimethylamido)aluminum (TDMAA) and NH_3 in the temperature range 180–400°C was later presented in [41].

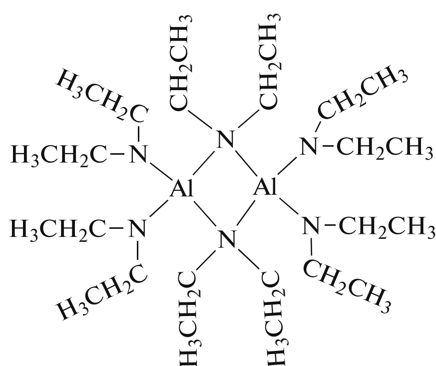

Fig. 1. Tris(diethylamido)aluminum (TDEAA).

The majority of the mentioned above studies used NH_3 as the nitrogen precursor for deposition of AlN films, but N_2H_4 has more advantageous thermochemistry to growth metal nitrides. The high reactivity of N_2H_4 is due to the relatively weak N–N bond in N_2H_4 compared to the N–H bond in NH_3 [42, 43].

The present work is devoted to the development of the optimum conditions to grow ALD AlN without employing plasma and using tris(diethylamido)aluminum (TDEAA) at temperatures below 300°C. The structure of the TDEAA molecule is shown in Fig. 1. AlN films have never been previously obtained by ALD using TDEAA. To successfully use this method, high vapor pressure and thermal stability of a organometallic precursor are required. TDEAA has lower melting point than TDMAA and possibly higher thermal stability. According to the manufacturer's database, TDEAA melts between 28 and 31°C, whereas TDMAA melts between 82 and 84°C. Earlier, it was reported that a similar precursor for CVD, tetrakis(diethylamido)titanium used for deposition of titanium nitride, is more thermally stable than tetrakis(dimethylamido)titanium [44].

Figure 2 shows the simplified ALD AlN deposition scheme consisting of the surface reactions of TDEAA and NH_3 or N_2H_4.

EXPERIMENTAL

The AlN films were obtained by successively dosing tris(diethylamido)aluminum and NH_3 (or N_2H_4) on ALD equipment (*ASO NanoTech*, Makhachkala, Russia). The unit was equipped with a vacuum chamber with hot walls, in which a dense stream of an inert gas was fed. Ultra high purity nitrogen (UHP, 99.999%) used as a carrier gas. The nitrogen pressure in the ALD reactor maintained at 0.9 Torr. The purity of tris(diethylamido)aluminum and hydrazine (Sigma-Aldrich) was 99.99% (CAS no. 352546-72-6) and 98% (CAS no. 302-01-2), respectively. TDEAA and hydrazine were loaded in to dosing containers in an inert atmosphere. To create sufficient vapor pressure, TDEAA was heated in a stainless steel container to 85–90°C. Hydrazine was dosed from a glass container connected via an inlet valve to the reactor. Since hydrazine is explosive, it was handled with care according to the recommendations of [45]. Ammonia (Sigma-Aldrich) with purity of 99.98% (CAS no. 7664-41-7) was stored in a cylinder with a regulator installed by the manufacturer. Ammonia and hydrazine were not heated because of their high vapor pressures at room temperature.

For *ex situ* analysis of the resulting films, silicon Si⟨100⟩ wafer coupons with dimensions of 1.5 × 1.5 cm were used as substrates. The substrates were cleaned with acetone and isopropanol and dried with a UHP nitrogen flow; then they were kept in the ALD reaction chamber for ~30 min before the deposition. The

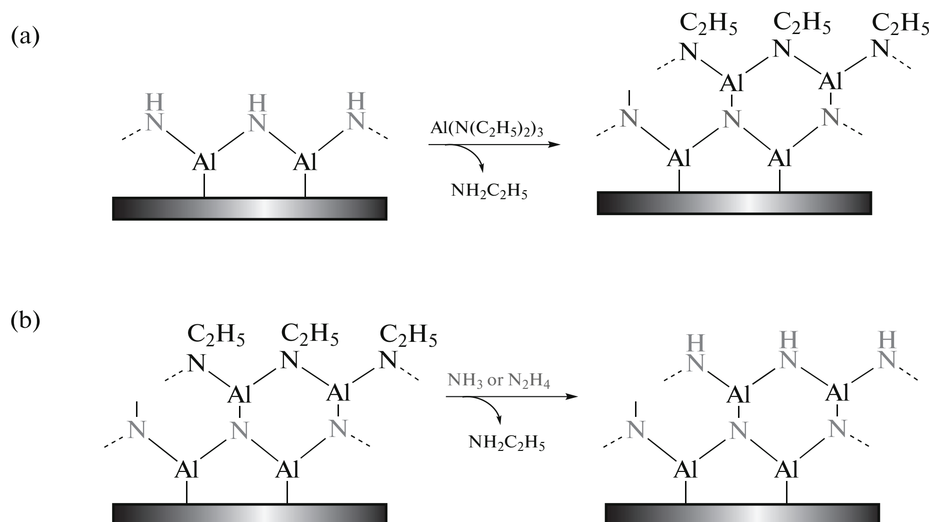

Fig. 2. Scheme of ALD of AlN using TDEAA and NH_3 or N_2H_4.

silicon substrates used for deposition had a native silicon oxide layer with a thickness of ~25 Å.

In situ monitoring of the deposition was performed by quartz crystal microbalance (QCM) for control of the growth parameters of AlN films and further optimization of the procedure [46]. Before the start of precursor dosing, the crystal used in QCM was coated by ALD in the same reactor with an Al_2O_3 film with a thickness of ~60 Å using trimethylaluminum ($Al(CH_3)_3$) and H_2O. The errors of QCM for each point of the saturation curves of the precursors were calculated from the standard deviations of 10–12 measurements. The error of thickness was evaluated from the data for three AlN films deposited simultaneously on the silicon substrates located at a distance of ~1 cm from each other along the gas flow direction.

The X-ray reflectivity (XRR) and diffraction (XRD) data were obtained with a Bede D1 high-resolution diffractometer (Bede Scientific, United States). The XRR experimental data were simulated using REFS software. The diffractometer was equipped with a copper anode; $\lambda = 1.54$ Å. The filament current was 40 mA at a voltage of 40 kV. The thickness, density, surface roughness, and crystal structure of the resulting films were determined from the XRR and XRD data. The X-ray photoelectron spectroscopy (XPS) data were obtained on a PHI 5400 instrument (Physical Electronics, United States) with a monochromatic AlK_α X-ray source (1486.6 eV) and Ar+ sputtering attachment. The argon ion energy during the etching was ~1.5 keV. The XPS enabled to determine the level of carbon and oxygen impurities and their depth distribution in the obtained AlN films. The ratio of the concentrations of nitrogen and aluminum atoms in the films was determined by Rutherford backscattering spectrometry (RBS). The analysis was performed on the RBS 400 equipment (Analytical Endstation, United States) using software from Charles Evans and Associates (United States). The energy of He+ ions was 2 MeV with a bombardment angle of 165°. The content of hydrogen impurities in the films was determined by forward recoil elastic spectrometry (FRES) on a National Electrostatics instrument (United States). For ERDA, calibration was performed using mica (9.5 at % hydrogen atoms). The He^{2+} ion energy was 2 MeV, and the bombardment angle 75°.

The times of introduction of precursors in the chamber and purge times are denoted as t_1, t_2, t_3, and t_4, where t_1 is the TDEAA exposure time; t_3 is the NH_3 or N_2H_4 dosing time; and t_2 and t_4 is the N_2 purge time after the introduction of the doses of the first and second reagents, respectively, in seconds.

RESULTS AND DISCUSSION

The data on the mass gain before saturation as a result of TDEAA and NH_3 exposures in to the reactor during the ALD of AlN at 175 and 200°C are shown in Fig. 3. The mass gain values for one A–B cycle depending on the TDEAA dose size are presented in Fig. 3a. The results presented in the plot were obtained at a TDEAA dosing time $t_1 = x$, purge times $t_2 = 40$ and $t_4 = 90$, and NH_3 dose time $t_3 = 3$ s, i.e., for one cycle $x/40/3/90$. According to Fig. 3, the mass gain reaches saturation at ~3.5 s for both temperatures. When the deposition temperature increased, the film growth rate increased from 18 to 21.5 ng/(cm^2 cycle). The TDEAA partial pressure was ~10 mTorr after dosing for 3.5 s, which corresponds to a dose of 3.5×10^4 L (1 L (Langmuir) = 1×10^{-6} Torr s). Figure 3b shows the saturation parameters for NH_3 obtained after dosings of $3.5/40/x/90$ where the TDEAA dose remained constant and equal to 3.5 s, and x is the variable NH_3 dosing time. The mass gain reached saturation at ~3 s for both temperatures. The maximum mass gain was 16.3 and 20.5 ng/(cm^2 cycle) at deposition temperatures of 175 and 200°C, respectively. These values are close to the parameters shown in Fig. 3a; i.e., both experiments were performed at fixed saturation parameters of the precursor. The partial pressure of NH_3 was ~225 mTorr when the valve was open for 3 s, which corresponds to a dose of 6.75×10^5 L.

The data on mass gain before saturation as a result of TDEAA and N_2H_4 exposures at 200 and 225°C are shown in Fig. 4. The dependence of mass gain per cycle on the TDEAA dose is shown in Fig. 4a. The dosing and purge parameters in this case were $x/40/1.3/90$ where x is the variable TDEAA dosing time, and 1.3 s is the size of the hydrazine dose, which remained constant. According to the plot, the mass gain reached saturation at a TDEAA dosing time of ~1 s. It slightly increased from 24.4 ng/(cm^2 cycle) at 200°C to 25 ng/(cm^2 cycle) at 225°C. Figure 4b shows how the mass gain changes depending on the N_2H_4 dose. The dosing parameters in this case were $1/40/x/90$, where 1 s is the fixed time for the TDEAA dose and x is the variable time for the N_2H_4 dose. The mass gain reached saturation when the N_2H_4 dose was introduced for 1.5 s. The mass gain slightly increased from 24.1 ng/(cm^2 cycle) at 200°C to 25.1 ng/(cm^2 cycle) at 225°C. As in the case of ammonia, the data in Fig. 4 were obtained at the saturation parameters of the fixed precursor. The partial pressure of N_2H_4 during dosing for 1.3 s was ~30 mTorr, which corresponds to a dose of 3.9×10^4 L.

Thus, the surface reactions of TDEAA and NH_3 or N_2H_4 were found to reach saturation, which satisfies the condition for ALD. The optimum growth conditions are achieved much faster when N_2H_4 is used. The saturation dose of N_2H_4 is 3.9×10^4 L, much lower than that of NH_3 (6.75×10^5 L). In addition, the purge time required for completely removing the by-products in the ammonia process took much longer time than in the hydrazine process. This showed itself as elongated pressure stabilization during the ammonia

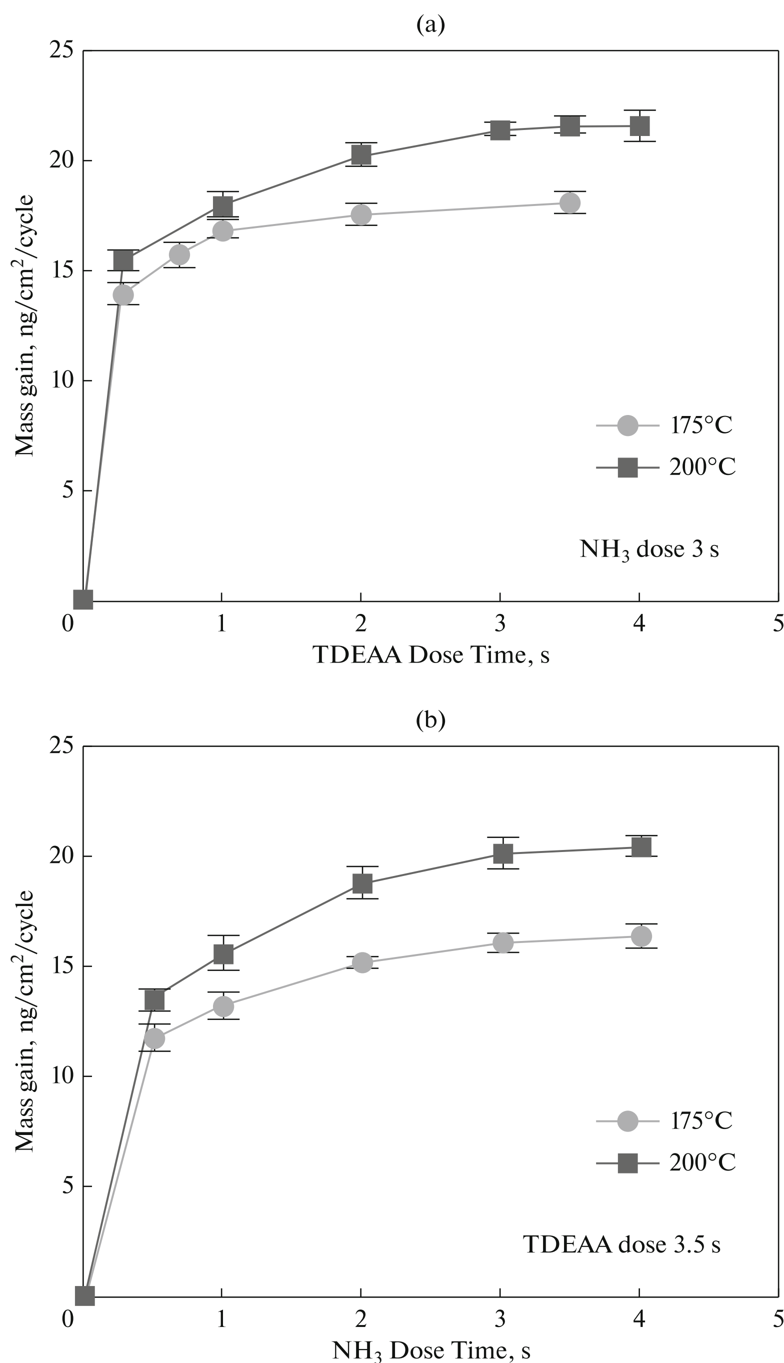

Fig. 3. QCM data on saturation of (a) TDEAA and (b) NH_3 during the ALD AlN at 175 and 200°C.

dose purge. The data of [47] suggest possible formation of ammonia and organometallic (OM) precursor adducts with a relatively low melting point over the volume of the vacuum chamber. In general, rapid evacuation precludes CVD reactions and reduces the film deposition time. Evacuation of 90 s after N_2H_4 dosing was performed only to minimize the variables for cleaner comparison with the TDEAA/NH_3 system and for stable operation of QCM.

Figure 5 presents the observed QCM signal during the ALD of AlN performed by alternating dosing of TDEAA and N_2H_4 at 200°C. The data of Fig. 5a show that the mass gain is linear for 25 cycles. The reagent dosing time was 1.5/40/1.3/90; the average growth rate is ~24.3 ng/(cm^2 cycle). The profile of the QCM signal obtained during the precursor dosing is shown in Fig. 5b. It can be seen that the dosing of TDEAA leads to a

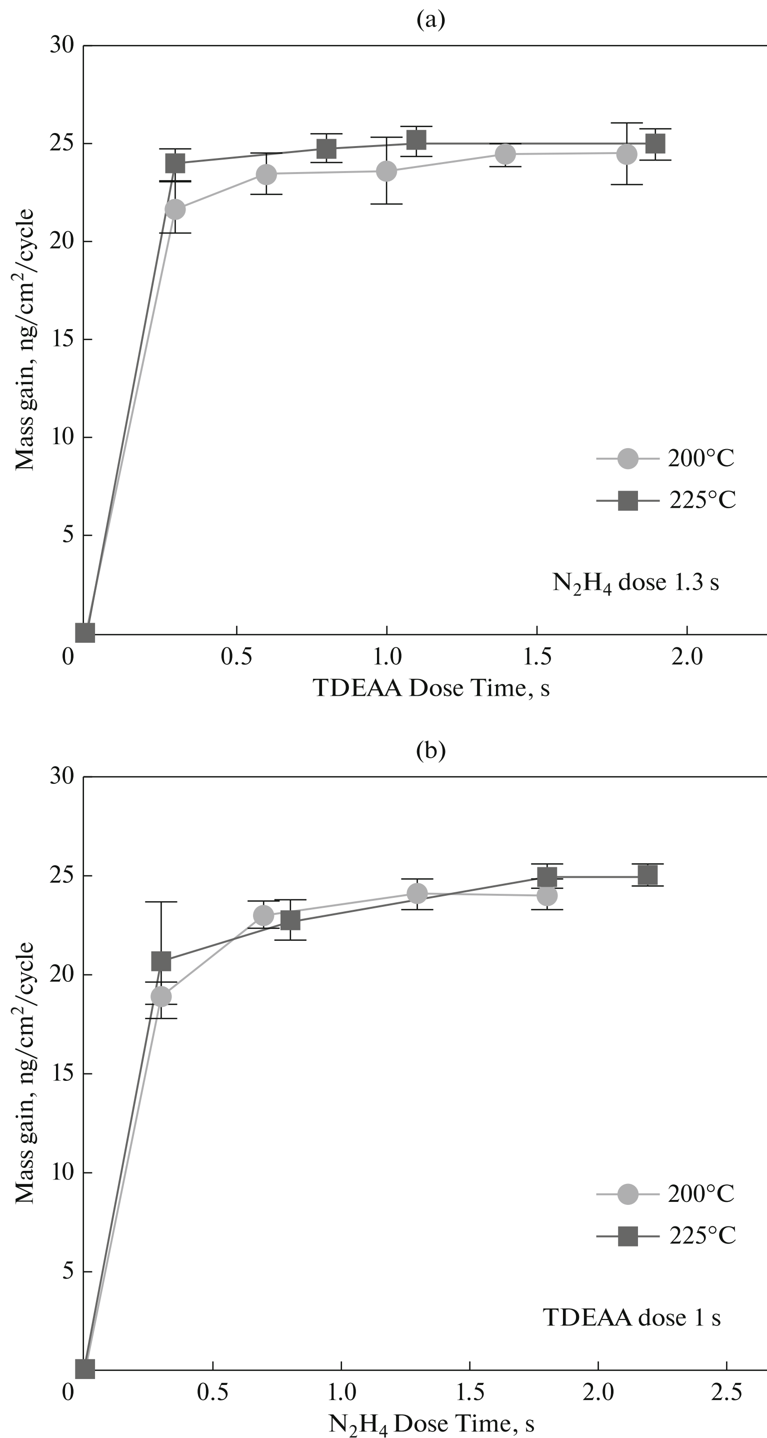

Fig. 4. QCM data on saturation of (a) TDEAA and (b) N_2H_4 during the ALD AlN at 200, and 225°C.

mass gain of 35.3 ng/cm^2, and the dosing of N_2H_4 to a mass loss of 12.1 ng/cm^2 with the resulting mass increase of 23.2 ng/cm^2 per cycle. The observed mass gain and loss during the dosing of TDEAA and N_2H_4 occur in accordance with the deposition mechanism shown in Fig. 1. The reaction of TDEAA proceeds effectively without surface recombinations that lead to mass loss after the dosing. The dip in Fig. 5b observed during the dose of N_2H_4 was attributed [48] to the overheated gas effect on the QCM crystal. Figure 5b shows good reproducibility of changes on the surface during the dosing of reagents. For all *ex situ* data pre-

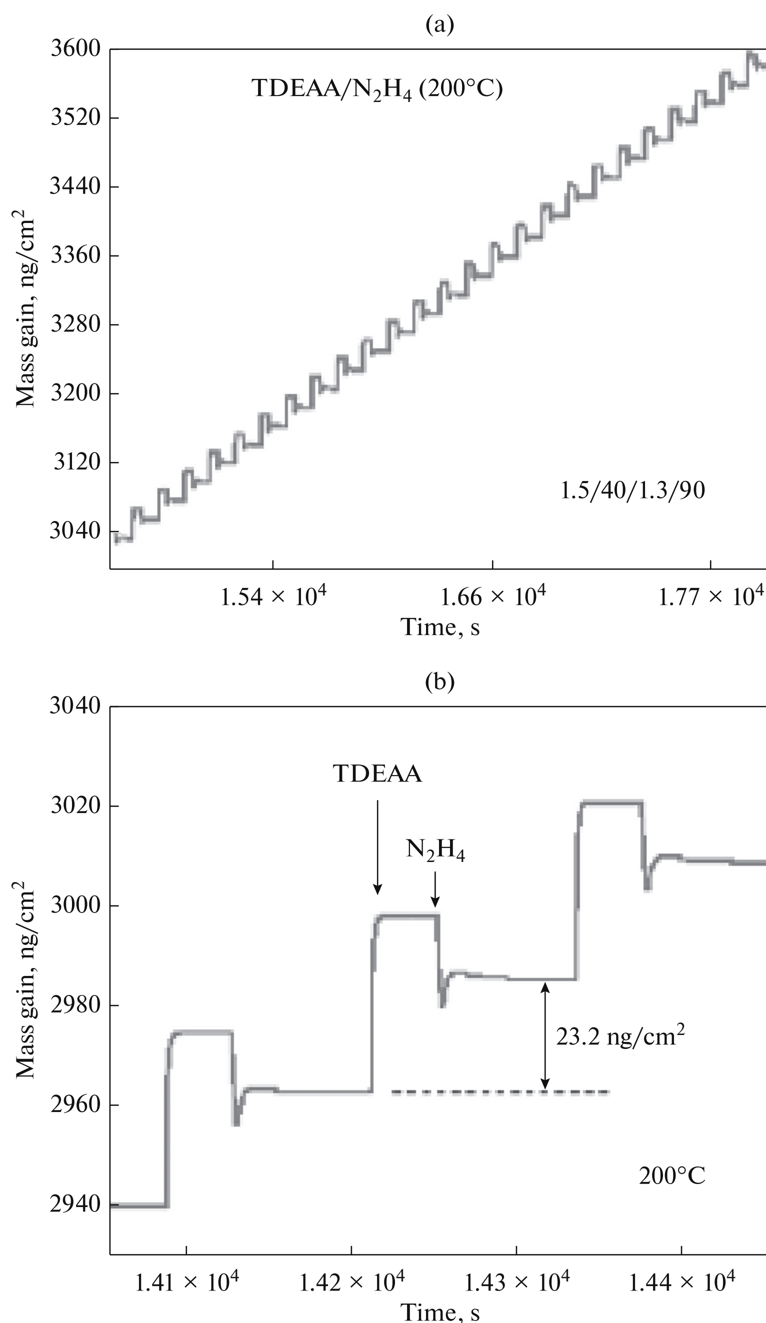

Fig. 5. QCM signal obtained at 200°C (a) during 25 ALD cycles of $TDEAA/N_2H_4$ and (b) zoom-in image of three ALD cycles of $TDEAA/N_2H_4$.

sented below, the ALD AlN was performed on condition of saturation for precursors.

XRR and XRD Analyses of ALD AlN Films

Figure 6 presents the XRR data for dependence of the growth rate of AlN film on silicon substrates on the deposition temperature varied from 150 to 280°C. One hundred A–B cycles were deposited on the substrates for each temperature. The dosing and purge time during ALD was 1.5/40/1.3/90 for $TDEAA/N_2H_4$ and 3.5/40/3/90 for $TDEAA/NH_3$. According to Fig. 6, in the case of NH_3, the growth rate gradually increases from 0.87 Å/cycle at 150°C to 1.47 Å/cycle at 225°C. The decrease in the growth rate above 225°C is associated with a reduction of the number of reactive surface sites. In this case, we think this is

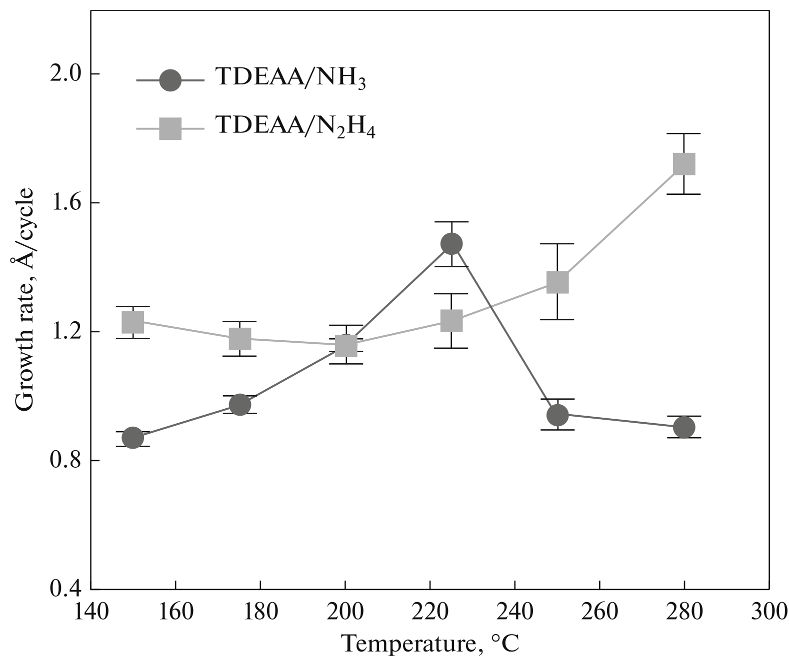

Fig. 6. XRR data on variation of the growth rate of AlN ALD films with temperature.

caused by the thermal decomposition of TDEAA. The similar organometallic precursors containing amido groups, namely, tetrakis(diethylamido)titanium ($Ti((C_2H_5)_2N)_4$) and tris(diethylamido)(*tert*-butylimido)tantalum ($(CH_3)_3CNTa(N(C_2H_5)_2)_3$), thermally decompose above 220°C [42, 44].

On the other hand, the rate of film deposition in the case of N_2H_4 at first decreased from 1.23 Å/cycle at 150°C to 1.16 Å/cycle at 200°C and then started to increase, reaching 1.72 Å/cycle at 280°C. The higher film deposition rate at 150°C is possibly related to the formation of multilayers of physisorbed molecules of N_2H_4 and/or stable adduct between the OM precursor and N_2H_4 [43]. The deposition rate also slightly increased during the ALD of TaN at 150°C with N_2H_4 used as a nitrogen precursor [42]. The increase in the deposition rate above 225°C observed for TDEAA/N_2H_4 may be associated with the decomposition of the OM precursor and, as a consequence, with film deposition by thermal CVD. Due to the presence of aluminum and nitrogen in the TDEAA molecule (Fig. 1), the thermal CVD of aluminum nitride can occur by decomposition without participation of the nitrogen precursor [47, 49]. The increased gradient of film thickness at higher temperatures is also indirect evidence for decomposition of TDEAA. Note that NH_3 and N_2H_4 thermally decompose at higher temperatures, ~800 and ~300°C, respectively [45, 47]. The observed considerable increase in the deposition rate at temperatures from 150 to 225°C for NH_3 indicates that the activation energy of surface reactions is higher than for N_2H_4. Therefore, we think the range of optimum ALD of AlN film with the use of TDEAA and N_2H_4 or NH_3 is between 200 and 225°C.

The linear growth of the ALD AlN films on silicon with increase in number of A–B cycles is presented in Fig. 7. The films were deposited at 200°C and reagent dosing times of 1.5/40/1.3/90 for the TDEAA/N_2H_4 system and 3.5/40/3/90 for TDEAA/NH_3 have been used. According to Fig. 7, as the number of cycles increases, the thickness of the deposited nitride film also increases linearly, with the growth rates being approximately equal for these systems (~1.1 Å/cycle). The films grow at a submonolayer rate if we take into account that the AlN monolayer thickness is ~2.5 Å [50]. The data of Fig. 7 confirm the observed by in situ QCM linear growth of the TDEAA/N_2H_4 film (Fig. 5a). In this case, the nucleation period of film growth on the native SiO_2 layer of the substrate is short for both systems. A relatively short film nucleation period of 5–10 cycles was also observed by QCM on the ALD Al_2O_3 film.

According to [40, 50] the thermal ALD of AlN film was performed using TDMAA and NH_3 at 200°C at a rate of 0.7–0.9 Å/cycle. The ALD of AlN was generally [22, 25, 26, 28] performed with TMA and NH_3 at temperatures from 320 to 470°C at deposition rates of 0.2–3.5 Å/cycle. Several studies [23, 29, 51], however, indicated that the ALD of AlN using trimethylaluminum and ammonia was possible only at temperatures of ≤327°C. The growth rate of AlN films deposited at 500°C using $AlCl_3$ and NH_3 is 1.0 Å/cycle [27, 28]. The films obtained by PE-ALD using TDMAA/N_2

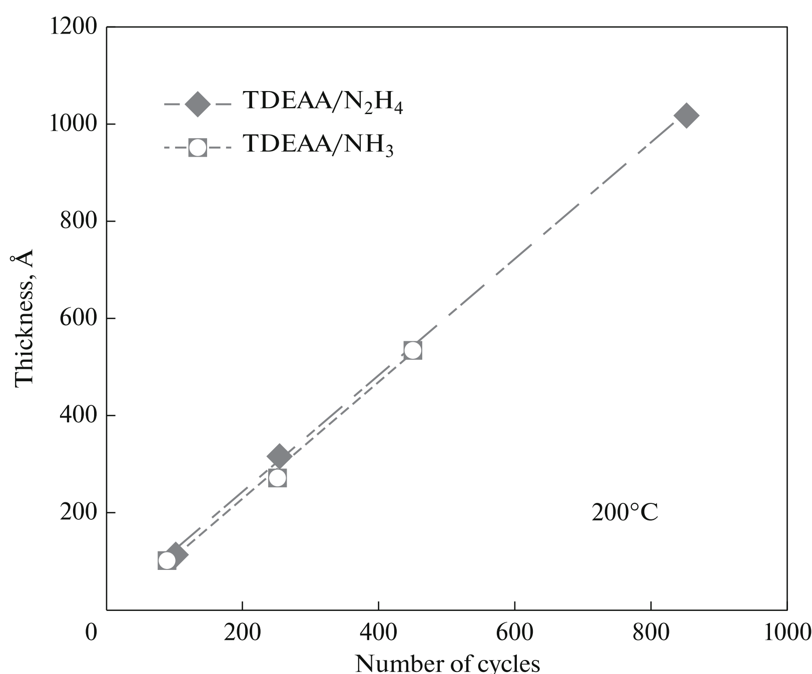

Fig. 7. XRR data on the linear growth of aluminum nitride films on silicon substrates for different numbers of ALD cycles.

[52] at 250°C were deposited at a rate of ~0.8 Å/cycle. The growth rates of PE-ALD AlN at 200°C using TMA and NH_3 [34, 35, 53, 54] were 0.9–1.02 Å/cycle; when using TMA and the N_2/H_2, $N_2/H_2/Ar$, N_2/Ar, NH_3/Ar, N_2 mixtures, the films grew at rates of 0.61–1.2 Å/cycle [34, 36, 53, 55, 56]. The PE-ALD AlN films sputtered at 350°C using $AlCl_3$ and $NH_3/Ar/H_2$ or NH_3/H_2 were deposited at a rate of ~0.4 Å/cycle [31, 32]. In our case, the film growth rates are higher than those published previously for thermal ALD of AlN at the same temperatures and close to the data obtained by PE-ALD of AlN at both low and high temperatures.

The densities and roughnesses of the obtained ALD AlN coatings were determined by XRR. The films synthesized at 200°C had densities on the average of 2.36 and 2.22 g/m^3 for processes with N_2H_4 and NH_3, respectively, which is 72.4 and 68% of the bulk density of aluminum nitride (3.26 g/cm^3) [57]. The densities of the films obtained at 225°C were slightly higher, ~2.41 g/m^3 (74%) and 2.25 g/m^3 (69%) for systems with N_2H_4 and NH_3, respectively. The mass gains per cycle at 200°C for ALD TDEAA/N_2H_4 recalculated from the XRR data on the density and deposition rate of the films (26 ng/(cm^2 cycle)) agree well with the experimental QCM data shown in Fig. 4 (~24.5 ng/(cm^2 cycle)). The high density of the films obtained using N_2H_4 compared with that for NH_3 must favor high stability against the oxidation in air. The (mean square) roughness of the AlN films obtained at 200 and 225°C varied from 1.5 to 9 Å depending on the film thickness.

The literature densities and roughnesses for ALD AlN films are mainly available for the films obtained by the plasma-chemical method. The density of the layers obtained by PE-ALD of AlN at 200°C using TMA and NH_3 was 2.56–2.58 g/cm^3 and the roughness was ~14 Å [53, 54]; for the layers obtained using TMA and NH_3/Ar, N_2/H_2, $N_2/H_2/Ar$, N_2 the density was 1.9–2.82 g/cm^3 and the roughness varied from 14.5 to 21.6 Å [34, 53, 56]. The AlN films obtained by ALD using TDEAA/N_2H_4 are slightly worse in density than the PE-ALD films, but had lower roughness because they are amorphous according to XRD analysis. The amorphous AlN films were obtained at 200°C by ALD and CVD using TDMAA and NH_3 [13, 16, 41, 58]. At the same time, the AlN films obtained by CVD and thermal and plasma-chemical ALD at temperatures of ≥300°C generally had a polycrystalline structure [16, 22, 26, 28, 32, 41]. The AlN films obtained by PE-ALD at relatively low temperatures of 100–250°C using TMA and N_2/H_2 or NH_3 were mixtures of polycrystalline and amorphous phases [33–36, 38]. The formation of amorphous aluminum nitride films at low temperatures was attributed [56] to the presence of certain impurities.

XPS and FRES Analyses of ALD AlN Films

Figure 8 shows the results of the XPS analysis of the nitride film with a thickness of 300 Å obtained using

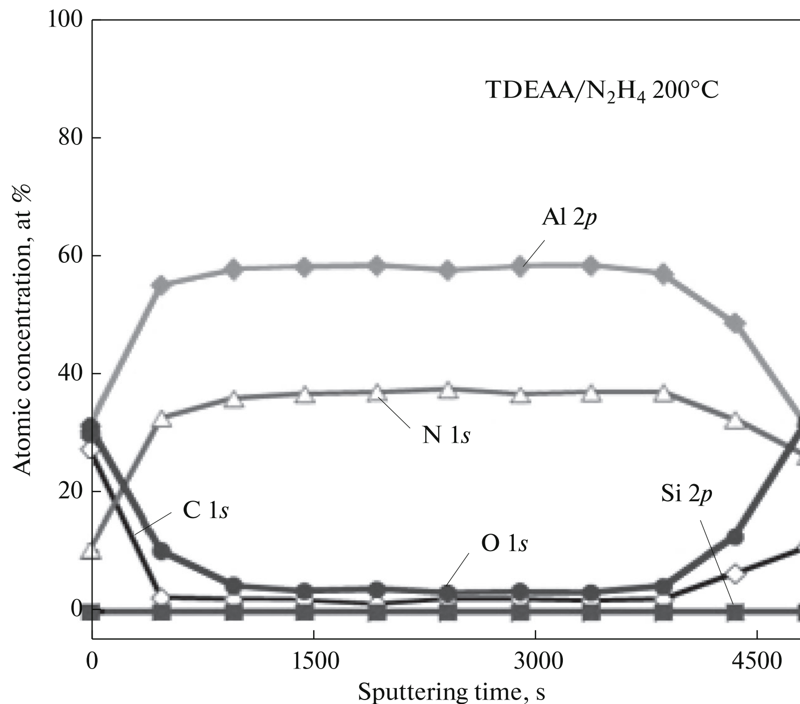

Fig. 8. XPS data on the atomic distribution in the bulk of the AlN ALD film obtained using hydrazine at 200°C.

ALD TDEAA/N_2H_4 at 200°C. The upper layer of nitride contains oxygen and carbon impurities. It's know [28], that the substrates with an aluminum nitride coating are oxidize in air, forming a passivation alumina film. Carbon on the film surface is gets deposited from air during the transfer of the sample from the ALD reactor into the XPS chamber. After etching of the film surface with argon ions, the oxygen and content decreases significantly. The oxygen and carbon carbon content in the bulk of the film is ~3.2 and 1.4 at %, respectively. The presence of oxygen in the bulk of the film explained by its presence in the form of an impurity in the dosed N_2H_4; in addition, it's known, that the hydrazine is hygroscopic [45]. The presence of carbon in the bulk of the film indicates that the surface processes are not ideal. The presence of a carbon impurity can affect the dielectric properties of the AlN film [59]. The absence of significant carbon impurities in our films suggests that reaction B (Fig. 2) at dosing of N_2H_4 proceeds close to completion.

The level of oxygen and carbon impurities in our (ALD) films synthesized using TDEAA and N_2H_4 is comparable or lower to that of the AlN films obtained by ALD and PE-ALD by other authors [13, 16]. According to [41], the AlN films obtained by ALD using TDMAA and NH_3 at 200°C contains ~6.5 at % oxygen and ~1.5 at % carbon. The CVD of AlN films at 200°C using TDMAA and NH_3 leads to the following impurity contents: ≤5 at % oxygen and ≤2.95 at % carbon [13, 16]. Using TMA and NH_3, one can obtain ALD AlN films at 330–450°C with 0.8–2.5 at % oxygen and ≤7 at % carbon impurities [22, 25]. The ALD AlN layers deposited at 500°C using $AlCl_3$ and NH_3 contain 6 at % chlorine impurities and a certain amount of oxygen [28]. The AlN films obtained PS-ALD at 150–200°C contain 0.07–3.0 at % oxygen and ≤2.5 at % carbon when TMA and NH_3 are used [33, 34, 37, 54] and 0.14–6.0 at % oxygen and ≤4 at % carbon when a combination with NH_3/Ar, N_2/H_2, N_2/H_2/Ar is used [34, 37, 53, 56]. Note that the PE-ALD AlN films obtained using TMA and N_2 plasma are unstable in air, the oxygen and carbon contents in them reaching 39–48.45 and 4–8 at %, respectively [53, 60]. In PE-ALD of AlN using $AlCl_3$ and a gas mixture of NH_3/H_2 [31] or NH_3/Ar/H_2 [32], however, the chlorine level is low, 0.21–0.23 at %.

According to Fig. 8, the ratio of N to Al atomic concentrations in the bulk of the films is 0.6. There is enough evidence [61, 62] for the preferential reactive removal of light elements by Ar^+ ions during the XPS analysis. In our case, the decreased nitrogen level is possibly explained by the removal of NH_3 and its derivatives. For more precise determination of the N to Al ratio, we analyzed the films by RBS. Figure 9 shows the RBS spectrum of the ALD AlN films with a thickness of 382 Å grown at 200°C by alternating doses of TDEAA and N_2H_4. The processing of the results showed that the N/Al concentration ratio is ~1.3. This value is close to the data of [16, 53] for CVD and PE-ALD of AlN films obtained at 200°C using TDEAA

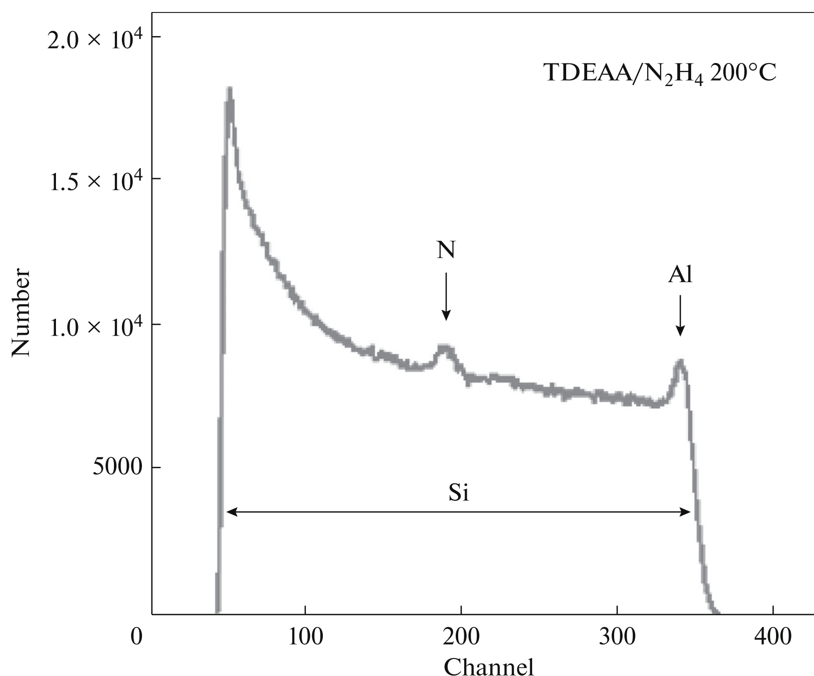

Fig. 9. RBS data obtained for the AlN ALD film grown using hydrazine at 200°C.

and NH_3, where the N/Al ratio was 1.15 and 1.1–1.2, respectively. Earlier, it was assumed that the nitrogen excess in the film could be in the form of (N–N) bonds [16, 63].

Hydrogen is one of the most frequent impurities in AlN films grown by thermal and plasma-stimulated ALD. In the present study, the content of hydrogen atoms in the films was determined by forward recoil elastic spectrometry (FRES). Figure 10 presents the FRES spectra of the ALD films of aluminum nitrides with thicknesses of 980 and 550 Å obtained at 200°C using N_2H_4 and NH_3, respectively. An analysis of the samples shows that hydrogen in the films is at the level of 22.7 and 26 at % for systems with N_2H_4 and NH_3, respectively. This indicates that the reaction of TDEAA with the surface (–NH_x) groups (reaction A, Fig. 2) is possibly incomplete, which may be the reason for the presence of hydrogen impurities.

The hydrogen concentrations in the films obtained in this work are slightly lower than in the films grown at 200°C using TDMAA/NH_3 by ALD (30 at %) [41] and CVD (11–31 at %) [13, 16]. The films obtained by ALD AlN at 350 and 500°C using NH_3 and TMA or $AlCl_3$ contain ~9–15 and 9 at % hydrogen, respectively [22, 28]. It is interesting that the hydrogen content in some PE-ALD AlN films obtained at 200°C using TMA and NH_3 is high enough, 20–21 at % [53, 54]; for N_2/H_2, it is 19–22 at % [53, 56]. In PE-ALD of AlN films obtained using $AlCl_3$ and the NH_3/H_2 [27] or $NH_3/Ar/H_2$ [32] gas mixtures at 350°C, the hydrogen content was low, 2.01 at %. It should be taken into account, however, that the deposition of films with hydrogen plasma and hydrogen mixtures can lead to gas diffusion into the substrate and modification of its surface [64], therefore, requires special control [32]. An increase in deposition temperature of AlN generally leads to a decrease in the hydrogen content in the synthesized films [41, 54]. In our case, the films obtained at a higher deposition temperature 225°C using ALD TDMAA and N_2H_4 or NH_3 should also contain less hydrogen impurities. An analysis shows that the hydrogen level in our samples (obtained at the same temperatures) is comparable to the literature data given above, but higher than for the films obtained by high-temperature PE-ALD.

Thus, hydrogen may be present in the films in the form of amino (–NH_2) or imide (–NH) groups and tetra-coordinated amino groups [63, 65, 66]. The excess of nitrogen and the presence of hydrogen impurities also suggest possible formation of stable complexes (adducts) between the OM precursor and NH_3 or N_2H_4 [43, 47, 63]. For effective decomposition of nitrogen–hydrogen bonds in AlN films, it was shown [24] that the deposition temperature should not be lower than 330°C. To refine the mechanism of the surface reactions that are specific for the systems considered, additional studies by infrared spectroscopy are required.

The amount of hydrogen can be reduced by annealing the films in an inert gas atmosphere [16] or vacuum [56] at 550–650°C or by treatment in nitrogen

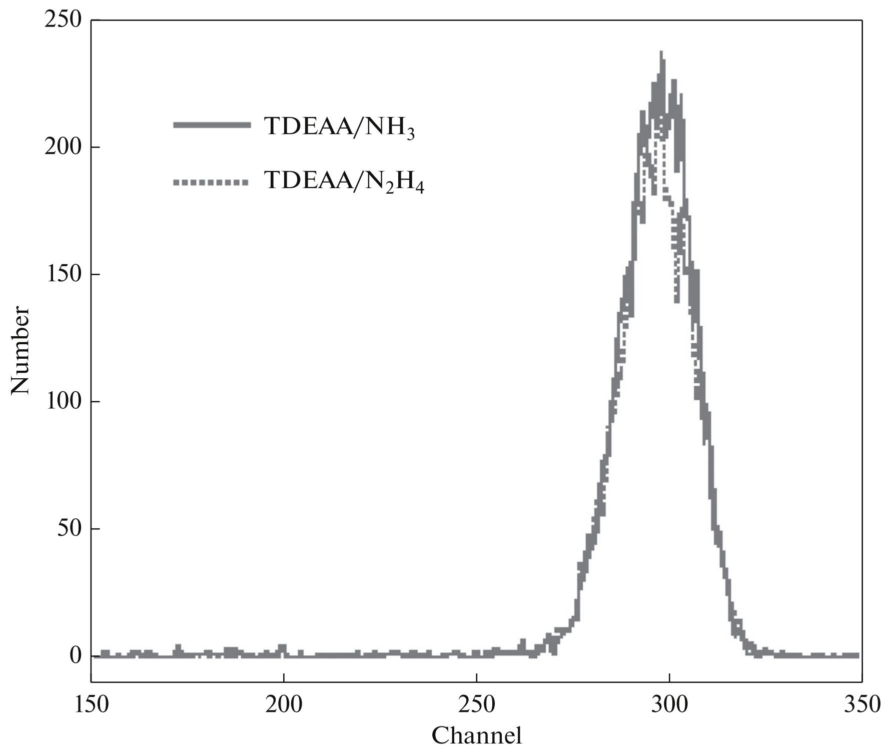

Fig. 10. FRES spectrum for AlN ALD samples deposited using ammonia and hydrazine at 200°C.

plasma at ~400°C [67] or argon plasma at 300°C [68]. The thermal and plasma treatments of the film should lead to increase in density and improved chemical stability, in particular, to its stability against oxidation in air [67]. We observed [50] a significant decrease in hydrogen concentration in ALD AlN films obtained using TDMAA and NH_3 after annealing in a nitrogen atmosphere for 1 h at 650°C. The films obtained in the present study were not annealed. Even with high hydrogen contents, the films obtained in this study can find potential application in microelectronics [16, 40, 66].

CONCLUSIONS

The results of the experimental studies showed that the films with an approximate composition AlNH and with some hydrogen and carbon impurities can be obtained by ALD using TDEAA and N_2H_4 or NH_3 with relatively high deposition rates and at relatively low temperatures. At the same time, hydrazine has more favorable surface reactivity with TDEAA, which leads to increased density of the films, all other conditions being equal. Level of impurities, density, and roughness, of our films are comparable to and occasionally exceed the AlN film samples obtained by other thermal and plasma-stimulated ALD processes. The oxygen content in the films obtained from TDEAA and N_2H_4 can be reduced by using hydrazine with higher than 98% purity. The AlN films obtained in this work have a relatively high level of hydrogen impurities, which is a problem for many ALD AlN systems. This problem can be solved by using high-temperature annealing of the samples which can help to preserve exclusive homogeneity of the resulting layer inherent only to thermal ALD. The precursors and deposition conditions of AlN films used in this work can be considered an alternative path to the conventional plasma or high-temperature methods.

REFERENCES

1. Slack, G.A., et al., The intrinsic thermal-conductivity of AlN, *J. Phys. Chem. Solids,* 1987, vol. 48, no. 7, pp. 641–647.
2. Goldberg, Y., *Properties of Advanced Semiconductor Materials: GaN, AlN, InN, BN, SiC, SiGe,* Levinshtein, M.E., Rumyantsev, S.L., and Shur, M.S., New York: Wiley, 2001.
3. Meng, W.J., *Properties of Group III Nitrides,* No. 11 of *EMIS Datareviews Series,* London: Edgar J.H., 1994.
4. Aita, C.R., Kubiak, C.J.G., and Shih, F.Y.H., Optical behavior near the fundamental absorption-edge of sputter-deposited microcrystalline aluminum nitride, *J. Appl. Phys.,* 1989, vol. 66, no. 9, pp. 4360–4363.
5. Edwards, J. et al., Space charge conduction and electrical behaviour of aluminium nitride single crystals, *Solid State Commun.,* 1965, vol. 3, no. 5, pp. 99–100.
6. Usman, M. et al., Toward the understanding of stacked Al-based high-k dielectrics for passivation of 4H-SiC

devices, *J. Electrochem. Soc.,* 2011, vol. 158, no. 1, pp. H75–H79.

7. Bosund, M. et al., GaAs surface passivation by plasma-enhanced atomic-layer-deposited aluminum nitride, *Appl. Surf. Sci.,* 2010, vol. 256, no. 24, pp. 7434–7437.
8. Kueck, D. et al., AlN as passivation for surface channel FETs on H-terminated diamond, *Diamond Relat. Mater.,* 2010, vol. 19, nos. 7–9, pp. 932–935.
9. Luc, Q.H. et al., Plasma enhanced atomic layer deposition passivated $HfO_2/AlN/In_{0.53}Ga_{0.47}As$ MOSCAPs with sub-nanometer equivalent oxide thickness and low interface trap density, *IEEE Electron Dev. Lett.,* 2015, vol. 36, no. 12, pp. 1277–1280.
10. Aissa, K.A. et al., AlN films deposited by dc magnetron sputtering and high power impulse magnetron sputtering for SAW applications, *J. Phys. D: Appl. Phys.,* 2015, vol. 48, no. 14.
11. Yusoff, M.Z.M. et al., Plasma-assisted MBE growth of AlN/GaN/AlN heterostructures on Si(111) substrate, *Superlatt. Microstruct.,* 2013, vol. 60, pp. 500–507.
12. Brubaker, M.D. et al., Effect of AlN buffer layer properties on the morphology and polarity of GaN nanowires grown by molecular beam epitaxy, *J. Appl. Phys.,* 2011, vol. 110, no. 5.
13. Hoffman, D.M. et al., Chemical vapor deposition of aluminum and gallium nitride thin films from metalorganic precursors, *J. Vacuum Sci. Technol. A,* 1996, vol. 14, no. 2, pp. 306–311.
14. Khan, M.A. et al., Low-pressure metalorganic chemical vapor-deposition of AlN over sapphire substrates, *Appl. Phys. Lett.,* 1992, vol. 61, no. 21, pp. 2539–2541.
15. Interrante, L.V. et al., Preparation and properties of aluminum nitride films using an organometallic precursor, *J. Electrochem. Soc.,* 1989, vol. 136, no. 2, pp. 472–478.
16. Gordon, R.G., Riaz, U., and Hoffman, D.M., Chemical vapor-deposition of aluminum nitride thin-films, *J. Mater. Res.,* 1992, vol. 7, no. 7, pp. 1679–1684.
17. Fathimulla, A. and Lakhani, A.A., Reactively Rf magnetron sputtered ain films as gate dielectric, *J. Appl. Phys.,* 1983, vol. 54, no. 8, pp. 4586–4589.
18. Mirpuri, C. et al., Low-temperature plasma-assisted growth of optically transparent, highly oriented nanocrystalline AlN, *J. Appl. Phys.,* 2007, vol. 101, no. 2.
19. Rosenberger, L. et al., XPS analysis of aluminum nitride films deposited by plasma source molecular beam epitaxy, *Surf. Interface Anal.,* 2008, vol. 40, no. 9, pp. 1254–1261.
20. Gacevic, Z. et al., Internal quantum efficiency of III-nitride quantum dot superlattices grown by plasma-assisted molecular-beam epitaxy, *J. Appl. Phys.,* 2011, vol. 109, no. 10.
21. George, S.M., Atomic layer deposition: an overview, *Chem. Rev.,* 2010, vol. 110, no. 1, pp. 111–131.
22. Ruhela, D. et al., Low temperature deposition of AlN films by an alternate supply of trimethyl aluminum and ammonia, *Chem. Vapor Deposit.,* 1996, vol. 2, no. 6, pp. 277–283.
23. Mayer, T.M., Rogers, J.W., and Michalske, T.A., Mechanism of nucleation and atomic layer growth of AlN on Si, *Chem. Mater.,* 1991, vol. 3, no. 4, pp. 641–646.
24. Liu, H., Bertolet, D.C., and Rogers, J.W., Reactions of trimethylaluminum and ammonia on alumina at 600-K, surface chemical aspects of AlN thin-film growth, *Surf. Sci.,* 1995, vol. 340, nos. 1–2, pp. 88–100.
25. Bui, H.V. et al., Self-limiting growth and thickness- and temperature-dependence of optical constants of ALD AlN thin films, *ECS J. Solid State Sci. Technol.,* 2014, vol. 3, no. 4, pp. P101–P106.
26. Liu, X.Y. et al., Atomic layer deposition of aluminum nitride thin films from trimethyl aluminum (TMA) and ammonia, in *Integration of Advanced Micro- and Nanoeletronic Devices—Critical Issues and Solutions, Proceedings of the Symposia, San Francisco, CA, April 13–16, 2004, MRS Symp. Proc.,* 2004, vol. 811, pp. 11–16.
27. Elers, K.E. et al., Atomic layer epitaxy growth of AlN thin-films, *J. Phys. IV,* 1995, vol. 5, no. C5, pp. 1021–1027.
28. Jokinen, J. et al., Analysis of AlN thin films by combining TOF-ERDA and NRB techniques, *Thin Solid Films,* 1996, vol. 289, nos. 1–2, pp. 159–165.
29. Puurunen, R.L. et al., Successive reactions of gaseous trimethylaluminium and ammonia on porous alumina, *Phys. Chem. Chem. Phys.,* 2001, vol. 3, no. 6, pp. 1093–1102.
30. Alevli, M., Ozgit, C., and Donmez, I., The influence of growth temperature on the properties of AlN films grown by atomic layer deposition, *Acta Phys. Polon. A,* 2011, vol. 120, no. 6A, pp. A58–A60.
31. Lee, Y.J. and Kang, S.W., Growth of aluminum nitride thin films prepared by plasma-enhanced atomic layer deposition, *Thin Solid Films,* 2004, vol. 446, no. 2, pp. 227–231.
32. Lee, Y.J., Formation of aluminum nitride thin films as gate dielectrics on Si(100), *J. Cryst. Growth,* 2004, vol. 266, no. 4, pp. 568–572.
33. Ozgit, C. et al., Self-limiting low-temperature growth of crystalline AlN thin films by plasma-enhanced atomic layer deposition, *Thin Solid Films,* 2012, vol. 520, no. 7, pp. 2750–2755.
34. Ozgit-Akgun, C. et al., Hollow cathode plasma-assisted atomic layer deposition of crystalline AlN, GaN and $Al_xGa_{1-x}N$ thin films at low temperatures, *J. Mater. Chem. C,* 2014, vol. 2, no. 12, pp. 2123–2136.
35. Alevli, M. et al., Structural properties of AlN films deposited by plasma-enhanced atomic layer deposition at different growth temperatures, *Phys. Status Solidi A,* 2012, vol. 209, no. 2, pp. 266–271.
36. Goerke, S. et al., Atomic layer deposition of AlN for thin membranes using trimethylaluminum and H-2/N-2 plasma, *Appl. Surf. Sci.,* 2015, vol. 338, pp. 35–41.
37. Alevli, M., et al., The influence of N-2/H-2 and ammonia N source materials on optical and structural properties of AlN films grown by plasma enhanced atomic layer deposition, *J. Cryst. Growth,* 2011, vol. 335, no. 1, pp. 51–57.
38. Motamedi, P. and Cadien, K., Structural and optical characterization of low-temperature ALD crystalline AlN, *J. Cryst. Growth,* 2015, vol. 421, pp. 45–52.

39. Profijt, H.B. et al., Plasma-assisted atomic layer deposition: basics, opportunities, and challenges, *J. Vacuum Sci. Technol. A,* 2011, vol. 29, no. 5.

40. Kim, K.H. et al., Atomic layer deposition of insulating nitride interfacial layers for germanium metal oxide semiconductor field effect transistors with high-kappa oxide/tungsten nitride gate stacks, *Appl. Phys. Lett.,* 2007, vol. 90, no. 21.

41. Liu, G. et al., Atomic layer deposition of AlN with tris(dimethylamido)aluminum and NH_3, in *Proceedings of the 7th Symposium on Atomic Layer Deposition Applications, Boston, MA, Oct. 10–12, 2011, ECS Trans.,* 2011, vol. 41, no. 2, pp. 219–225.

42. Burton, B.B., Lavoie, A.R., and George, S.M., Tantalum nitride atomic layer deposition using (*tert*-butylimido) tris(diethylamido) tantalum and hydrazine, *J. Electrochem. Soc.,* 2008, vol. 155, no. 7, pp. D508–D516.

43. Gaskill, D.K., Bottka, N., and Lin, M.C., OMVPE of GaN and AlN films by metal alkyls and hydrazine, *J. Cryst. Growth,* 1986, vol. 77, nos. 1–3, pp. 418–423.

44. Yun, J.Y., Park, M.Y., and Rhee, S.W., Comparison of tetrakis(dimethylamido)titanium and tetrakis(diethylamido)titanium as precursors for metallorganic chemical vapor deposition of titanium nitride, *J. Electrochem. Soc.,* 1999, vol. 146, no. 5, pp. 1804–1808.

45. Schmidt, E.W., *Hydrazine and Its Derivatives, Preparation, Properties, Applications,* New York: Wiley, 2001.

46. Elam, J.W., Groner, M.D., and George, S.M., Viscous flow reactor with quartz crystal microbalance for thin film growth by atomic layer deposition, *Rev. Sci. Instrum.,* 2002, vol. 73, no. 8, pp. 2981–2987.

47. Neumayer, D.A. and Ekerdt, J.G., Growth of group III nitrides. A review of precursors and techniques, *Chem. Mater.,* 1996, vol. 8, no. 1, p. 9–25.

48. Rocklein, M.N. and George, S.M., Temperature-induced apparent mass changes observed during quartz crystal microbalance measurements of atomic layer deposition, *Anal. Chem.,* 2003, vol. 75, no. 19, pp. 4975–4982.

49. Takahashi, Y. et al., Low-temperature deposition of a refractory aluminum compound by the thermal-decomposition of aluminum dialkylamides, *Surf. Sci.,* 1979, vol. 86, pp. 238–245.

50. Holtz, M. et al., Preparation of optoelectronic devices based on AlN/AlGaN superlattices, in *Progress in Semiconductors II, Electronic and Optoelectronic Applications, MRS Symp. Proc.,* 2003, vol. 744, pp. 621–626.

51. Bertolet, D.C., Liu, H., and Rogers, J.W., Mechanistics of early-stage growth of AlN on Alumina. 2. TmAl and NH_3, *Chem. Mater.,* 1993, vol. 5, no. 12, pp. 1814–1818.

52. Buttera, S.C., Mandia, D.J., and Barry, S.T., Tris(dimethylamido) aluminum(III): an overlooked atomic layer deposition precursor, *J. Vacuum Sci. Technol. A,* 2017, vol. 35, no. 1.

53. Perros, A.P. et al., Influence of plasma chemistry on impurity incorporation in AlN prepared by plasma enhanced atomic layer deposition, *J. Phys. D: Appl. Phys.,* 2013, vol. 46, no. 50.

54. Bosund, M. et al., Properties of AlN grown by plasma enhanced atomic layer deposition, *Appl. Surf. Sci.,* 2011, vol. 257, no. 17, pp. 7827–7830.

55. Kim, K.H., Kwak, N.W., and Lee, S.H., Fabrication and properties of AlN film on GaN substrate by using remote plasma atomic layer deposition method, *Electron. Mater. Lett.,* 2009, vol. 5, no. 2, pp. 83–86.

56. Broas, M. et al., Structural and chemical analysis of annealed plasma-enhanced atomic layer deposition aluminum nitride films, *J. Vacuum Sci. Technol. A,* 2016, vol. 34, no. 4.

57. *The CRC Handbook of Chemistry and Physics,* Lide, D.R., Ed., 88th ed., Gaithersburg, MD: Natl. Inst. Standards Technol., 2007, p. 2640.

58. Abdulagatov, A.I. et al., Atomic layer deposition of AlN and AlON with tris(dimethylamido)aluminum, NH_3 and H_2O, 2017, in preparation.

59. Nepal, N. et al., Epitaxial growth of AlN films via plasma-assisted atomic layer epitaxy, *Appl. Phys. Lett.,* 2013, vol. 103, no. 8.

60. Ozgit-Akgun, C., Donmez, I., and Biyikli, N., Plasma-enhanced atomic layer deposition of III-nitride thin films, in *Proceedings of the 9th Symposium on Atomic Layer Deposition Applications, ECS Trans.,* 2013, vol. 58, no. 10, pp. 289–297.

61. Kelly, R., Attempt to understand preferential sputtering, *Nucl. Instrum. Methods Phys. Res.,* 1978, vol. 149, nos. 1–3, pp. 553–558.

62. Sigmund, P., Mechanisms and theory of physical sputtering by particle impact, *Nucl. Instrum. Methods Phys. Res. B,* 1987, vol. 27, no. 1, pp. 1–20.

63. Liu, H.N., Bertolet, D.C., and Rogers, J.W., The surface-chemistry of aluminum nitride MOCVD on alumina using trimethylaluminum and ammonia as precursors, *Surf. Sci.,* 1994, vol. 320, nos. 1–2, pp. 145–160.

64. Fonash, S.J., An overview of dry etching damage and contamination effects, *J. Electrochem. Soc.,* 1990, vol. 137, no. 12, pp. 3885–3892.

65. Soto, C., Boiadjiev, V., and Tysoe, W.T., Spectroscopic study of AlN film formation by the sequential reaction of ammonia and trimethylaluminum on alumina, *Chem. Mater.,* 1996, vol. 8, no. 9, pp. 2359–2365.

66. Hoffman, D.M., Chemical-vapor-deposition of nitride thin-films, *Polyhedron,* 1994, vol. 13, no. 8, pp. 1169–1179.

67. Cho, M.H. et al., Enhancement of the chemical stability of hydrogenated aluminum nitride thin films by nitrogen plasma treatment, *Electrochem. Solid State Lett.,* 2001, vol. 4, no. 2, pp. F7–F9.

68. Shih, H.Y. et al., Low-temperature atomic layer epitaxy of AlN ultrathin films by layer-by-layer, in-situ atomic layer annealing, *Sci. Rep.,* 2017, vol. 7, p. 39717.

Translated by L. Smolina

5 AlN thin films deposited by thermal ALD using Hydrazinium Chloride and Triisobutylaluminum as precursors

5.1 Motivation of the article

Despite generally positive results described in the previous article (Chapter 4), it was decided that the search for optimal precursors for deposition of AlN must continue. The reasoning behind this is that despite its decent reactivity, hydrazine as a precursor, unfortunately, also has a number of disadvantages. Due to its flammable nature, the usage of hydrazine poses certain difficulties during transportation and immediate handling, it is also a relatively costly compound. All of these issues on the other hand are completely solved by replacing hydrazine with its salt - hydrazine chloride (N_2H_5Cl). Hydrazine chloride is widely available chemical compound, it is cheap and its usage does not require as much precaution as that of hydrazine. In terms of reactivity, however, N_2H_5Cl is expected to yield results similar to those of hydrazine, as it dissociates in the chamber into hydrazine and HCl. Thus, this reasoning constitutes the motivation of the following research.

5.2 Conclusion on the article

As a result of this study it was established that hydrazine chloride is a viable nitrogen precursor in AlN ALD process. The XPS and SIMS analysis of the obtained films confirmed the presence of Al-N bonds. Another positive aspect lies in the fact that despite expectation, no amount of chlorine impurities was detected by either of methods. This unambiguously proves that chlorine is removed from the chamber during the purge stage in the form of HCl. Furthermore, a solution to oxidization was proposed which implies high-temperature annealing in nitrogen atmosphere. After such procedure, chemical composition of AlN layers was significantly improved. Unfortunately, at the period of writing this paper there was no option to quantify hydrogen impurities within the obtained films. Nonetheless, since upon entering the chamber hydrazine chloride decomposes into hydrazine, we can speculate that the amount of hydrogen should be of similar values as reported in Chapter 4.

5.3 Contribution

I conducted all the measurements and wrote the entirety of the manuscript. The co-authors contribution lies in providing resources, help with the visualisation and annealing, as well as making minor corrections and giving valuable advice throughout the study.

5.4 Article 3

The paper **Aluminum Nitride Nanofilms by Atomic Layer Deposition Using Alternative Precursors Hydrazinium Chloride and Triisobutylaluminum** was published in the **Coating** journal (2079-6412; IF: 2.436) in the year of 2020. This is an Open Access paper.

coatings

MDPI

Article

Aluminum Nitride Nanofilms by Atomic Layer Deposition Using Alternative Precursors Hydrazinium Chloride and Triisobutylaluminum

Rashid Dallaev [1,*], Dinara Sobola [1,2], Pavel Tofel [1], Ľubomir Škvarenina [1] and Petr Sedlák [1,2]

[1] The Faculty of Electrical Engineering and Communication, Brno University of Technology, Technická 3058/10, 616 00 Brno, Czech Republic; sobola@vutbr.cz (D.S.); tofel@feec.vutbr.cz (P.T.); xskvar01@stud.feec.vutbr.cz (Ľ.Š.); sedlakp@feec.vutbr.cz (P.S.)

[2] Central European Institute of Technology, Purkyňova 123, 61600 Brno, Czech Republic

* Correspondence: xdalla03@vutbr.cz

Received: 13 September 2020; Accepted: 30 September 2020; Published: 3 October 2020

Abstract: The aim of this study is motivated by the pursuit to investigate the performance of new and as yet untested precursors such as hydrazinium chloride (N_2H_5Cl) and triisobutylaluminum $Al(C_4H_9)_3$ in the AlN atomic layer deposition (ALD) process as well as to study effects of successive annealing on the quality of the resulting layer. Both precursors are significantly cheaper than their conventional counterparts while also being widely available and can boast easy handling. Furthermore, $Al(C_4H_9)_3$ being a rather large molecule might promote steric hindrance and prevent formation of undesired hydrogen bonds. Chemical analysis is provided by X-ray photoelectron spectroscopy (XPS) and secondary-ion mass spectrometry (SIMS) techniques; surface morphology was studied using atomic force microscopy (AFM). Chlorine containing precursors such as $AlCl_3$ are usually avoided in ALD process due to the risk of chamber contamination. However, experimental data of this study demonstrated that the use of N_2H_5Cl does not result in chlorine contamination due to the fact that temperature needed for HCl molecules to become reactive cannot be reached within the AlN ALD window (200–350 °C). No amount of chlorine was detected even by the most sensitive techniques such as SIMS, meaning it is fully removed out of the chamber during purge stages. A part of the obtained samples was subjected to annealing (1350 °C) to study effects of high-temperature processing in nitrogen atmosphere, the comparisons with unprocessed samples are provided.

Keywords: aluminum nitride; triisobutylaluminum; hydrazinium chloride; atomic layer deposition; atomic force microscopy; X-ray photoelectron spectroscopy; secondary-ion mass spectrometry

1. Introduction

Aluminum nitride is a wide band gap semiconducting material with covalent bonds, which has a hexagonal crystalline structure that is analogous to the structure of zinc sulfide known as wurtzite. It has a wide range of applications in optoelectronics UV detectors, surface acoustic wave devices, piezoelectric energy convertors and other fields; devices that can benefit from this material are: ultraviolet (UV) optoelectronic devices, such as UV light-emitting diodes (LEDs) and UV laser diodes (LDs) [1].

Ever increasing popularity of AlN-based nanostructures is well justified considering the abundance of its remarkable characteristics. Besides having a wide band gap, AlN boasts such properties as: high electrical resistance, high breakdown voltage, mechanical durability, chemical stability, low deposition temperatures and a potential for piezoelectric applications [2]. This material is resistant to high temperatures in inert atmospheres and has a low expansion coefficient [3]. Lower deposition

temperatures within the range of 150–400 °C (depending on a chosen method) ensure compatibility of AlN for applications such as post-processing of integrated circuits. Furthermore, it appears to be an appropriate material to be implemented in surface acoustic wave sensors and bulk acoustic wave filters [4]. Taking into consideration that the conventional silicon monolithic systems also require lower temperatures of deposition, AlN seems to be a more favorable option in comparison to other piezoelectric materials such as zinc oxide (ZnO) or zinc zirconate ($ZnZrO_3$) [5]. AlN has also been reported to exhibit resistive switching properties [6].

Being such an attractive semi-conductive material, it is well expected for there to be a plethora of studies and reports featuring AlN deposited by a variety of multiple tools (magnetron sputtering, ion-beam deposition, metalorganic vapor-phase epitaxy etc.) [7–11]. This particular paper focuses on the atomic layer deposition (ALD) method. ALD is a subtype of the bigger group of methods known as chemical vapor deposition (CVD) methods which are employed for obtaining thin films of various materials in vapor phase. The main feature of an ALD is the sequential introduction of the precursors followed by purging stage which increases homogeneity, purity and quality of the films altogether. ALD has established itself as a promising technique in the semiconductor manufacturing process and technologies for energy conversion [12–14]. For application in nanoelectronics, it is essential to have atomic precision in materials manufacturing. Over the last decades ALD proved to be a relatively affordable method with high scalability and repeatability while also providing the necessary precision of the atomic layer for films fabrication at the nanoscale level [15–17].

Nowadays, the most common precursors for obtaining AlN by ALD are: N_2/H_2 plasma, ammonia (NH_3), aluminum chloride ($AlCl_3$), hydrazine (N_2H_4) with each having its advantages and deficiencies. The usage of $AlCl_3$ as an aluminum precursor results in considerable chlorine impregnation into the layer, and also leads to chamber contamination. Ammonia requires high energy for activation and is reported for its limited reactivity under temperatures below 475 °C [18,19]. Hydrazine on the other hand has a more favorable thermochemistry but despite the generally positive results, the use of hydrazine (N_2H_4) is associated with a number of complications, such as transportation difficulties, explosiveness, instability and expensiveness [20]. The two most common precursors nowadays for obtaining AlN seem to be $Al(CH_3)_3$ and N_2/H_2 plasma. There are numerous reports demonstrating the use of these two precursors in deposition of AlN thin films, the quality of which mostly is within reasonable bounds [6,13,14].

However, the search for more affordable and efficient precursors is always a relevant and justifiable task. In this study, we will be exploring alternatives to the well-established precursors.

Triisobutylaluminum (hence TiBA) is a metalorganic compound with an exact formula $[(CH_3)_2CHCH_2]_3Al$ or $Al(C_4H_9)_3$ in a compressed form, which is mostly used as an Al precursor in CVD processes [7,8]. The following reasons speak in favor of choosing TiBA as an alternative Al precursor:

(1) Triisobutylaluminum is 1.7 times cheaper than the conventional Trimethylaluminum according to "Sigmaaldrich":

Triisobutylaluminum; CAS Number: 100-99-2; Triisobutylaluminum (~97% purity grade); price: USD 147 (100 g); trimethylaluminum; CAS Number: 75-24-1; trimethylaluminum (97% purity grade); price: USD 250 (100 g).

(2) $Al(C_4H_9)_3$ may actually be a more favorable choice in terms of reactivity with Si and a higher chamber pressure due to its being a larger molecule [21,22].

(3) Novelty factor—we have already seen multiple times AlN films grown using conventional precursors, so it seems only reasonable to test out something new, especially when there is no apparent reason why $Al(C_4H_9)_3$ should perform poorer than the well-established $Al(CH_3)_3$.

Much like TiBA, N_2H_5Cl is a relatively cheap compound (USD 62 for 100 g according to Sigma-Aldrich) and thus seems to be an attractive choice for nitrogen precursor. Another aspect which speaks in favor of N_2H_5Cl lies in the fact that, although it requires some basic precaution measures it is much easier to handle compared to hydrazine in its pure form [23]. As was stated above, chlorine is an aggressive element that might lead to the instrument contamination, which is why chlorine-containing

precursors are usually overlooked when it comes to ALD. However, as will be demonstrated in the experimental section, the use of hydrazinium chloride does not result in chlorine contamination since HCl into which N_2H_5Cl decomposes upon entering the ALD chamber never reaches energy to become reactive and is removed out of the chamber as a waste product.

Annealing in nitrogen is known to produce a positive effect on the quality of AlN thin films [10,24,25], hence, we also performed high-temperature annealing of the deposited layers. Simplification, optimization and price reduction in the technological aspects of obtaining AlN films will help in creating a single technological cycle for obtaining products working in the UV spectral region, buffer layers for LED structures, as well as piezo-crystalline layers in NEMS structures.

2. Experimental Detail

Deposition of the AlN thin films was carried out on the ALDCERAM ML-200 setup located in the physics department of the Dagestan State University. Prior to deposition, substrates were cleaned with acetone, isopropanol and dried in a stream of UHP nitrogen. Then the substrates were placed in the ALD chamber and were kept there for ~30 min until the chamber temperature reached 250 °C, allowing to initiate deposition. The container with TiBA has been heated to its vaporization temperature (86 °C).

In total, 150 ALD cycles were performed with the following parameters: the exposure time of TiBA $Al(C_4H_9)_3$ was 4 s, after which the reactor chamber was purged with the inert gas (N_2) for 5 s; the next stage was the introduction of hydrazinium chloride N_2H_5Cl, the duration of which was 0.2 s followed by a nitrogen purging of 30 s; then, again introduction of $Al(C_4H_9)_3$ for 4 s, followed by a nitrogen purging of 30 s. The image of the ALD equipment used is presented in Figure 1a. One cycle of the ALD process, as well as the change in the chamber pressure during precursor introduction, is presented in Figure 1b. The gradual decrease in the chamber pressure during precursor exposure time indicates chemisorption which takes place on the substrate.

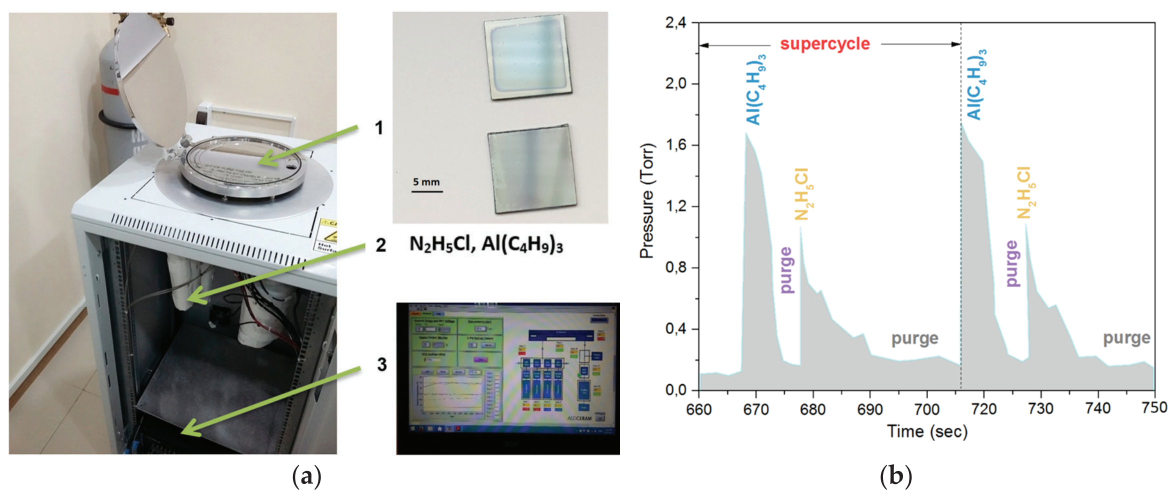

Figure 1. (**a**) Atomic layer deposition (ALD) equipment and its main units: 1—vacuum chamber, 2—section for containers with precursors, 3—controller with a custom-built software; (**b**) Dependency of the chamber pressure on the precursor exposure time.

Growth per cycle (GPC) as a function of precursor exposure time and temperature is given in Figure 2a,b. The values were calculated from spectroscopic ellipsometry data on thickness. The average growth rate was found to be ~0.072 nm/cycle. The stable value of GPC is reached at ~1 s of exposure for N_2H_5Cl and at ~20 s for TiBA (Figure 2a). According to Figure 2b, the self-limiting growth takes place in the temperature range of 150–250 °C. The rapid increase in GPC after 250 °C might be attributed to self-decomposition of TiBA as is the case for TMA after 300 °C [26].

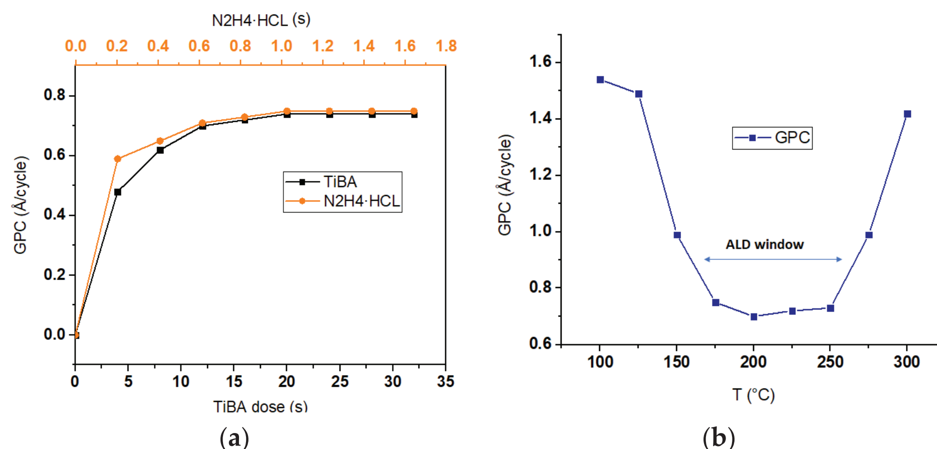

Figure 2. Growth per cycle (GPC) as a function of (**a**)—precursor exposure time; (**b**)—deposition temperature.

For informative and illustrative reasons, we include the scheme of an assumed ideal ALD process presented in Figure 3. In the middle we can see the result of the reaction of TiBA with the activated substrate on the left; C_4H_{10} is a waste product. On the right is the result of the reaction of N_2H_5Cl with the surface of the middle product; C_4H_{10}, C_4H_9Cl and HCl are the expected waste products.

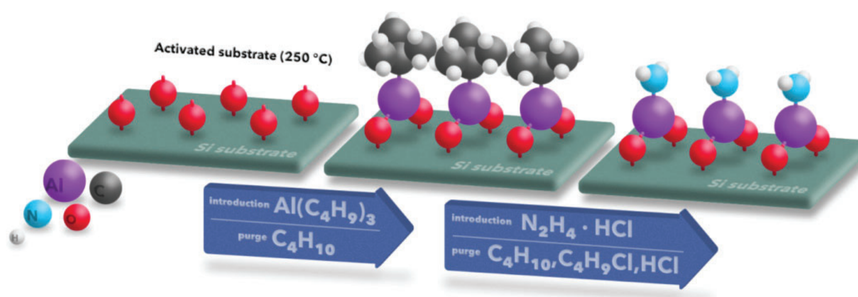

Figure 3. The scheme of an ideal ALD process.

Heating of the container with hydrazinium chloride was carried out at temperature up to 90 °C (T_m of N_2H_5Cl ~ 89 °C). The deposition temperature of the sample batch used for analysis was 250 °C, which is within the AlN ALD window according to our GPC measurements and a plethora of other studies [2,3,6,12,13,18,20]. A part of the obtained films has been also subjected to a high-temperature annealing (1350 °C) in the nitrogen (N_2) atmosphere for 1 h to remove possible impurities (in particular, hydrogen impurities).

AFM images were taken on a Scanning Probe Microscope Bruker Dimension Icon (ICON-SPM) in tapping mode. Gwyddion software was used for processing and extracting values for surface roughness.

Kratos Analytical Axis Supra instrument with Al Kα excitation source and emission current of 15 mA was employed to perform XPS analysis. Wide spectrum was taken at 80 eV. High resolution spectra were taken at 20 eV. All spectra were calibrated by shifting major C 1s peak (C–C bond) to 284.8 eV. The presented spectra were made in CasaXPS software (Version 2.3.19.PR1.0), SG linear smoothing and background subtraction tools were used.

SIMS analysis was performed on ION-TOF TOF.SIMS 5 instrument in positive mode. The instrument utilizes the dual gun mode of analysis. An oxygen gun with energy of 2 KeV was used for aggressive sputtering (material removal only), whereas a Bi gun provides a much slower sputtering rate and the secondary ions produced by it are collected by the analyzer. The area of the crater was chosen to be 100 nm × 100 nm and the area of analysis 50 nm × 50 nm. The 3D modelling was carried out using the native software SurfaceLab 7.1 provided by the manufacturer.

All aforementioned instruments used for analysis of the obtained samples are located at the CEITEC Nano Research Infrastructure in Brno, Czech Republic.

3. Experimental Data

3.1. Atomic Force Microscopy (AFM) and X-ray Diffraction (XRD) Data

In our study, the AFM method has been employed to investigate topography of AlN thin films before and after annealing at 1350 °C. The obtained AFM images are presented in Figure 4.

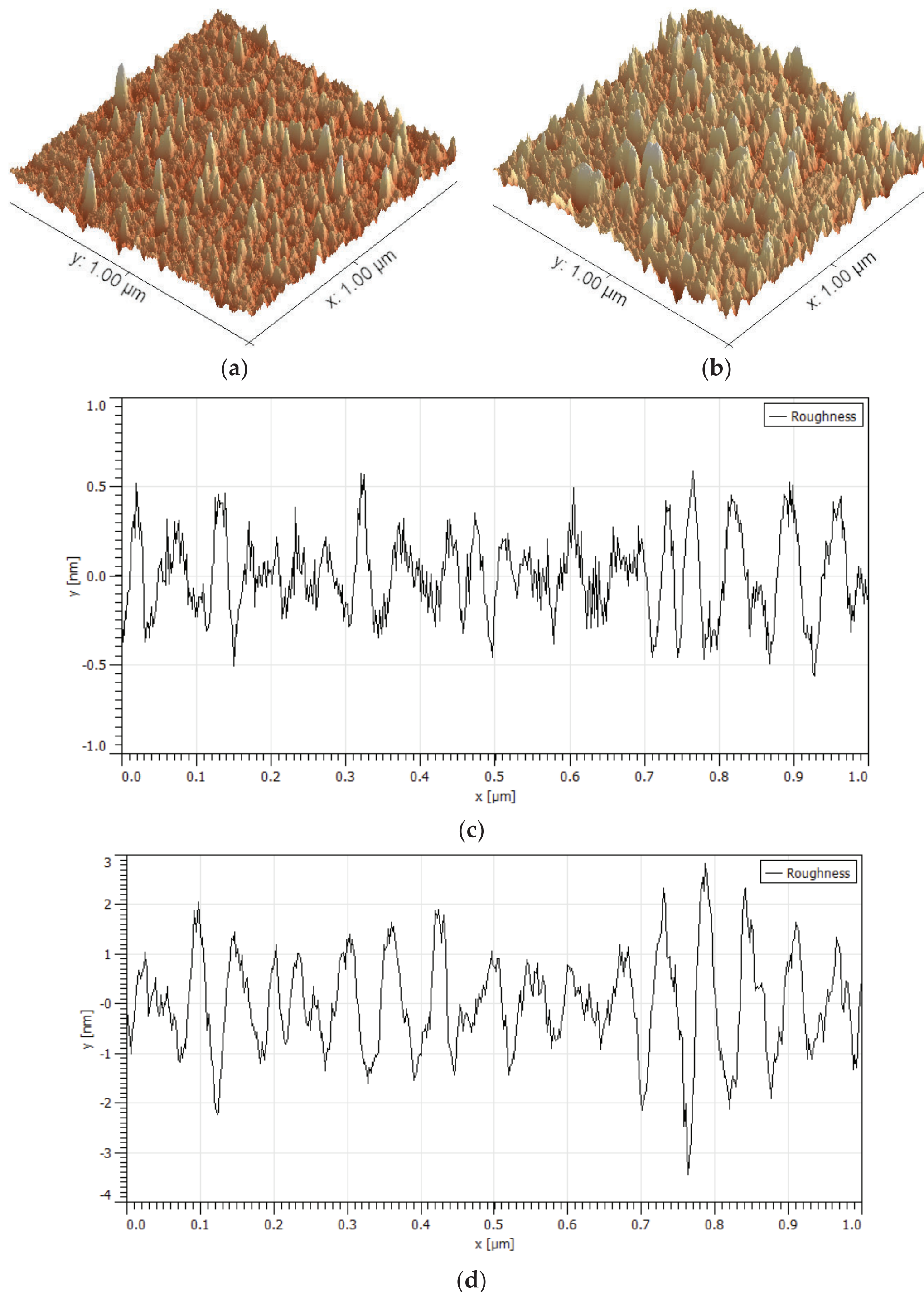

Figure 4. AFM images scan area 1 µm × 1 µm, (**a**)—before annealing; (**b**)—after annealing; (**c**,**d**) profiles of the films before and after annealing correspondingly.

Obtained results enable observation of changes caused by annealing of the films (Figure 4a,b). AFM data confirm that annealing contributes to the increase in roughness; coalescence of particles on the surface is likely to occur as well as removal of the residual hydrocarbon bonds from the film.

Annealing also leads to an increase in the topography uniformity and regularity of the surface texture (Figure 4c,d).

We assume that the film is in the crystallization stage, that is, in the intermediate state between amorphous and polycrystalline. Annealing completes the crystallization process which is proved by the XRD spectra provided in Figure 5. The increase in existing reflections and appearance of new ones indicated that the annealed films consist of crystallites of a larger size [24,27]. The root mean square of the surface roughness (S_a) for as-deposited AlN layer equaled to 0.23 nm which is within the norm for ALD AlN [15,28]. However, we can observe a rather significant increase after annealing of up to 0.84 nm, which suggests once again that temperature treatment promotes the tendency of the layer to coalesce into clusters. Huan-Yu Shih et al. report in their work an increase in the similar magnitude (from 0.223 nm to 0.663 nm) after annealing [18]. An increase in surface roughness can be explained by an increase in the grain size in the AlN layer, resulting in an improvement of crystallinity. In addition, the high conformity of films obtained by the ALD method leads to the filling of surface pits and pinholes with each deposited layer, which helps to reduce the density of pits or point defects on the surface. In addition, thermal stress caused by the difference in the thermal expansion coefficient between AlN and silicon can lead to formation of pits and cracks.

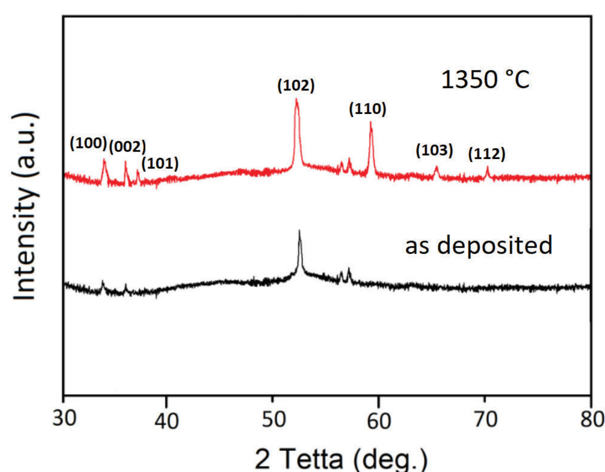

Figure 5. XRD spectra for as-deposited and annealed samples.

3.2. X-ray Photoelectron Spectroscopy (XPS) Data

XPS comparison of as-deposited and annealed samples of AlN. Annealing was carried out in N_2 atmosphere at 1350 °C for 1 h, heating/cooling rate was at 100 °C/min. All spectra have been calibrated by setting the C–C bond at 248.8 eV. The most important and notable change is the considerable increase in N1s peak intensity after annealing (Figure 6). Distinguishing nitrogen peak on the wide-spectrum of as-deposited films is somewhat challenging, which is why it is best instead to consult the high-resolution spectra provided below. The proneness of AlN to extensive oxidation is a notorious issue reported by multiple studies [6,17,18,29]. Carbon is also an unavoidable contaminant occurring from atmosphere [6,17,30].

The N 1s peak on the wide spectrum of unannealed samples is of rather low intensity; nonetheless it is still well-defined in high-resolution mode. We speculate that intensity of the nitrogen peak might be enhanced by increasing exposure time of N_2H_5Cl, since the optimal saturation may not have been reached. However, this minor detail should by no means be a hindrance to drawing conclusions regarding the efficiency of N_2H_5Cl. As will be demonstrated in the discussion section, N_2H_5Cl basically decomposes into hydrazine in the ALD chamber and the latter has already demonstrated positive

results as a nitrogen precursor for AlN thin films [20]. Moreover, imperfections of the ALD process have then been rectified by consecutive annealing in nitrogen.

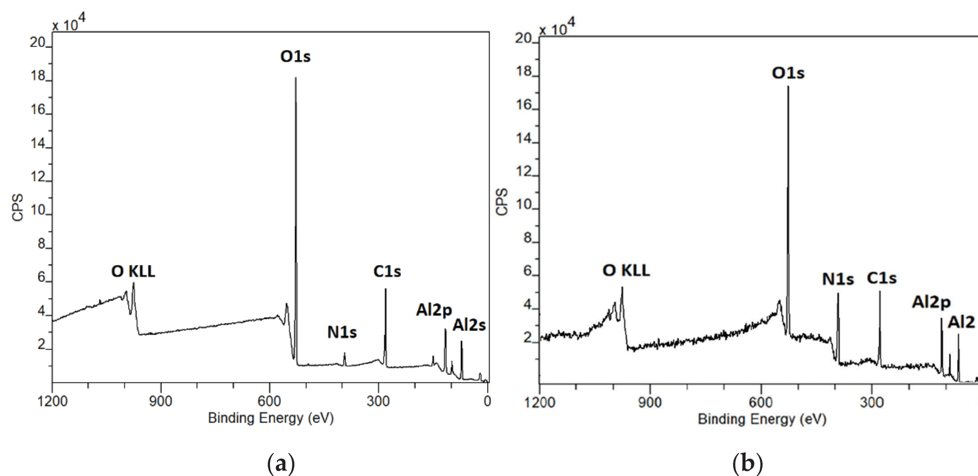

Figure 6. Comparison of XPS wide spectra of: (**a**) as-deposited AlN sample; (**b**) annealed AlN sample.

Both peaks are located at ~396.8 eV which is the energy widely attributed to Al–N bond [9,17,31–33]. The subpeak at ~400 eV is ascribed to C–NH_2 bonds (Figure 7). It is also worth emphasizing that, despite expectations, neither of the N 1s peaks shows any sign of oxidization; C–NH_2 bonds apparently occur as a result of side reaction between the two used precursors and remain unaffected by high-temperature annealing given the strong nature of these bonds. The dramatic increase in Al–N bond intensity is explained by influx of new nitrogen atoms during the annealing in the N_2 flow which induced reaction with the Al atoms still engaged in Al–Al bonds.

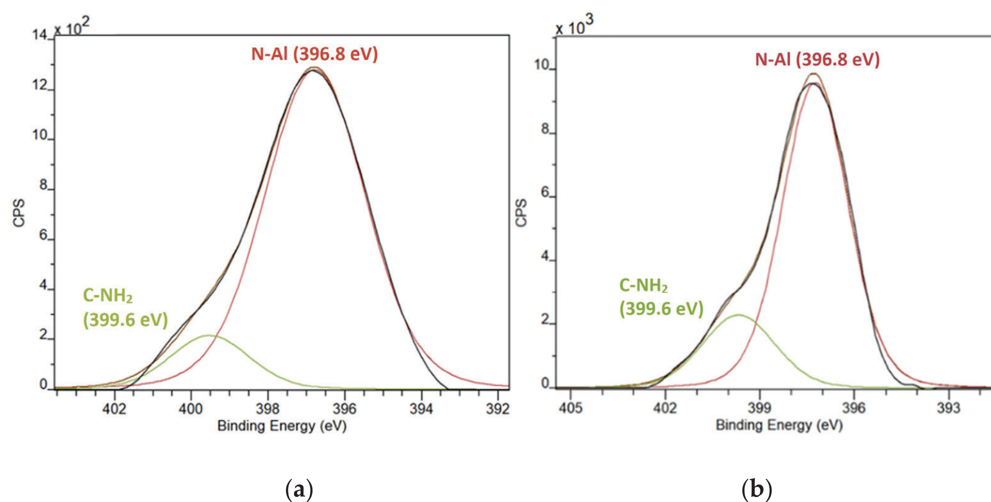

Figure 7. Comparison of high resolution N1s spectra of: (**a**) as-deposited AlN sample; (**b**) annealed AlN sample.

Figure 8a shows that the Al 2p peak can be deconvoluted into several subpeaks, the major one at 75.5 eV is related to Al–O and the smaller at 74.4 eV is attributed to Al–N [10,17,30,34–36]. Both peaks persist after high-temperature treatment (Figure 8b) and remain at the same binding energies. However, there is also a third peak that can be observed for as-deposited samples which is located at 77 eV. The literature is very scant on that matter, there is a record on Al–F bond located at 77 eV [37], however, no fluoride has been detected in our wide spectra, which is why this third peak more likely belongs to the Al–O bond affected by nitrogen as this is suggested by P.W. Wang et al. [38].

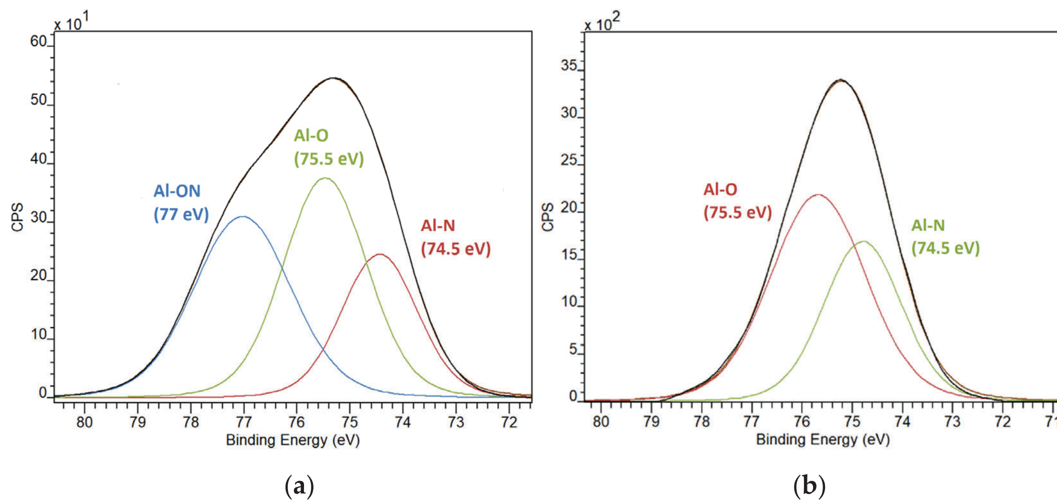

Figure 8. Comparison of high resolution Al 2p spectra of: (**a**) as-deposited AlN sample; (**b**) annealed AlN sample.

Extensive study of literature compels us to conclude that there is no consensus whatsoever among researchers on the exact position of the Al–N bond and the records vary greatly. Which is why we are also including a table with values of Al–N binding energy reported by other research studies (Table 1).

Table 1. Energies values assigned to Al–N bond by different authors.

Bond	Peak	Binding Energies (eV)
Al–N	Al 2p	74.7 [17], 73.5 [30], 74.3 [35], 74.4 [39], 74.2 [40], 74.0 [11], 74.6 [41]
	N 1s	397.8 [29], 396.4 [30], 397.3 [39], 397.4 [40], 396.5 [41], 397.7 [29], 397.1 [42]

Analysis of C 1s peak (Figure 9) shows the presence of different organic bonds, which are O–C=O at 2884 eV for as-deposited sample and O–C=O 287.6 eV, C–O–C 285.9 at eV for annealed sample [6,25,30]. The formation of new types of bonds is well expected when high temperature treatment is applied (Figure 9b), especially with a reactive element such as oxygen, the coalescence of the layer during extreme heating is also a promoting factor for such reactivity. The new C–O–C is likely to be formed not only from the C atoms in the C–C bond but also as a result of breaking of π–π bonds in O–C=O which are less stable in comparison with σ bonds in C–O–C.

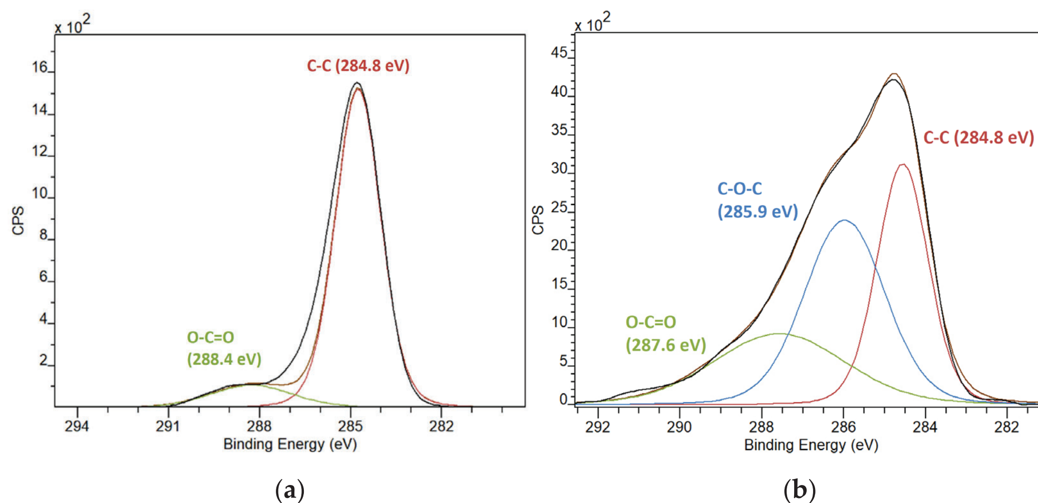

Figure 9. Comparison of high-resolution C 1s spectra of: (**a**) as-deposited AlN sample; (**b**) annealed AlN sample.

O1s high-resolution spectra are presented in Figure 10 and there we can observe the same tendency as in the C 1s peak a shift from C=O bond at 533.2 eV to C–O–C bond at 532.9 eV. The Al–O bond at 531.6 eV is present in both scenarios due to AlN's high affinity to oxidation [6,17,18,29,30].

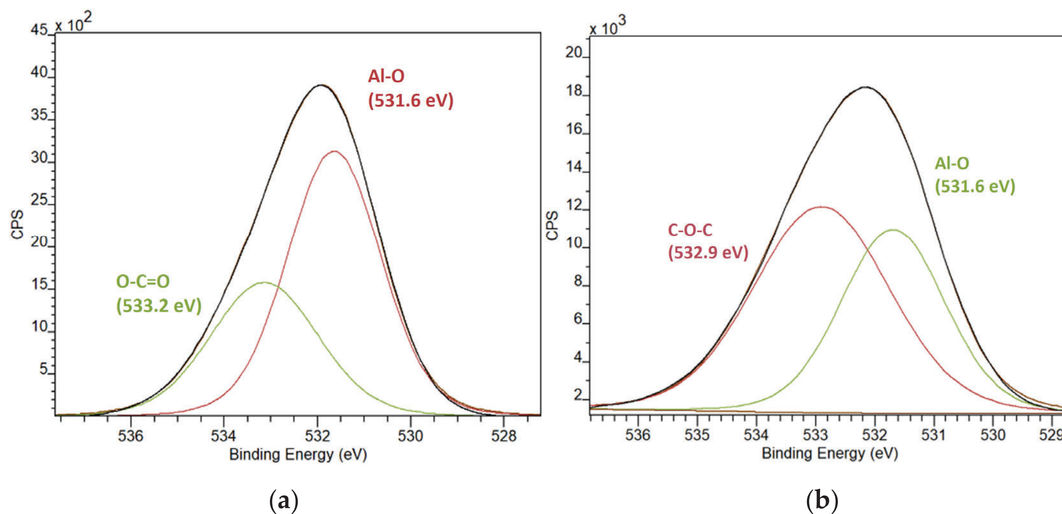

(**a**) (**b**)

Figure 10. Comparison of high-resolution O 1s spectra of: (**a**) as-deposited AlN sample; (**b**) annealed AlN sample.

3.3. Secondary-Ion Mass Spectrometry

To further investigate the chemical composition as well as to provide depth profiling of the films obtained, the secondary-ion mass spectrometry (SIMS) was utilized in time-of-flight mode. The main principle of this mode is that different ions require different periods of time to reach the analyzer due to mass discrepancy; this period of time is then counted and used to detect and identify an ion using the software with an extensive built-in database.

The SIMS equipment used in this work utilizes two ion-guns, one of which is used for sputtering only and the other with much lower energy is used for analysis. For sputtering, we used oxygen ions with energy of 2 keV for creating a crater and bismuth ions for analyzing the sputtered area along the way. Every 2 s of sputtering was followed by 3 s of analysis. The area of the crater was 200 nm × 200 nm; the area of analysis was 50 nm × 50 nm. The depth profiling spectra for O^-, AlO^-, Si^-, Al^-, AlN^- and SiO^- for both annealed and unannealed samples are given in Figure 11a,b.

Sputter time on X-axis is 80 s which can be translated into approximately 20 nm of crater depth. The Si spectrum maximizes at around 42 s which translates into ~8 nm, indicating the end of the layer and beginning of the substrate. At the same point, we can observe a rapid decrease in intensity of Al and AlN peaks. SiO spectrum exhibits a hill between 20 and 50 s which is the region of the substrate oxidization. It is worth mentioning that SIMS spectra are unusable for quantification. It can be noticed that the intensity of O^- and AlO^- ions is high, which also correlates with XPS data. As we mentioned in the section describing XPS results, the extensive oxidization of AlN films grown by ALD is a notorious issue and by no means limited to our particular case [6,17,18,29]. Partially, the amount of oxygen can be explained by the fact that we utilized oxygen primary beam, a portion of that beam is scattered back to the analyzer either in the form of pure ions or ions formed by the interaction with the atoms in the sample. Thus, the real amount of oxygen or oxygen containing ions is significantly lower.

In Figure 10 below, images of 2D and 3D distribution of ions are presented. A sample without temperature treatment (Figure 12a) shows a rather uniform distribution of AlN^- ions, whereas there is a noticeable grain of ~20 nm × 20 nm containing AlN^- on a sample that has undergone temperature treatment (Figure 12b); such grains have been spotted throughout the entire surface of all samples. This discovery unambiguously confirms the clustery nature of the layer on annealed samples. The 3D distribution of the grain is presented in Figure 12c.

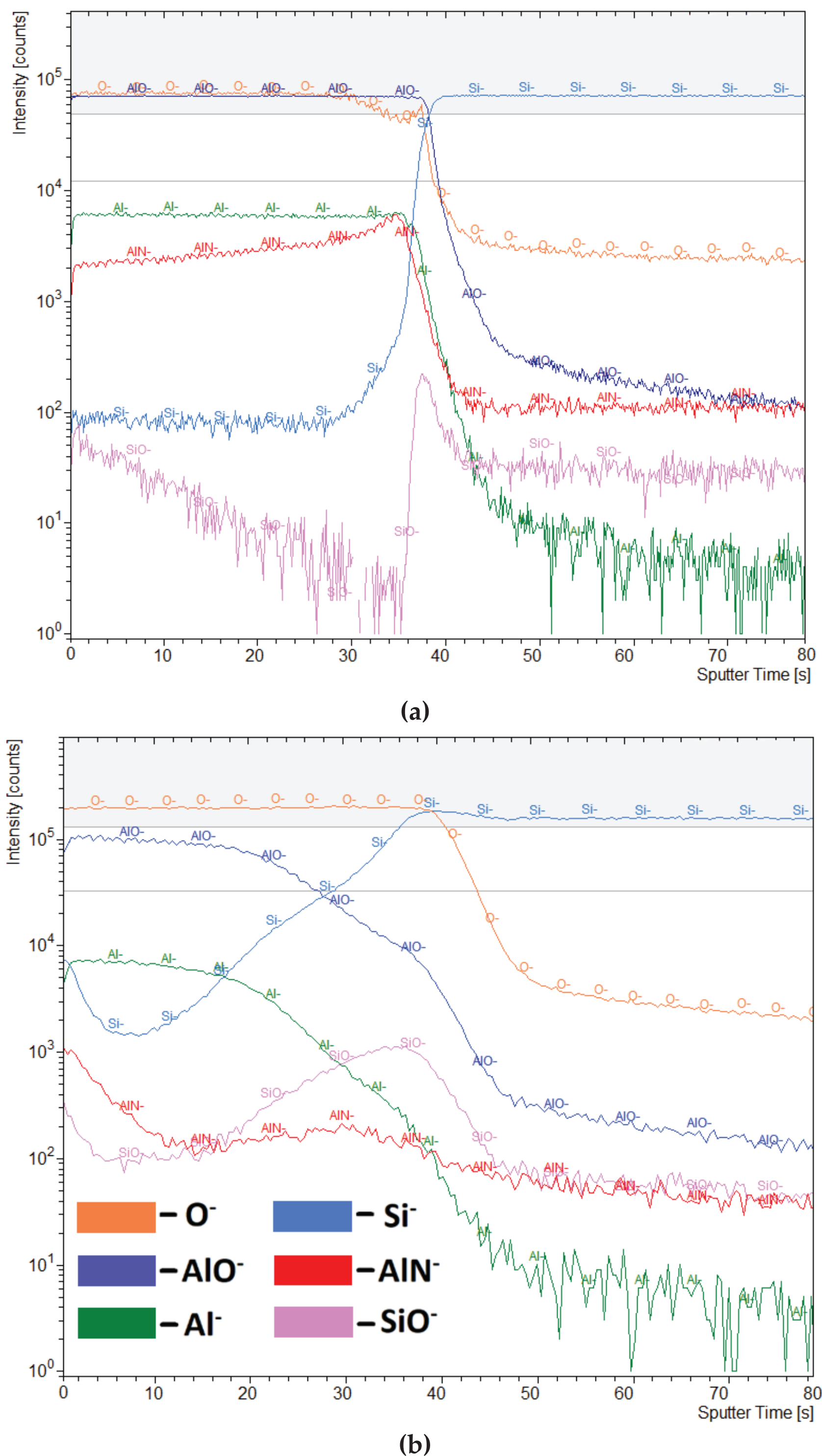

Figure 11. (**a**) Depth profile SIMS spectra for different ions for a sample without temperature treatment; (**b**) depth profile SIMS spectra for different ions for a sample with temperature treatment.

Now it is important to state here, that there is a known issue that comes into play while modeling 3D distribution of elements on uneven surfaces which lies in the fact that the model begins with the lowest point on the surface and all the features (including grains) that are higher than the lowest point are shown to be distributed downwards in the model instead of upward. So the continuation of the AlN grain (dark green color) which we see after the SiO_2 native layer (purple color) actually resides above the 3D model and not in the bulk of the substrate as the picture misleadingly implies.

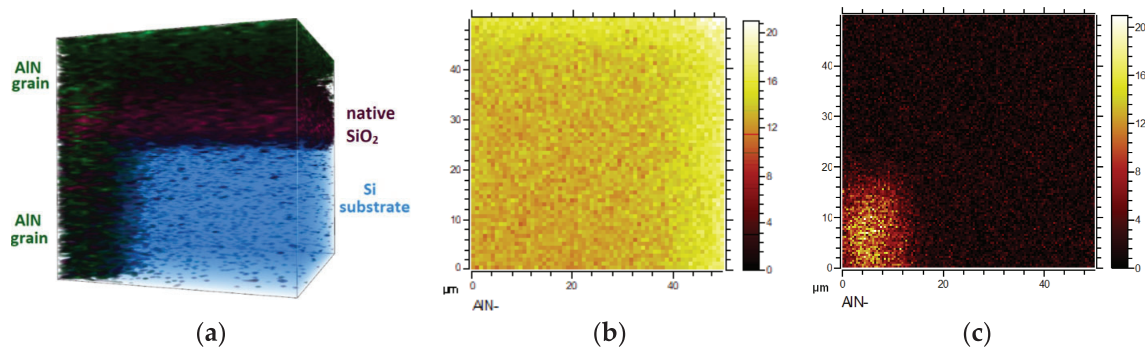

(**a**) (**b**) (**c**)

Figure 12. (**a**) 2D distribution of AlN^{-} ions for samples without temperature treatment; (**b**) 2D distribution of AlN^{-} ions for samples with temperature treatment; (**c**) 3D distribution of AlN^{-}, SiO^{-}, and Si^{-} ions of a sample with temperature treatment.

4. Discussion

The experimental results suggest clusterization of the grown layer after annealing. The plethora of different peaks and artefacts observed in the XPS spectra is likely due to the fact that XPS beam captures clusters of AlN as well as part of the oxidized substrate.

The first step was the introduction of the Al precursor; the low-energy metalorganic bonds can be broken at relatively low temperatures (~200–250 °C) [7,8]. The ion formed as a result will connect with the surface oxygen:

$$[\text{substrate}]\text{-SiO}_2 + \text{Al(C}_4\text{H}_9)_3 \rightarrow [\text{substrate}]\text{-Si-O-Al-(C}_4\text{H}_9)_2 + \text{C}_4\text{H}_9{}^{+}$$

Then, the chamber is purged and hydrazinium chloride is introduced. The hydrazinium chloride salt first decomposes into hydrazine and hydrogen chloride [43].

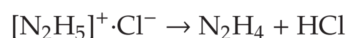

$$[\text{N}_2\text{H}_5]^{+}\cdot\text{Cl}^{-} \rightarrow \text{N}_2\text{H}_4 + \text{HCl}$$

It is worth indicating that no presence of the latter has been detected neither by XPS nor SIMS analyses, which means HCl molecules are completely removed out of the chamber during the purge stage. It has to do with the fact the that the deposition temperature is not nearly enough to ionize HCl, hydrazine on the other hand can be activated at temperatures <250 °C [20] and, theoretically, reaction should proceed as following:

$$\text{N}_2\text{H}_4 \rightarrow (\text{-N-H}_2)_2 \quad (1)$$

$$[\text{substrate}]\text{-Si-O-Al- (C}_4\text{H}_9)_2 + (\text{-N-H}_2)_2 \rightarrow [\text{substrate}]\text{-Si-O-Al-N- (H)}_2 + \text{C}_4\text{H}_{10} \quad (2)$$

Further annealing is necessary since the optimal saturation with nitrogen atoms has not been reached and oxygen atoms that might have been in the chamber have much higher affinity to Al than nitrogen atoms. Annealing in nitrogen is supposed to rectify inadequacies of the ALD process and improve the quality of AlN in general (crystallization).

Thus, the deposited samples have then been submitted to high-temperature (1350 °C) annealing in nitrogen atmosphere which promoted formation of nitridic and oxynitridic bonds in different proportions throughout the sample.

$$\text{Al}_2\text{O}_3 + \text{N}_2 \rightarrow \text{Al-N-O-(main reaction)} \quad (3)$$

$$\text{Al}_2\text{O}_3 + \text{N}_2 \rightarrow \text{Al-O-N-(side reaction)} \quad (4)$$

The XPS spectra unambiguously suggest an increased amount of Al–N bonds for annealed samples, which is why we assume that some of the Al–O–Al and Al–O–N bonds are decomposed

under the thermal stress and new Al–N–Al and Al–N–O bonds are formed either through reaction with molecular nitrogen of through diffusion process. The fact that molecular nitrogen might become reactive at temperatures exceeding 1000 °C has also been reported by C. F. Cullis and J. G. Yates in their study on reaction of carbon with molecular nitrogen [44]. The diffusion implies the release of nitrogen atoms that are seated deep down in the layer, beyond the range of the X-ray. Upon release, these atoms are distributed equally throughout the layer forming new bonds. To corroborate our assumption, we refer to the work of Cao D. et al. [25] who also studied the effect of high-temperature annealing on AlN films deposited by PE-ALD and reported similar tendency. The overall observation in their work is that high-temperature annealing seems to promote formation of new Al–N bonds and causes decomposition of Al–O–N bonds. Furthermore, they also indicated that the annealing of AlN in a nitrogen atmosphere generally improves the quality of the film while eliminating the defects that might have occurred during the growth through diffusion and rearrangement of the atoms. Annealing also produces a favorable effect on the crystalline qualities of the layer.

5. Conclusions

The main purpose of this work was to test out the new cheap and accessible precursors, hydrazinium chloride (N_2H_5Cl) and triisobutylaluminum (TiBA), in the AlN ALD process. Obtained samples have been analyzed using AFM, XPS and SIMS methods. The data collected from these analyses incline us to conclude that optimal saturation with nitrogen might not have been reached; however, temperature treatment fixed that issue and resulted in the film taking the “clustery” nature. These small crystals with diameters of ~20 mm × 20 nm cover the substrate in a uniform manner. Overall, it can be said that hydrazinium chloride showed positive results, though of course with several stipulations. We believe that by optimization of the technology and growing films with higher thickness, more reassuring results can be achieved. Thus, based on the data provided within the scope of this study, additional research regarding these precursors is warranted.

Author Contributions: Data curation, R.D.; Formal analysis, R.D.; Resources, P.T. and P.S.; Supervision, D.S. and P.S.; Visualization, L.Š.; Writing—original draft, R.D.; Writing—review & editing, R.D. and D.S. All authors have read and agreed to the published version of the manuscript.

Funding: Research described in this paper was financially supported by the Ministry of Education, Youth and Sports of the Czech Republic under the project CEITEC 2020 (LQ1601), by the National Sustainability Program under grant LO1401 and by Internal Grant Agency of Brno University of Technology, grant No. FEKT-S-20-6352. The research infrastructure of the SIX Center was used in this work. CzechNanoLab project LM2018110 funded by MEYS CR is gratefully acknowledged for the financial support of the measurements/sample fabrication at CEITEC Nano Research Infrastructure.

Conflicts of Interest: The authors declare that they have no conflict of interest.

References

1. Nieminen, M.; Lehto, S.; Niinistö, L. Atomic layer epitaxy growth of AlN thin films. *J. Mater. Chem.* **2001**, *11*, 3148–3153. [CrossRef]
2. Van Bui, H.; Wiggers, F.B.; Gupta, A.; Nguyen, M.D.; Aarnink, A.A.I.; De Jong, M.P.; Kovalgin, A.Y. Initial growth, refractive index, and crystallinity of thermal and plasma-enhanced atomic layer deposition AlN films. *J. Vac. Sci. Technol. A Vac. Surf. Film* **2015**, *33*, 01A111. [CrossRef]
3. Tarala, V.A.; Altakhov, A.S.; Martens, Y.A.; Lisitsyn, S.V. Growing aluminum nitride films by Plasma-Enhanced Atomic. *Inorg Mater.* **2015**, *51*, 728–735. [CrossRef]
4. Andrei, A.; Krupa, K.; Jozwik, M.; Delobelle, V.; Hirsinger, L.; Gorecki, C.; Nieradko, L.; Meunier, C. AlN as an actuation material for MEMS applications. The case of AlN driven multilayered cantilevers. *Sens. Actuators A Phys.* **2008**, *141*, 565–576. [CrossRef]
5. Giordano, C.; Ingrosso, I.; Todaro, M.; Maruccio, G.; De Guido, S.; Cingolani, R.; Passaseo, A.; De Vittorio, M. AlN on polysilicon piezoelectric cantilevers for sensors/actuators. *Microelectron. Eng.* **2009**, *86*, 1204–1207. [CrossRef]

6. Zhang, J.; Zhang, Q.; Yang, H.; Wu, H.; Zhou, J.; Hu, L. Bipolar resistive switching properties of AlN films deposited by plasma-enhanced atomic layer deposition. *Appl. Surf. Sci.* **2014**, *315*, 110–115. [CrossRef]
7. Găluşcă, D.G.; Perju, M.C.; Nejneru, C.; Nergiş, D.D.B.; E Lăzărescu, I. Aluminum coating influence on nitride layer performance deposited by MO-CVD in fluidized bed on austenitic stainless steel substrate. *IOP Conf. Ser. Mater. Sci. Eng.* **2018**, *374*. [CrossRef]
8. Czok, G.S.; Werther, J. Liquid spray vs. gaseous precursor injection—Its influence on the performance of particle coating by CVD in the fluidized bed. *Powder Technol.* **2006**, *162*, 100–110. [CrossRef]
9. Meng, J.P.; Liu, X.P.; Fu, Z.Q.; Wang, X.J.; Hao, L. Thermal stability of AlN films prepared by ion beam assisted deposition. *Appl. Surf. Sci.* **2015**, *347*, 109–115. [CrossRef]
10. Jose, F.; Ramaseshan, R.; Dash, S.; Bera, S.; Tyagi, A.K.; Raj, B. Response of magnetron sputtered AlN films to controlled atmosphere annealing. *J. Phys. D Appl. Phys.* **2010**, *43*, 075304. [CrossRef]
11. Ma, D.; Liu, H.; Deng, Q.; Yang, W.; Silins, K.; Huang, N.; Leng, Y. Optimal target sputtering mode for aluminum nitride thin film deposition by high power pulsed magnetron sputtering. *Vacuum* **2019**, *160*, 410–417. [CrossRef]
12. Johnson, R.W.; Hultqvist, A.; Bent, S.F. A brief review of atomic layer deposition: From fundamentals to applications. *Mater. Today* **2014**, *17*, 236–246. [CrossRef]
13. Ozgit, C.; Donmez, I.; Alevli, M.; Biyikli, N.; Ozgit-Akgun, C. Self-Limiting low-temperature growth of crystalline AlN thin films by plasma-enhanced atomic layer deposition. *Thin Solid Films* **2012**, *520*, 2750–2755. [CrossRef]
14. Goerke, S.; Ziegler, M.; Ihring, A.; Dellith, J.; Undisz, A.; Diegel, M.; Anders, S.; Huebner, U.; Rettenmayr, M.; Meyer, H.G. Atomic layer deposition of AlN for thin membranes using trimethylaluminum and H_2/N_2 plasma. *Appl. Surf. Sci.* **2015**, *338*, 35–41. [CrossRef]
15. Sadeghpour, S.; Ceyssens, F.; Puers, R. Crystalline growth of AlN thin films by atomic layer deposition. *J. Phys. Conf. Ser.* **2016**, *757*, 6–11. [CrossRef]
16. Shih, H.Y.; Lee, W.H.; Kao, W.C.; Chuang, Y.C.; Lin, R.M.; Lin, H.C.; Shiojiri, M.; Chen, M.-J. Low-Temperature atomic layer epitaxy of AlN ultrathin films by layer-by-layer, in-situ atomic layer annealing. *Sci. Rep.* **2017**, *7*, 1–8. [CrossRef]
17. Motamedi, P.; Cadien, K. XPS analysis of AlN thin films deposited by plasma enhanced atomic layer deposition. *Appl. Surf. Sci.* **2014**, *315*, 104–109. [CrossRef]
18. Rontu, V.; Sippola, P.; Broas, M.; Ross, G.; Sajavaara, T.; Lipsanen, H.; Paulasto-Kröckel, M.; Franssila, S. Atomic layer deposition of AlN from $AlCl_3$ using NH_3 and Ar/NH_3 plasma. *J. Vac. Sci. Technol. A Vac. Surf. Film* **2018**, *36*, 021508. [CrossRef]
19. Chen, Z.; Zhu, Z.; Härkönen, K.; Salmi, E. Batch processing of aluminum nitride by atomic layer deposition from $AlCl_3$ and NH_3. *J. Vac. Sci. Technol. A* **2019**, *37*, 020925. [CrossRef]
20. Abdulagatov, A.I.; Ramazanov, S.; Dallaev, R.S.; Murliev, E.K.; Palchaev, D.; Rabadanov, M.K.; Abdulagatov, I.M. Atomic layer deposition of aluminum nitride using tris(diethylamido)aluminum and hydrazine or ammonia. *Russ. Microelectron.* **2018**, *47*, 118–130. [CrossRef]
21. Jones, A.C.; Hitchman, M.L. *Overview of Chemical Vapor Deposition; Chemical Vapor Deposition: Precursors, Processes and Applications*; Jones, A.C., Hitchman, M.L., Eds.; Royal Society of Chemistry: London, UK, 2009; pp. 327–328.
22. Kermagoret, A.; Kerber, R.N.; Conley, M.P.; Callens, E.; Florian, P.; Massiot, D.; Copéret, C.; Delbecq, F.; Rozanska, X.; Sautet, P. Triisobutylaluminum: Bulkier and yet more reactive towards silica surfaces than triethyl or trimethylaluminum. *Dalton Trans.* **2013**, *42*, 12681–12687. [CrossRef] [PubMed]
23. Cellier, P.P.; Spindler, J.-F.; Taillefer, M.; Cristau, H.-J. Pd/C-catalyzed room-temperature hydrodehalogenation of aryl halides with hydrazine hydrochloride. *Tetrahedron Lett.* **2003**, *44*, 7191–7195. [CrossRef]
24. Xiao, S.; Suzuki, R.; Miyake, H.; Harada, S.; Ujihara, T. Improvement mechanism of sputtered AlN films by high-temperature annealing. *J. Cryst. Growth* **2018**, *502*, 41–44. [CrossRef]
25. Cao, D.; Cheng, X.; Xie, Y.-H.; Zheng, L.; Wang, Z.; Yu, X.; Wang, J.; Shen, D.; Yu, Y. Effects of rapid thermal annealing on the properties of AlN films deposited by PEALD on AlGaN/GaN heterostructures. *RSC Adv.* **2015**, *5*, 37881–37886. [CrossRef]
26. Liu, S.; Peng, M.; Hou, C.; He, Y.; Li, M.; Zheng, X. PEALD-Grown Crystalline AlN Films on Si (100) with Sharp Interface and Good Uniformity. *Nanoscale Res. Lett.* **2017**, *12*, 1–6. [CrossRef]

27. Ozgit-Akgun, C.; Goldenberg, E.; Okyay, A.K.; Biyikli, N. Hollow cathode plasma-assisted atomic layer deposition of crystalline AlN, GaN and $Al_xGa_{1-x}N$ thin films at low temperatures. *J. Mater. Chem. C* **2014**, *2*, 2123–2136. [CrossRef]
28. Motamedi, P.; Cadien, K. Structural and optical characterization of low-temperature ALD crystalline AlN. *J. Cryst. Growth* **2015**, *421*, 45–52. [CrossRef]
29. Kim, H.; Kim, N.D.; An, S.C.; Yoon, H.J.; Choi, B.J. Improved interfacial properties of thermal atomic layer deposited AlN on GaN. *Vacuum* **2019**, *159*, 379–381. [CrossRef]
30. Rosenberger, L.; Baird, R.; McCullen, E.; Auner, G.; Shreve, G. XPS analysis of aluminum nitride films deposited by plasma source molecular beam epitaxy. *Surf. Interface Anal.* **2008**, *40*, 1254–1261. [CrossRef]
31. Lin, Y.-H.; Hsu, J.-C.; Ding, Y.; Wang, P.W. Optical properties of high transmittance aluminum oxynitride thin films for spectral range from near ultraviolet to visible. *Opt. Rev.* **2009**, *16*, 400–403. [CrossRef]
32. Morgan, D.J. Imaging XPS for industrial applications. *J. Electron Spectrosc. Relat. Phenom.* **2018**, *231*, 109–117. [CrossRef]
33. Reddy, N.; Bera, P.; Reddy, V.R.; Sridhara, N.; Dey, A.; Anandan, C.; Sharma, A.K. XPS study of sputtered alumina thin films. *Ceram. Int.* **2014**, *40*, 11099–11107. [CrossRef]
34. Chen, D.; Xu, D.; Wang, J.; Zhang, Y. Investigation of chemical etching of AlN film with different textures by X-ray photoelectron spectroscopy. *J. Phys. D Appl. Phys.* **2008**, *41*. [CrossRef]
35. Radwan, A.B.; Shakoor, R.A. Aluminum nitride (AlN) reinforced electrodeposited Ni–B nanocomposite coatings. *Ceram. Int.* **2020**, *46*, 9863–9871. [CrossRef]
36. Graniel, O.; Kempiński, M.; Jancelewicz, M.; Zaleski, K.; Jurga, S.; Smyntyna, V. Structural and XPS characterization of ALD Al_2O_3 coated porous silicon. *Vacuum* **2015**, *113*, 52–58. [CrossRef]
37. Zhang, T.; Park, J.Y.; Huang, W.; Somorjai, G.A. Influence of reaction with XeF_2 on surface adhesion of Al and Al_2O_3 surfaces. *Appl. Phys. Lett.* **2008**, *93*. [CrossRef]
38. Wang, P.W.; Hsu, J.-C.; Lin, Y.-H.; Chen, H.-L. Structural investigation of high-transmittance aluminum oxynitride films deposited by ion beam sputtering. *Surf. Interface Anal.* **2010**, *43*, 1089–1094. [CrossRef]
39. Wang, C.C.; Chiu, M.C.; Shiao, M.H.; Shieu, F.S. Characterization of AlN Thin Films Prepared by unbalanced magnetron sputtering. *J. Electrochem. Soc.* **2004**, *151*, 252–256. [CrossRef]
40. Garcia-Mendez, M.; Morales-Rodríguez, S.; Shaji, S.; Krishnan, B.; Bartolo-Pérez, P. Structural properties of ALN films with oxygen content deposited by reactive magnetron sputtering: XRD and XPS characterization. *Surf. Rev. Lett.* **2011**, *18*, 23–31. [CrossRef]
41. Zhu, M.; Chen, P.; Fu, R.K.; Liu, W.; Lin, C.; Chu, P.K. AlN thin films fabricated by ultra-high vacuum electron-beam evaporation with ammonia for silicon-on-insulator application. *Appl. Surf. Sci.* **2005**, *239*, 327–334. [CrossRef]
42. Oikawa, H.; Akiyama, R.; Kanazawa, K.; Kuroda, S.; Harayama, I.; Nagashima, K.; Sekiba, D.; Ashizawa, Y.; Tsukamoto, A.; Nakagawa, K.; et al. Deposition and characterization of amorphous aluminum nitride thin films for a gate insulator. *Thin Solid Films* **2015**, *574*, 110–114. [CrossRef]
43. Shimizu, W.; Nakamura, S.; Sato, T.; Murakami, Y. Creation of high-refractive-index amorphous titanium oxide thin films from low-fractal-dimension polymeric precursors synthesized by a sol-gel technique with a hydrazine monohydrochloride catalyst. *Langmuir* **2012**, *28*, 12245–12255. [CrossRef] [PubMed]
44. Cullis, C.F.; Yates, J.G. Reaction of carbon with nitrogen. *Trans. Faraday Soc.* **1964**, *60*, 141–148. [CrossRef]

© 2020 by the authors. Licensee MDPI, Basel, Switzerland. This article is an open access article distributed under the terms and conditions of the Creative Commons Attribution (CC BY) license (http://creativecommons.org/licenses/by/4.0/).

6 Study of the chemical composition of AlN layers obtained by PE-ALD

6.1 Motivation of the article

This short communication was published as a result of my participation in the 9th International Conference on Materials Structure and Micromechanics of Fracture (MSMF9). This study is an attempt at investigation of hydrogen phenomenon within AlN layer with the use of conventional and widely available technique such as Fourier-transform infrared spectroscopy (FTIR) as well as less common secondary-ion mass spectrometry (SIMS). In general, hydrogen quantification requires the use of advanced methods which utilize high-energy ions species (ERDA, NRA). However, more common methods could still provide us with a tentative idea on the hydrogen presence as well as indicate what type of bonding it is engaged in. Since, hydrogen contamination is potentially detrimental to the quality of the resulting layers, its investigation is a justifiable task which constitutes the motivation of the following study.

6.2 Conclusion on the article

The AlN thin films were deposited by PE-ALD. The XPS indicated the presence of Al-N bonds. FTIR has detected the presence of C-H bonds, which exist in rather small concentration given the low intensity of the corresponding peak. This data overlap with what we could observe in SIMS analysis, which indeed confirms the hydrogen presence within the bulk of the AlN layer. Such conclusion can be made based on the fact that the concentration of H ion drastically decreases upon reaching the substrate by sputtering ions. However, there is no possibility to estimate the degree of hydrogen contamination, which is why the use of more advanced and capable of quantification techniques is warranted, which is the implication for future study.

6.3 Contribution

I conducted all the measurements and wrote the entirety of the manuscript. The co-authors contribution lies in providing resources, making minor corrections and giving valuable advice throughout the study.

6.4 Article 4

The paper **Investigation Of Structure Of Aln Thin Films Using Fourier-Transform Infrared Spectroscopy** was published **Procedia Structural Integrity** journal (ISSN: 2452-3216; indexed in WoS and Scopus databases) in the year of 2019.

Available online at www.sciencedirect.com

ScienceDirect

Procedia Structural Integrity 23 (2019) 601–606

Structural Integrity Procedia

www.elsevier.com/locate/procedia

9th International Conference on Materials Structure and Micromechanics of Fracture

Investigation of structure of AlN thin films using Fourier-transform infrared spectroscopy

Rashid Dallaev[a,b], Nikola Papěž[a*], Dinara Sobola[a,b], Shikhgasan Ramazanov[c], Petr Sedlák[a]

[a]*Department of Physics, Faculty of Electrical Engineering and Communications, Brno University of Technology, Technická 2848/8, Brno, 61600, Czech Republic*

[b]*Central European Institute of Technology, Purkyňova 123, 61600 Brno, Czech Republic*

[c]*Dagestan State University,Faculty of Physics, Department of condensed matter physics 367002, Dagestan Republic, Makhachala, st. Gadzhieva*

Abstract

This study focuses on structural imperfections caused by hydrogen impurities in AlN thin films obtained using atomic layer deposition method (ALD). Currently, there is a severe lack of studies regarding the presence of hydrogen in the bulk of AlN films. Fourier-transform infrared spectroscopy (FTIR) is one of the few methods that allow detection bonds of light elements, in particular - hydrogen. Hydrogen is known to be a frequent contaminant in AlN films grown by ALD method, it may form different bonds with nitrogen, e.g. amino (–NH2) or imide (–NH) groups, which impair the quality of the resulting film. Which is why, it is important to investigate the phenomenon of hydrogen as well as to search for the suitable methods to eliminate or at least reduce its quantity. In this work several samples have been prepared using different precursors, substrates and deposition parameters and characterized using FTIR and additional techniques such as AFM, XPS and EDS to provide a comparative and comprehensive analysis of topography, morphology and chemical composition of AlN thin films.

© 2019 The Authors. Published by Elsevier B.V.
This is an open access article under the CC BY-NC-ND license (http://creativecommons.org/licenses/by-nc-nd/4.0/)
Peer-review under responsibility of the scientific committee of the ICMSMF organizers

Keywords: thin-films, aluminum nitride, Fourier-transform infrared spectroscopy, hydrogen impurities, structural analysis.

* Corresponding author. Tel.: +420-607-335-321
E-mail address: nikola.papez@vutbr.cz

2452-3216 © 2019 The Authors. Published by Elsevier B.V.
This is an open access article under the CC BY-NC-ND license (http://creativecommons.org/licenses/by-nc-nd/4.0/)
Peer-review under responsibility of the scientific committee of the ICMSMF organizers
10.1016/j.prostr.2020.01.152

1. Introduction

Aluminum nitride is a wide band gap semiconducting material with covalent bonds, which has a hexagonal crystalline structure that is an analog of the structure of zinc sulfide known as wurtzite. This material is resistant to high temperatures in the inert atmospheres [1].

Thin films of aluminum nitride (AlN) are gaining a lot of attention lately, due to the excellent characteristics of this material such as wide band gap, remarkable mechanical properties, high chemical stability, high electrical resistance, high breakdown voltage, low deposition temperature and impressive piezoelectric properties [2]. Another advantage of AlN thin films in comparison to other piezoelectric materials such as lead zirconate titanate and zinc oxide is the possibility of their integration in traditional silicon monolithic systems, for synthesis of which a low temperature deposition processes is demanded [3]. A low deposition temperature (below 400 °C) of AlN makes it a compatible material when it comes to post-processing of the integrated circuits. Also, it seems to be a promising candidate for bulk acoustic wave filters and surface acoustic wave [4].

Atomic layer deposition (ALD) is a vapor phase method used for obtaining thin films of different materials. ALD has established itself as a promising technique in semiconductor manufacturing process and technologies for energy conversion [5]. For application in nanoelectronics it is crucial to have atomic precision in materials manufacturing. Over the last several years ALD proved to be a relatively cheap and scalable method which provides the necessary precision of the atomic layer for fabrication of films at the nanoscale level [6].

But there is still a lack of study regarding contaminations in AlN obtained by various methods [7, 8]. This paper in particular aims to fill the gap in knowledge of preparation AlN thin films grown by ALD.

Infrared reflectance is a spectroscopic non-destructive techniques providing information on the nature of chemical bonds. By evaluating the intensity of light dispersed from and through a sample, NIR reflectance spectra can be employed to quickly define material's properties without changing the sample.

Another technique that allows detection of light elements is Secondary ion-mass spectrometry (SIMS). In this work it was employed in time-of-flight mode, the sputtering of the film was conducted using Ar cluster. As a result, we managed to create 3D profile images for certain elements in the bulk of the film. The depth of the sputtering was around 200nm (the density of the AlN layer is around 70nm).

2. Preparation of the samples

In this work we obtained AlN thin films using plasma enhanced atomic layer deposition (PE-ALD) on silicon substrates and highly oriented pyrolytic graphite (HOPG). Obtained films have been analyzed using AFM, XPS, EDS methods.

In total 634 ALD cycles have been performed which translates into thickness of approximately 40nm (1cycle ≈ 0,629 Å). The temperature of deposition was 250 °C. The energy of plasma was 300W. The sequence of each cycle consisted of following steps: 1) introduction of TMA (0,06sec), 2) purge 10sec, 3) initiate flow of N2/H2 (20 sccm) and enable plasma (40 sec), 4) purge 5sec. Annealing duration was of 1h, 10min of which under 1250 °C, the rest 50 min under 1000 °C. Silicon substrates with (100) orientation and dimensions of 1x1x0,1cm are polished to atomic thickness and were cleaned with isopropanol prior to deposition.

3. Results and discussion

3.1. Atomic force microscopy

In order to investigate surface morphology and topography of the films obtained we utilized atomic force microcopy technique in tapping mode. AFM images are given in fig. 1.

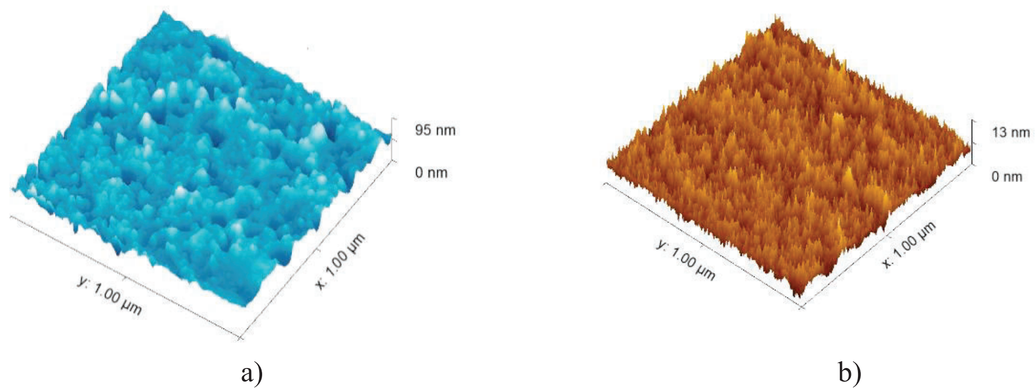

a) b)

Figure 1. AFM imgaes of: a) AlN on Si substrate, b) AlN on HOPG

Average rougness (Ra) has also been calculated. For AlN on Si its values equals to 12.5 Å and for AlN on HOPG – 9.7 Å. Which suggests that the films grown on HOPG have more uniform topography and therefore better quality.

3.2. Fourier-transform infrared spectroscopy data

FTIR reflectance spectrum of AlN on HOPG is given in fig 2.

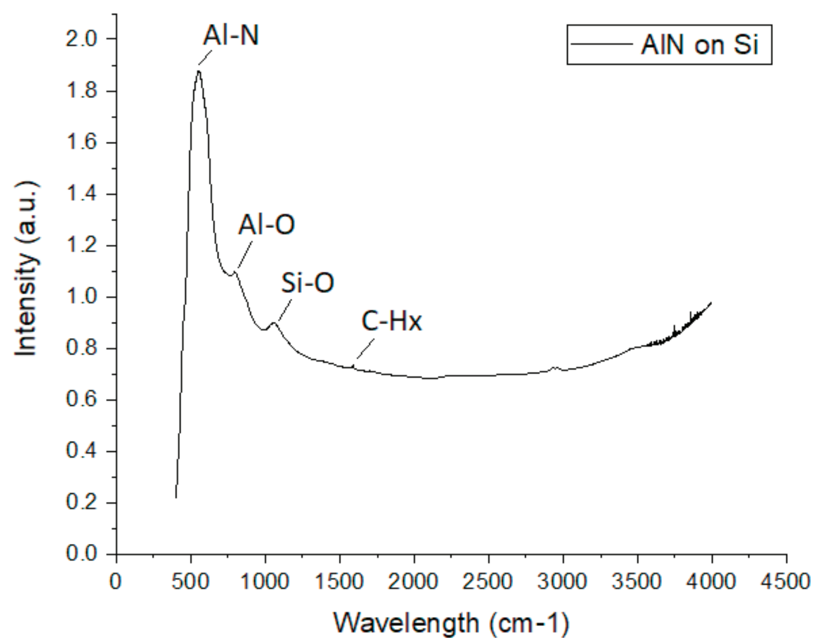

Figure 2. FTIR spectra for AlN on HOPG

The major peak at ~615 cm^{-1} is assigned to Al–N, vibration mode A1(TO); smaller peaks at 735 cm^{-1} and ~1100 cm^{-1} are attributed to ν(Al–O), vibration mode Al–O and to Si-O vibration mode ν(Si–O) correspondingly [9, 10]. There is also a slightly visible peak at ~1500eV which is according to [11] corresponds to C-H bonds. This peak is of particular interest since FTIR used in this work mostly to detect the presence of hydrogen.

3.3. Secondary ion-mass spectrometry

3D SIMS images are given in fig. 3.

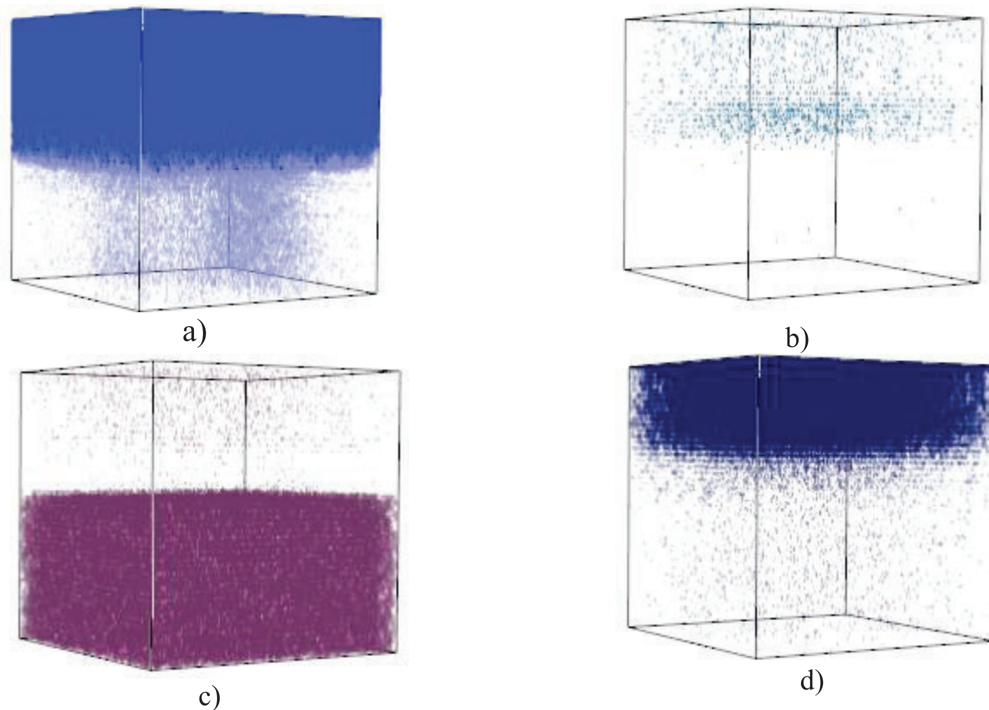

Figure 3. SIMS 3D profiling images of: a) Aluminum, b) Nitrogen, c) Silicon, d) Hydrogen.

As expected, we have a dense distribution of aluminum atoms and less so of nitrogen in the surface of the sample (fig 3a and fig. 3b). According to [16] annealing of AlN in the nitrogen atmosphere might improve the quality of the layer and therefore increase the amount of nitrogen atoms.
Once the sputtering beam has broken through the AlN layer, no more aluminum is detected, instead we can observe the dense distribution of Si atoms of the substrate (fig 3c). The hydrogen 3D profile is given in fig 3d. Since SIMS detector picks up not only atoms emitted from the surface but also from the atmosphere it is nearly impossible to tell how much of the hydrogen exactly belongs to the AlN layer. Nevertheless, we still can reasonably assume that at least part of it resides in the bulk of the AlN layer, given that there is almost none of the hydrogen in the substrate.

3.4. X-ray photoelectron spectroscopy (XPS) data

To provide comprehensive analysis of chemical composition X-ray photoelectron spectroscopy (XPS) method was utilized. Fitted elemental high resolution spectra are presented in fig. 4.

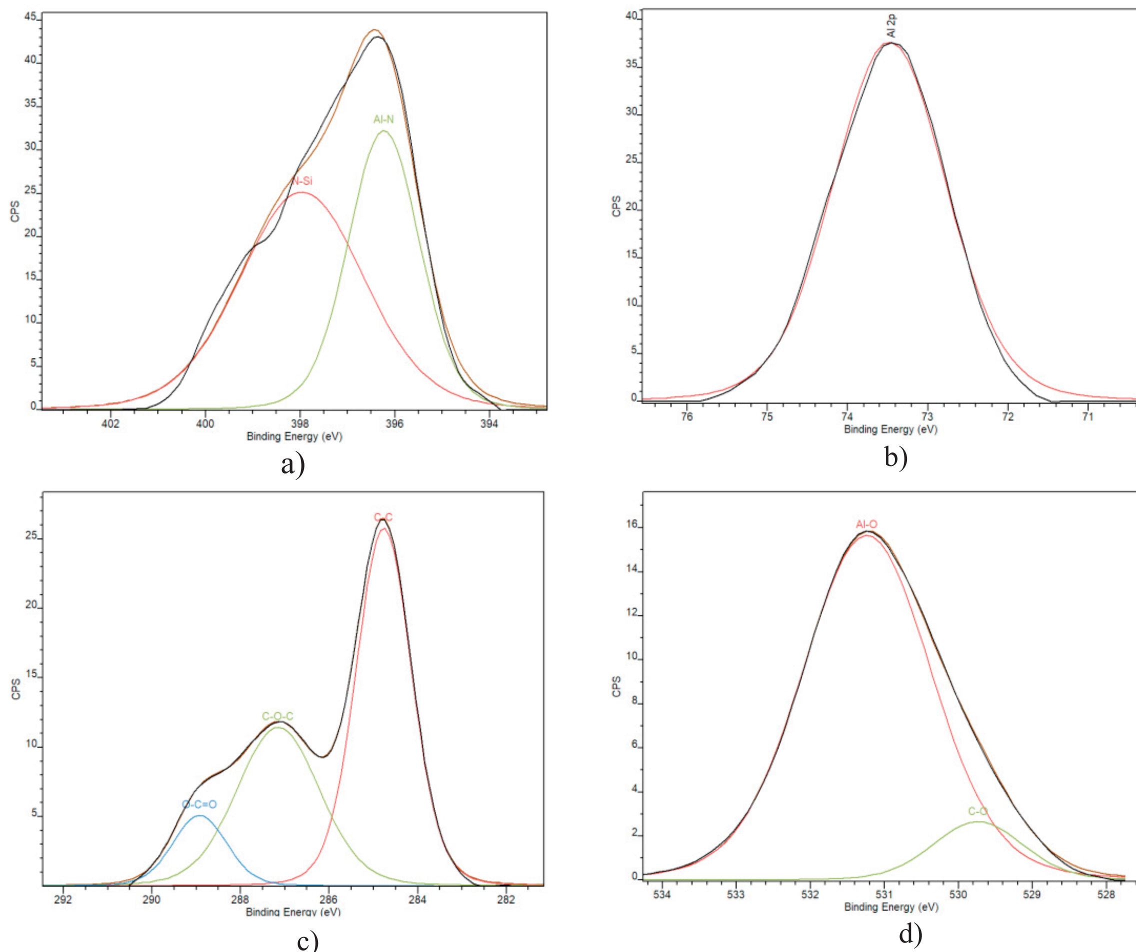

Figure 4. XPS elemental spectra for AlN on Si: a) N1s, b) Al2p, c) C1s, d) O1s

The nitrogen peak (fig. 4a) consists of two subpeaks of binding energies of 397eV and 398,3eV. The bigger suppeak at 397eV is one belonging to Al-N bond and the smaller one is ascribed to N-Si [12].
Aluminum has just one intense peak (fig.4b) at ~73,5 eV which is exacly the binding energy of Al-N accoridng to literature [13], which perfectly correlates with the data of the nitrogen peak
Peaks of unavoidable contaminants in form of carbon (fig.4c) and oxygen(fig.4d) are also presented. Carbon forms a triplet of peaks at 284,8eV; 286,5eV and 288,5 eV which are attributed to C-C; C-O-C and O-C=O correspondingly. Oxygen doublet consits of peaks at 529,8 eV (C-O) and 531eV (Al-O) [14, 15].

4. Conclusion

In this paper AlN thin films have been deposited using PE-ALD equipment on two different substrates – silicon and HOPG. Surface analysis of the samples using AFM indicated that AlN layer on HOPG has a more uniform topography as compared to the one on silicon. Chemical structure of the samples obtained has been thoroughly studied using such techniques as FTIR, SIMS and XPS. FITR analysis showed the presence of Al-N bonds which was also confirmed by XPS analysis. Hydrogen has also been detected by FTIR in the form of C-Hx bonds. Using data obtained by SIMS method with Ar cluster, 3D profiles of the aluminum, nitrogen, silicon and hydrogen have been generated which provided information on distribution of these elements in the stratum of the sample. As a result of this study we have confirmed the presence of nitrogen in the bulk of the AlN layer using several methods while at the same time providing a comprehensive analysis of AlN thin films obtained by PE-ALD.

Acknowledgement. Research described in this paper was financially supported by the Ministry of Education, Youth and Sports of the Czech Republic under the project CEITEC 2020 (LQ1601), by the National Sustainability Program under grant LO1401 and by Internal Grant Agency of Brno University of Technology, grant No. FEKT-S-17-4626. The research infrastructure of the SIX Center was used in this work. Part of the work was carried out with the support of CEITEC Nano Research Infrastructure (ID LM2015041, MEYS CR, 2016–2019), CEITEC Brno University of Technology.

References

[1] V. A. Tarala, A. S. Altakhov, V. Ya. Martens, S. V. Lisitsyn, Growing aluminum nitride films by Plasma-Enhanced Atomic. (2015). doi:10.1088/1742-6596/757/1/012003

[2] Y. Bian, M. Liu, G. Ke, Y. Chen, J. DiBattista, E. Chan, Y. Yang, Aluminum nitride thin film growth and applications for heat dissipation, Surf. Coatings Technol. 267 (2015) 65–69. doi:10.1016/j.surfcoat.2014.11.060

[3] C. Giordano, I. Ingrosso, M.T. Todaro, G. Maruccio, S. De Guido, R. Cingolani, A. Passaseo, M. De Vittorio, AlN on polysilicon piezoelectric cantilevers for sensors/actuators, Microelectron. Eng. 86 (2009) 1204–1207. doi:10.1016/j.mee.2008.12.075

[4] A. Andrei, K. Krupa, M. Jozwik, P. Delobelle, L. Hirsinger, C. Gorecki, L. Nieradko, C. Meunier, AlN as an actuation material for MEMS applications. The case of AlN driven multilayered cantilevers, Sensors Actuators, A Phys. 141 (2008) 565–576. doi:10.1016/j.sna.2007.10.041.

[5] R.W. Johnson, A. Hultqvist, S.F. Bent, A brief review of atomic layer deposition: From fundamentals to applications, Mater. Today. 17 (2014) 236–246. doi:10.1016/j.mattod.2014.04.026

[6] M. Schlesinger, M. Paunovic, Electroless deposition of copper, Mod. Electroplat. 1 (2010) 433–446. doi:10.1002/9780470602638.

[7] M. Reusch, K. Holc, L. Kirste, P. Katus, L. Reindl, O. Ambacher, V. Lebedev, Piezoelectric AlN films for FPW sensors with improved device performance, Procedia Eng. 168 (2016) 1040–1043. doi:10.1016/j.proeng.2016.11.335.

[8] A.I. Abdulagatov, Sh. M. Ramazanov, R.S. Dallaev, E.K. Murliev, D. K. Palchaev, M. Kh. Rabadanov and I.M. Abdulagatov, Atomic Layer Deposition of Aluminum Nitride Using Tris(diethylamido)aluminum and Hydrazine or Ammonia. Russian Microelectronics (2008), Vol. 47, No. 2, 118–130 doi: 10.1134/s1063739718020026

[9] C. John, Interpretation of Infrared Spectra, A Practical Approach, Encycl. Anal. Chem. (2000).

[10] M. Broas, P. Sippola, T. Sajavaara, V. Vuorinen, A. Pyymaki Perros, H. Lipsanen, M. Paulasto-Kröckel, Structural and chemical analysis of annealed plasma-enhanced atomic layer deposition aluminum nitride films, J. Vac. Sci. Technol. A Vacuum, Surfaces, Film. (2016). doi:10.1116/1.4953029.

[11] P. Motamedi, K. Cadien, Structural and optical characterization of low-temperature ALD crystalline AlN, J. Cryst. Growth. (2015). doi:10.1016/j.jcrysgro.2015.04.009.

[12] H. Kim, H. Ju, B. Joon, Optic Investigation of fast and slow traps in atomic layer deposited AlN on 4H-SiC, Opt. - Int. J. Light Electron Opt. 184 (2019) 527–532. doi:10.1016/j.ijleo.2019.05.002.

[13] Y. Li, C. Zhang, X. Luo, Y. Liang, D. Wuu, C. Tin, X. Lu, Applied Surface Science Surface , structural and optical properties of AlN thin films grown on different face sapphire substrates by metalorganic chemical vapor deposition, Appl. Surf. Sci. 458 (2018) 972–977. doi:10.1016/j.apsusc.2018.07.138.

[14] Z. Tseng, L. Chen, W. Li, S. Chu, Resistive switching characteristics of sputtered AlN thin films, Ceram. Int. 42 (2016) 9496–9503. doi:10.1016/j.ceramint.2016.03.022.

[15] D. Rashid, S. Stach, Ş. Ţălu, D. Sobola, A. Méndez-Albores, G.T. Córdova, L. Grmela, Stereometric Analysis of Effects of Heat Stressing on Micromorphology of Si Single Crystals, Silicon. (2019). doi:10.1007/s12633-019-0085-4.

[16] D. Cao, X. Cheng, Y.H. Xie, L. Zheng, Z. Wang, X. Yu, J. Wang, D. Shen, Y. Yu, Effects of rapid thermal annealing on the properties of AlN films deposited by PEALD on AlGaN/GaN heterostructures, RSC Adv. 5 (2015) 37881–37886. doi:10.1039/c5ra04728e.

7 Analysis of AlN layers deposited on the surface of HOPG by PE-ALD

7.1 Motivation of the article

This is another short communication that was published as a result of a student national conference EEICT 2021, organized by Brno University of Technology. In this study, HOPG was chosen to be the substrate for deposition of AlN by PE-ALD. The choice of HOPG as a substrate is explained by several factors. First of all, HOPG has not been utilized before and it is always a good idea to test new substrates in terms of their viability, to increase amount of available options. Aside from that, HOPG actually has certain advantages over more conventional substrates:

1) Since HOPG is basically just carbon, it has extremely high melting point (~3550 °C), this greatly facilitates post-processing and unlocks the possibility of annealing of deposited layers under very high temperatures without affecting the substrate.

2) Another reason lies in the laminated nature of HOPG which makes possible the transfer of the deposited layer from the substrate onto a different foundation, if such necessity arises.

7.2 Conclusion on the article

The obtained films were investigated by AFM, XPS and SIMS methods. AFM indicated good uniformity of the obtained layers with the surface roughness of only ~3.6nm. The presence of Al-N bonds was confirmed by XPS. SIMS has provided additional information on the chemical composition, such as distribution patterns of certain ions within the layers. AlN ion was detected on the SIMS mass spectrum, which is a positive aspect and correlates well with XPS results. Both methods, however, also discovered impurities in the form of carbon and oxygen, just as was the case with previous studies. This issue would require appropriate post-processing which is made easier due to the nature of HOPG substrate.

7.3 Contribution

As a sole author I am responsible for the entirety of the given research.

7.4 Article 5

The article is accepted and will be published as proceeding of EEICT 2021 conference, Brno, Czech Republic. This contribution was awarded 1st place during the conference, and as result, will be indexed in Web of Science database. ISBN: 978-80-214-5943-4

STUDENT EEICT
ELECTRICAL ENGINEERING, INFORMATION SCIENCE, AND COMMUNICATION TECHNOLOGIES

Accepted: 6.5.2021
ISBN: 978-80-214-5943-4

Characterization of AlN nanolayers deposited on a surface of HOPG by PE-ALD

Rashid Dallaev

Doctoral Degree Programme (4th year), FEEC BUT

E-mail: xdalla03@vutbr.cz

Supervised by: Petr Sedlák

E-mail: sedlakp@feec.vutbr.cz

Abstract: In this study plasma-enhanced atomic layer deposition process of AlN has been performed with the purpose to test the expediency of highly oriented pyrolytic graphite (HOPG) to serve as a substrate in such process. The obtained samples were thoroughly analyzed using various analytical techniques. Atomic force microscopy was employed for studying topographic and morphological features of the surface; x-ray photoelectron spectroscopy (XPS) analysis supported by second ion-mass spectrometry method (SIMS) has been conducted on the obtained sample to investigate the chemical nature of the deposited films as well as elemental distribution. Temperature stability of HOPG makes it a suitable substrate for preparation of AlN films, being a bottom contact for further testing of the films electrical properties. The data gathered from the aforementioned techniques have indicated that HOPG is a viable choice for AlN ALD process.

Keywords: aluminium nitride, atomic layer deposition, highly oriented pyrolytic graphite, x-ray photoelectron spectroscopy, atomic force microscopy, second ion-mass spectrometry.

1 INTRODUCTION

Aluminium nitride (AlN) is a semi-conductive piezoelectric material with various promising physical and piezoelectric properties which attract attention of scientists from all over the world. AlN demonstrates an outstanding performance in a variety of electronics and covers quite a large range of applications which have been abundantly described by many researchers [1-11]. There is a lot of reports of AlN thin films grown using different physical and chemical vapour deposition methods (PVD, CVD) [2, 8, 9]. Atomic layer deposition (ALD) is one of the methods of CVD group. Its main advantages over others stem from the fact that reactions in ALD are sequential and self-limiting which enables a precise control over the film's growth at the atomic level [2, 8, 9, 11]. Further benefit of ALD is that after each reaction cycle the deposition chamber is purged from unreacted components of metalorganic precursors by an inert gas which leads to excellent purity and homogeneity of the film. So far, AlN thin films have been mostly deposited on silicon and sapphire wafers which proved to be reliable substrates to be employed in the process [8, 9, 11]. However, it remains a relevant topic of research to test out different substrates for AlN atomic layer deposition since chemical reactions that take place on the surface of the substrate as well as the nature of film/substrate interface may define the resulting quality of the entire deposited film. Thus, in this paper it has been decided to test out highly oriented pyrolytic graphite (HOPG) as a substrate for AlN ALD process. HOPG appears to be a promising substrate for AlN deposition process due to the carbon's ability to withstand extremely high temperatures, 3550 °C (a potential for high-temperature processing of the sample). Another advantage of HOPG is that its laminated nature allows for easy transferring of films grown on it onto a different foundation should such a need arise [12, 13].

2. EXPERIMENTAL DETAIL

To deposit AlN thin films using plasma enhanced atomic layer deposition (PE-ALD) on highly oriented pyrolytic graphite (HOPG) substrate Ultratech/CambridgeNanoTech Fiji 200 ALD instrument have been used. Obtained films have been analyzed using AFM, XPS and SIMS methods.

In total 1500 ALD cycles have been performed which translates into thickness of approximately 100nm (1cycle ≈ 0,629 Å). The temperature of deposition was 300 °C. The energy of plasma was 300W. The sequence of each cycle consisted of following steps:

1) introduction of TMA (0,06sec),
2) purge 10sec,
3) initiate flow of N2/H2 (20 sccm) and enable plasma (40 sec),
4) purge 5sec.

To ensure to purity of the surface, first layers of HOPG substrate were removed using an adhesive tape right before loading the samples into the ALD chamber.

SIMS analysis was carried out on ION-TOF TOF.SIMS 5 instrument in positive mode. The instrument enables analysis in dual gun mode. Oxygen gun with energy of 2KeV was employed for rough sputtering (material removal only), whereas Bi gun provides much slower sputtering rate and secondary ions produced by it are collected in an analyzer. Area of the crater was chosen to be 200x200nm, area of analysis 80x80 nm. The 3D modelling was done in the native software SurfaceLab 7.1 provided by the manufacturer.

Kratos Analytical Axis Supra instrument with Al Kα excitation source and emission current of 15mA was employed to perform XPS analysis. Wide spectrum was taken at of 80 eV. High resolution spectra were taken at of 20 eV. All spectra were calibrated by shifting major C1s peak (C-C bond) to 284.8 eV. The presented spectra were made in CasaXPS software, SG linear smoothing and background subtraction tools were used.

2 RESULTS AND DISCUSSION

3.1 Atomic force microscopy

Figure 1 shows surface images obtained by AFM. The average roughness for 2x2 and 5x5 μm images are 36,4 Å and 34,7 Å correspondingly. In total, around 15 images have been taken with different resolutions (0,5x0,5 μm, 2x2 μm, 10x10 μm). Several images have been taken at different spots all across the sample and exhibited the similar pattern. The average surface roughness value (Ra) fluctuates around ~35 Å for all of them, this indicates excellent uniformity of the deposited layer and conformal growth.

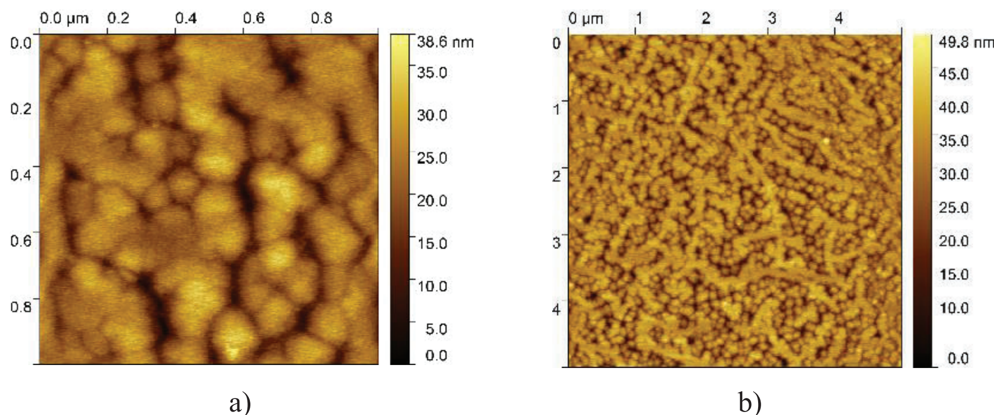

a) b)

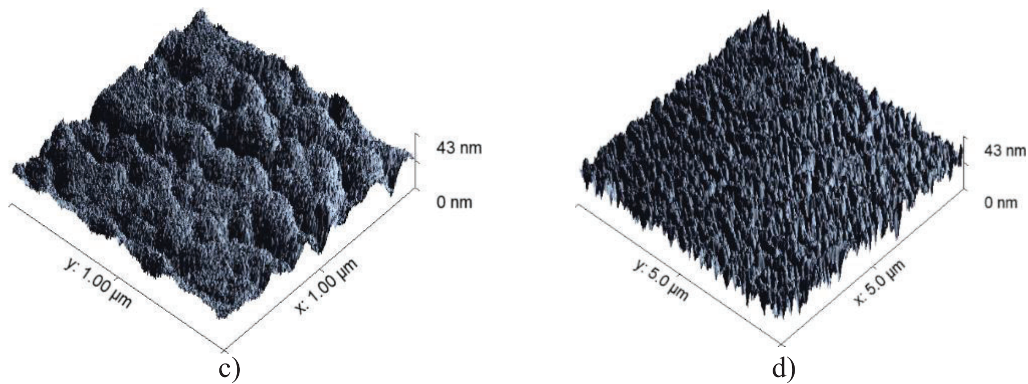

Figure 1. AFM images of: a) 2D 1x1 μm , b) 2D 5x5 μm, c) 3D 1x1 μm , d) 3D 5x5 μm

3.2 Secondary ion-mass spectrometry

Elemental distribution patterns according to SIMS are provided in Figure 2. During sputtering in SIMS not only individual ions are ejected from a material (C+, N+, O- etc.) but also composite ions (OH-, CH3-, AlO+ etc.) and even molecules. Which is why, in order to get a complete picture about the target compound we need to search for all possible combinations of its constituents, in our case those they are N+, AlN (a, b) and Al (c). By looking at these 3D images of ejected ions distribution we can clearly tell at which points the AlN ends and HOPG substrate begins. 3D profile of carbon (d) is also given to emphasize that shift. Furthermore, some of the carbon can also be noticed in the AlN layer, that is explained by the fact that the precursor employed in the ALD process (TMA) contains carbon some of which might have formed different bonds within the layer, which is also confirmed by XPS results.

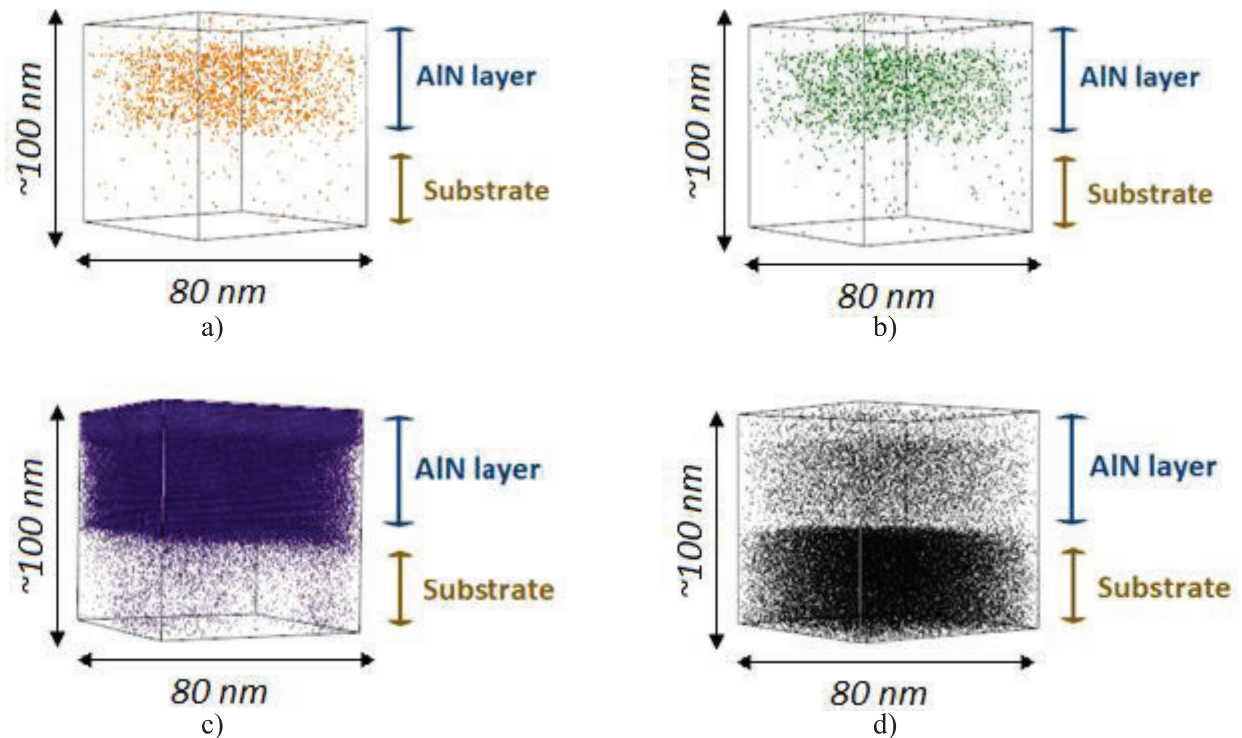

Figure 2. SIMS 3D distribution for AlN on HOPG: a) N+, b) AlN+, c) Al+, d) C+

3.1 X-ray photoelectron spectroscopy (XPS) data

XPS spectra are given in Figure 3. Wide spectum (fig. 3a) shows that the surface of the films is heavily oxidized and some carbon impurities are also present. The presence of carbon and oxygen is the result

of the samples exposure to atmosphere after the deposition. Thus, the bulk of the sample is expected to have superior degrees of purity. The nitrogen peak (fig. 3b) consists of three subpeaks with binding energies of 396,7 eV, 398,3 eV and 399,9 eV. The biggest of them located at 396,7 eV and according to a number of sources [14-18] is the one belonging to N-Al. The remaining two are located at 398,2 eV and 400 eV and attributed to N-O and N-Al-O correspondingly [14, 16].

Aluminum exhibits two subpeaks (fig.3c) the biggest occurs at 74 eV and is assigned as Al-N bond, the same energy values for Al-N bond are reportied in literature [15, 16]. There is also a good correlation with the nitrogen pieak in this regard, which also exhibits the presence of Al-N bond. The second peak has energy of ~73,5 eV and we speculate belongs to Al-Al defects which are though small in percentage but nonetheless present in the film. Given the high affinity of Al/AlN to oxidization [15, 16], both during the deposition process as well as in the open air, Al-O subpeak could also be reasonably anticipated here, however, it occurs at higher binding energies (>75eV) [19, 20] and hasn't been noted in this particular sample. XPS spectra have been taken at several different points on the sample surface and proved to be practically identical.

It appears instead that the bulk of the oxygen is bound to carbon in one way or the other which can be seen from C1s and O1s high-resolution spectra (fig. 3d and fig. 3e). Deconvolution of C1s resulted in 3 subpeaks located at 289,2 eV, 287,4eV and 284,8eV which correspond to O-C=O, C-O-C and C-C bond correspondingly [21]. By looking at O1s spectrum (fig. 3e) it can be inferred that the rest of the oxygen is bound to nitrogen forming N-O bond (530,3 eV). Overall, carbon and oxygen are undesirable but inevitable contaminants in ALD AlN their presence can be minimized by adjustments in the ALD process (temperature, pressure, precursor type) or by post-treatment of deposited samples (annealing, etching). Studying of oxygen impurities in AlN films is important since it is known to have negative effects on the resulting qualities of the film such as optical absorption and thermal conductivity [16].

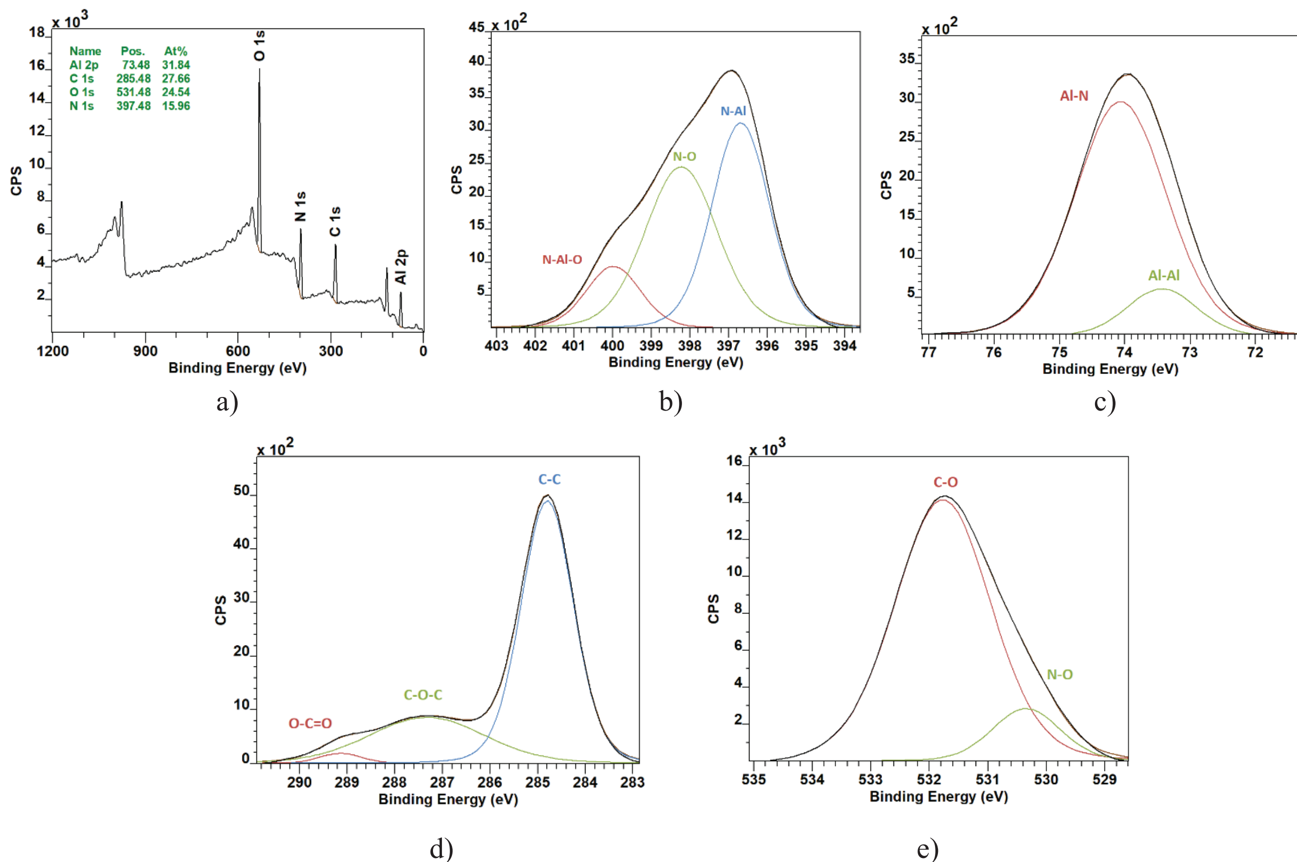

Figure 3. XPS high -resolution spectra for AlN on HOPG: a) wide spectrum, b) N1s, c) Al2p, d) C1s, e) O1s

3 CONCLUSION

In this paper we attempted to deposit AlN thin films using PE-ALD equipment on a previously untested substrate - HOPG. Surface analysis of the samples done by AFM indicates that deposited AlN layer exhibits quite uniform surface topography. Such methods as XPS and SIMS have been employed to investigate the chemical structure of the samples obtained. The data provided by these methods unambiguously confirms the presence of AlN compound, although not in the pure form. We can also observe formation of Al-Al and N-O defects as well as some impregnation of carbon in the XPS spectra which probably occur due to imperfection of the equipment's vacuum system or post-deposition surface oxidization. The removal of the undesired compounds from the films is the implication for future research, high-temperature annealing in nitrogen atmosphere might have a positive effect in this regard which is made possible thanks to carbon extremely high melting point. Presently, however, HOPG seems to be a promising substrate to be utilized in AlN deposition process.

ACKNOWLEDGEMENT

Research described in this paper was financially supported by the Ministry of Education, Youth and Sports of the Czech Republic under the project CEITEC 2020 (LQ1601) and by Internal Grant Agency of Brno University of Technology, grant No. FEKT-S-20-6352. A part of the work was carried out with the support of CEITEC Nano Research Infrastructure supported by MEYS CR (LM2018110).

REFERENCES

[1] A. Pandey, J. Kaushik, S. Dutta, A.K. Kapoor, D. Kaur, Electrical and structural characteristics of sputtered c-oriented AlN thin films on Si (100) and Si (110) substrates, Thin Solid Films. 666 (2018) 143–149. doi:10.1016/j.tsf.2018.09.016.

[2] L. Tian, S. Ponton, M. Benz, A. Crisci, R. Reboud, G. Giusti, F. Volpi, L. Rapenne, C. Vallée, M. Pons, A. Mantoux, C. Jiménez, E. Blanquet, Aluminum nitride thin films deposited by hydrogen plasma enhanced and thermal atomic layer deposition, Surf. Coatings Technol. 347 (2018) 181–190. doi:10.1016/j.surfcoat.2018.04.031.

[3] D.L. Ma, H.Y. Liu, Q.Y. Deng, W.M. Yang, K. Silins, N. Huang, Y.X. Leng, Optimal target sputtering mode for aluminum nitride thin film deposition by high power pulsed magnetron sputtering, Vacuum. 160 (2019) 410–417. doi:10.1016/j.vacuum.2018.11.058.

[4] I. Gablech, V. Svatoš, O. Caha, A. Dubroka, J. Pekárek, J. Klempa, P. Neužil, M. Schneider, T. Šikola, Preparation of high-quality stress-free (001) aluminum nitride thin film using a dual Kaufman ion-beam source setup, Thin Solid Films. 670 (2019) 105–112. doi:10.1016/j.tsf.2018.12.035.

[5] Y. Wu, C.H. Jia, W.F. Zhang, Growth of conductive and insulative highly-orientated aluminum nitride thin films using laser molecular beam epitaxy, Diam. Relat. Mater. 25 (2012) 139–143. doi:10.1016/j.diamond.2012.02.022.

[6] Y. Bian, M. Liu, G. Ke, Y. Chen, J. DiBattista, E. Chan, Y. Yang, Aluminum nitride thin film growth and applications for heat dissipation, Surf. Coatings Technol. 267 (2015) 65–69. doi:10.1016/j.surfcoat.2014.11.060.

[7] E. Österlund, J. Kinnunen, V. Rontu, A. Torkkeli, M. Paulasto-Kröckel, Mechanical properties and reliability of aluminum nitride thin films, J. Alloys Compd. 772 (2019) 306–313. doi:10.1016/j.jallcom.2018.09.062.

[8] R. Dallaev S. Stach, Ş. Ţălu, D. Sobola, A. Méndez-Albores, G.T. Córdova, L. Grmela, Stereometric Analysis of Effects of Heat Stressing on Micromorphology of Si Single Crystals, Silicon. (2019). doi:10.1007/s12633-019-0085-4.

[9] A.I. Abdulagatov, S.M. Ramazanov, R.S. Dallaev, E.K. Murliev, D.K. Palchaev, M.K. Rabadanov, I.M. Abdulagatov, Atomic Layer Deposition of Aluminum Nitride Using Tris(diethylamido)aluminum and Hydrazine or Ammonia, Russ. Microelectron. (2018). doi:10.1134/S1063739718020026.

[10] H. Zhang, C.L. Marshall, Atomic layer deposition: Catalytic preparation and modification technique for the next generation, Chinese J. Catal. 40 (2019) 1311–1323. doi:10.1016/s1872-2067(19)63321-8.
[11] Y. Li, C. Zhang, X. Luo, Y. Liang, D. Wuu, C. Tin, X. Lu, Applied Surface Science Surface , structural and optical properties of AlN thin films grown on different face sapphire substrates by metalorganic chemical vapor deposition, Appl. Surf. Sci. 458 (2018) 972–977. doi:10.1016/j.apsusc.2018.07.138.
[12] R. Dallaev, N. Papež, D. Sobola, S. Ramazanov, P. Sedlák, Investigation of structure of AlN thin films using Fourier-transform infrared spectroscopy. In Procedia Structural Integrity. Procedia Structural Integrity. Elsevier B.V., 2020. s. 601-606. ISSN: 2452-3216.
[13] P. Kaspar, D. Sobola,; R. Dallaev, S. Ramazanov, A. Nebojsa, S. Rezaee, L. Grmela, Characterization of Fe2O3 thin film on highly oriented pyrolytic graphite by AFM, Ellipsometry and XPS. Applied Surface Science, 2019, roč. 493, č. 1, s. 673-678. ISSN: 0169-4332.
[14] F. Dwikusuma, T.F. Kuech, X-ray photoelectron spectroscopic study on sapphire nitridation for GaN growth by hydride vapor phase epitaxy: Nitridation mechanism, J. Appl. Phys. 94 (2003) 5656–5664. doi:10.1063/1.1618357.
[15] P. Motamedi, K. Cadien, XPS analysis of AlN thin films deposited by plasma enhanced atomic layer deposition, Appl. Surf. Sci. 315 (2014) 104–109. doi:10.1016/j.apsusc.2014.07.105.
[16] L. Rosenberger, R. Baird, E. McCullen, G. Auner, G. Shreve, XPS analysis of aluminum nitride films deposited by plasma source molecular beam epitaxy, Surf. Interface Anal. 40 (2008) 1254–1261. doi:10.1002/sia.2874.
[17] H. Kim, N. Do, S. Chul, H. Ju, B. Joon, Improved interfacial properties of thermal atomic layer deposited AlN on GaN, Vacuum. 159 (2019) 379–381. doi:10.1016/j.vacuum.2018.10.067.
[18] M. Zhu, P. Chen, R.K.Y. Fu, W. Liu, C. Lin, P.K. Chu, AlN thin films fabricated by ultra-high vacuum electron-beam evaporation with ammonia for silicon-on-insulator application, Appl. Surf. Sci. 239 (2005) 327–334. doi:10.1016/j.apsusc.2004.05.287.
[19] O.H. Kim, D. Kim, T. Anderson, Atomic layer deposition of GaN using GaCl3 and NH3, J. Vac. Sci. Technol. A Vacuum, Surfaces, Film. 27 (2009) 923–928. doi:10.1116/1.3106619.
[20] F. Jose, R. Ramaseshan, S. Dash, S. Bera, A.K. Tyagi, B. Raj, Response of magnetron sputtered AlN films to controlled atmosphere annealing, J. Phys. D. Appl. Phys. 43 (2010) 075304. doi:10.1088/0022-3727/43/7/075304.
[21] N.C. David, D. Anavi, M. Milanovich, Y. Popowski, L. Frid, E. Amir, Preparation and properties of electro-conductive fabrics based on polypyrrole: Covalent vs. non-covalent attachment, IOP Conf. Ser. Mater. Sci. Eng. 254 (2017). doi:10.1088/1757-899X/254/3/032002.

8 Study of hydrogen content in AlN nanolayers deposited by PE-ALD

8.1 Motivation of the study

As was demonstrated in the results of the Chapters 4 and 5, samples obtained using thermal ALD exhibited rather high amount of hydrogen impurities (22-26 at.%). Given, the fact that hydrogen presence can drastically worsen the quality of the AlN layer, this issue has become somewhat concerning. Which is why, it was decided to look into the problem further. This time the AlN thin layer were deposited with the use of entirely different recipe and with the involvement of plasma. The research described in this chapter is the result of my 35-day internship in Sweden (Uppsala University, The Tandem Laboratory) where I have been working with the advanced equipment utilizing 5MV NEC PELLETRON particle accelerator. The results described in this chapter are currently under consideration in an impact journal.

8.2 Relevance of the study

The main focus of the current study is to investigate the degree of hydrogen impurities occurring in AlN deposited by PE-ALD with the use of trimethylaluminum (TMA) and N_2/H_2 plasma as precursors for aluminum and nitrogen respectively. By investigating the deposited films one can draw conclusions on how PE-ALD compares to its thermal counterpart in terms of hydrogen impregnations. The reason why the mixture of these two gases is used instead, for instance, pure nitrogen is that hydrogen atoms seem to positively affect the growth kinetics of the AlN layers by maximizing density of Al–N bonds, reducing the oxygen contamination, passivating defects, and so on. Therefore, the use of hydrogen alongside nitrogen during ALD of AlN minimizes the frequency of Al–O and Al-Al defects and allows to obtain resulting layers of superior quality overall [59, 60].

Since both precursors in this experiment contain hydrogen atoms, they both can be considered as potential sources of hydrogen contamination. Investigation of hydrogen contamination is important due to the fact that its presence in the structure may severely damage electrical, mechanical and optical properties of semi-conductive and metallic materials, especially in high concentrations. Most commonly, however, hydrogen causes embrittlement which is understood as increase in brittleness over time. Altogether, a great amount of materials may deteriorate in quality as a result of hydrogen absorption. [61, 62].

The most common and informative methods to study hydrogen content are the ones belonging to so-called ion-beam analysis (IBA) group. IBA group encompasses a large amount of methods which utilize medium or high energy primary ions in order to analyze the chemical composition of samples, however their usage is not limited to that. Some of the most prominent of IBA methods are: Rutherford backscattering spectrometry (RBS); secondary ion mass spectrometry (SIMS); elastic recoil detection analysis (ERDA) and nuclear resonance analysis (NRA), the latter two being widely employed for detection of hydrogen [63]. While other more readily available and conventional techniques such as for instance XPS and FTIR can be employed to detect hydrogen bonds, there is no possibility to use these methods for adequate estimation of the hydrogen concentration and distribution.

Not all IBA methods, however, are suitable for the task of hydrogen evaluation. For instance, RBS processing can get particularly problematic in cases when analyzed samples contain heavy elements (e.g. layer consisting of light elements on a heavy substrate), in which case peaks of light elements end up being drowned in those of heavy elements [64]. Additionally, the specifics of RBS make it impossible to detect elements which are lighter than the ones constituting the primary beam.

SIMS while not being specifically designed for detection of hydrogen can still be partially employed for this purpose by looking for hydrogen-containing ions. While any sort of quantification of hydrogen is unachievable (even with the use of standards) one can still draw conclusion by investigating and juxtaposing intensity of hydrogen atoms detected in different spectra, provided they were taken under the same parameters and at the same time. SIMS can also give a tentative idea on the hydrogen distribution [65].

Thus, when it comes to the study of quantity and distribution of hydrogen atoms, there are mainly two IBA methods which are up to the challenge. These methods are: elastic recoil detection analysis (ERDA) and nuclear resonance analysis (NRA), namely its subtype - resonance NRA, otherwise called nuclear resonance broadening (NRB). Additionally, oftentimes these methods employed particularly for the purpose of hydrogen investigation. These techniques are capable of detection and relatively accurate quantification of light elements in samples in a non-destructive manner and up to ~1 μm depth, which renders them extremely valuable tools when such analysis is required [66].

8.3 Sample preparation

For deposition of AlN thin films an ALD instrument *Ultratech/CambridgeNanoTech Fiji* 200 located at *CEITEC Nano* cleanrooms in Czech Republic, Brno was used. A recipe for a single ALD cycle consisted of the following stages:

1) TMA pulse → 2) wait 10 sec → 3) turn on N_2/H_2 flux → 4) wait 1 sec → 5) turn on plasma 300W (40 sec) → 6) turn off N_2/H_2 flux → 7) wait 5 sec

In total 3 separate depositions were performed with the following deposition parameters:

1) The flux intensity of N2/H2 = 20sccm; TMA pulse time = 0.06s; 1200 cycles in total; LSAT substrate which has the following chemical formula $(LaAlO_3)_{0.3}(Sr_2TaAlO_6)_{0.7}$

2) The flux intensity of N2/H2 = 100sccm; TMA pulse time = 0.12s; 700 cycles in total; SiC 6H substrate

3) The flux intensity of N2/H2 = 150sccm; TMA pulse time = 0.15s; 600 cycles in total; Si substrate

These changes in recipe were introduced with an aim to analyse how the difference in intensity of N_2/H_2 flux and TMA dosing would affect the resulting layer. The different amount of cycles was tried with the purpose to investigate if the thickness of the film has any effect on the distribution of hydrogen and other impurities. Parameters that remained constant for all depositions are: power of the plasma source - 300 Watt; chamber temperature - 300 °C; the pulse time of N_2/H_2 gas mixture - 40s; chamber pressure – 2.4×10^{-3} Torr. It should be also stated that not one but several samples were obtained as a result of each deposition process. All consecutive measurements were performed for every sample in order to ensure precision of the experiment. Thus, the samples belonging to the same deposition batch demonstrated results indistinguishable from one another.

Additionally, some of the samples from the 3rd deposition batch were subjected to high temperature annealing (1350 °C) in nitrogen atmosphere for 1 hour in order to investigate what sorts of changes such temperature processing would introduce into the samples structure, and most importantly how it would affect hydrogen concentration. As will be shown below, the samples from the 3rd batch demonstrated superior quality in comparison to others, which is the reason why they were chosen for post-processing. Furthermore, Si substrate being by far the most

common among the three is of greater interest in terms of utilization in post-processing procedures. For convenience, all the samples obtained and discussed within this study have been assigned designations as given in Table 1.

Table 1. Details and IDs of prepared samples

Samples	Description
#1	20sccm/0.06sec TMA; LSAT substrate; 1200 cycles
#2	100sccm/0.12sec TMA; SiC substrate; 700 cycles
#3	150sccm/0.15sec TMA; Si substrate; 600 cycles
#4	150sccm/0.15sec TMA; Si substrate, 600 cycles; annealed (1350 °C)

The substrates were purchased from *Biotain Crystal Co., Ltd* and were sealed in airtight packages upon manufacturing, therefore no pre-treatment was necessary. All three substrates are heat-resistant with very high melting points: 1414, 1840 and 2730 °C for Si, SiC and LSAT correspondingly. All three substrates were preliminarily tested in terms of growth tendency. The GPC values for all substrates turned out to be practically indistinguishable, suggesting that all three substrate provide similar degree of chemisorption for initial Al atoms. Given the aforementioned, in this study, it was decided to set aside speculations on advantages of a certain substrate over the others. Instead, the focus will be made on how the change in the flux intensity affects the GPC and chemical composition in the resulted layers. The GPC values as a function of temperature and precursor pulse times are given in Figure 4 for three different flux intensities of N_2/H_2 and TMA dosing. The values were calculated based on the data provided by spectroscopic ellipsometry.

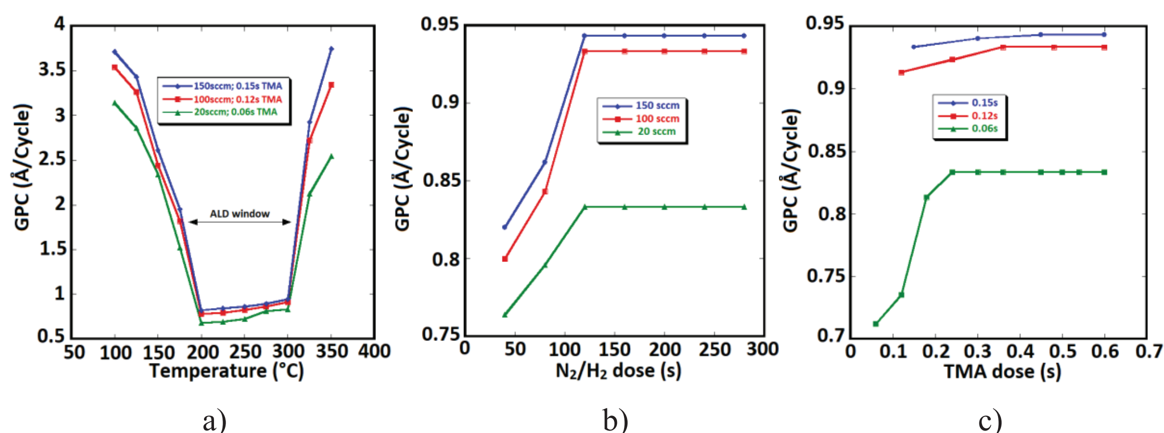

a) b) c)

Figure 4. GPC as a function of: a) temperature of deposition; b) pulse time of N_2/H_2, c) pulse time of TMA

According to Figure 4a The ALD windows appears to fall within 200-300 °C temperature range. In this regard the temperature of 300 °C was chosen for all depositions. The growth rate at the chosen deposition temperature was 0.83, 0.93 and 0.94 Å for 20, 100 and 150sccm of N_2/H_2 flux respectively. Taking into account these values and the total amount of cycles one can calculate thickness values of the resulting films, which are: 99,6 nm; 65.1nm and 55.8nm for 1, 2 and 3rd depositions correspondingly. Figure 4 (b, c) shows us GPC as a function of pulse time for both precursors. It can be observed that the deposition rate stabilizes after at the 3rd introduction of both precursors, indicating stoichiometric growth. Intensity of flux seems to be directly proportional to the growth with the difference being most noticeable between 20 and 100 sccm and not so much between 100 and 150 sccm. The growth tendency is analogous to the one of TMA precursor where growth rate maximizes at ~0.2s of pulse time. Increasing the pulse time of TMA and intensity of the flux of N_2/H_2 beyond the maximum values presented here has also been tested and did not produce any noticeable changes. Based on these results in can be inferred that optimal saturation occurs at the maximum values presented here (150sccm/0.15s), at least for the equipment used in this study. Even though the samples from the 1st and 2nd batches were found to be deposited under suboptimal parameters, the obtained data and discussion on them will be provided for comparative purposes. However, the data most relevant to the overall conclusion of this study should be made based on the results obtained for the samples from the 3rd batch and their annealed variants.

8.4 Characterization methods

Atomic force microscopy (AFM) setup

AFM images were taken using scanning probe microscope Bruker Dimension Icon (ICON-SPM) equipment in ScanAsyst mode of analysis devised by Bruker (*CEITEC Nano*, Czech Republic, Brno). The processing of the images and extraction of the data on average roughness was carried out with the Gwyddion software.

Secondary-ion mass spectrometry (SIMS) setup

SIMS analysis was conducted using *ION-TOF TOF.SIMS5* instrument (*CEITEC Nano*, Czech Republic, Brno) in dual-gun non-interlaced mode, which means sputtering and analysis is done alternately. One gun is utilized for aggressive sputtering/quick material removal with 2keV Cs primary ions, while the second gun utilizes low energy Bi^+ ions during which secondary ions are sent to analyser where they are measured by the time of flight detector. The raster size was set to be 200x200µm, the analysing area to 100x100 µm. All measurements were done in the negative mode. The raw data were exported from the native software *SurfaceLab 7* and then rebuilt in *OriginPro 2015*.

Nuclear reaction analysis (NRA) setup

Both NRA and ERDA measurements are implemented using the 5MV NEC PELLETRON accelerator at the surface and profile measurement at Tandem Laboratory which is a part of Uppsala university, Sweden. The resonance at 6.385 MeV for the reaction $^{1}H(^{15}N,\alpha\gamma)^{12}C$ was used in the present experiment. A sample with a known amount of artificially implanted hydrogen (18 at.%) was used as a reference in order to calibrate γ-yield intensity. To avoid the loss of hydrogen during the measurement the beam was broadened to ~6-7mm and its current was minimized. Background noise was measured and subtracted from all values. Hydrogen percentage was further normalized according to stopping power and density. The graph from the collected values was built in *KaleidaGraph* software.

Elastic recoil detection analysis (ERDA) setup

The ERDA setup utilizes the same accelerator as that in NRA. For the measurement described in this study 36 MeV ^{127}I-ions were employed. The detector angle for backscattered ions and the elements constituting the samples was set to be 45°. The values on elemental distribution were extracted using a non-commercial community-built *Potku* software [67]. The more detailed description of the ERDA setup can be found elsewhere [68]. The ERDA images were further processed for the purpose of removing redundant noise in a graphical software.

8.5 Atomic force microscopy (AFM) results

AFM measurements were performed in order to investigate the surface morphology and how it is affected by the alterations in deposition recipes and as a result of high-temperature treatment. The 3D AFM images are presented in Figure 5. The roughness profiles are given in Figure 6. Average roughness (R_a) was calculated for all samples and was found to be 1.07 nm, 0.31 nm; 0.28nm; 4.35 nm for *#1, #2, #3* and *#4* correspondingly. The sample *#2* and *#3* indicate similar roughness values which is expected since the difference in the recipes and layer thickness for these samples is not significant. The *#1* sample which was obtained using the least 20sccm N_2H_2 and 0.06sec TMA shows inferior surface roughness, which higher than that of *#2* (Figure 5 b) and *#3* (Figure 5 c) almost by a factor of three. That is due to the fact that 20sccm N_2H_2 and 0.06 sec TMA are not optimal (as could be seen from the GPC measurement in Figure 4), and the increase in the roughness is a clear sign of undersaturation and suboptimal stoichiometry. The other reason is that sample *#1* has AlN layer almost two times thicker than #2 and #3 (1200 vs 700 and 600 cycles), and it is a general tendency that thicker layer demonstrate higher values of surface roughness [69].

The annealed sample *#4* (Figure 5 d) also demonstrates a massive increase in roughness and one can also see the formation of trenches. This coarsening of the surface and the tendency to coalesce into clusters has been discussed in the author's previous work [70] and indicates the crystallization of the AlN layer.

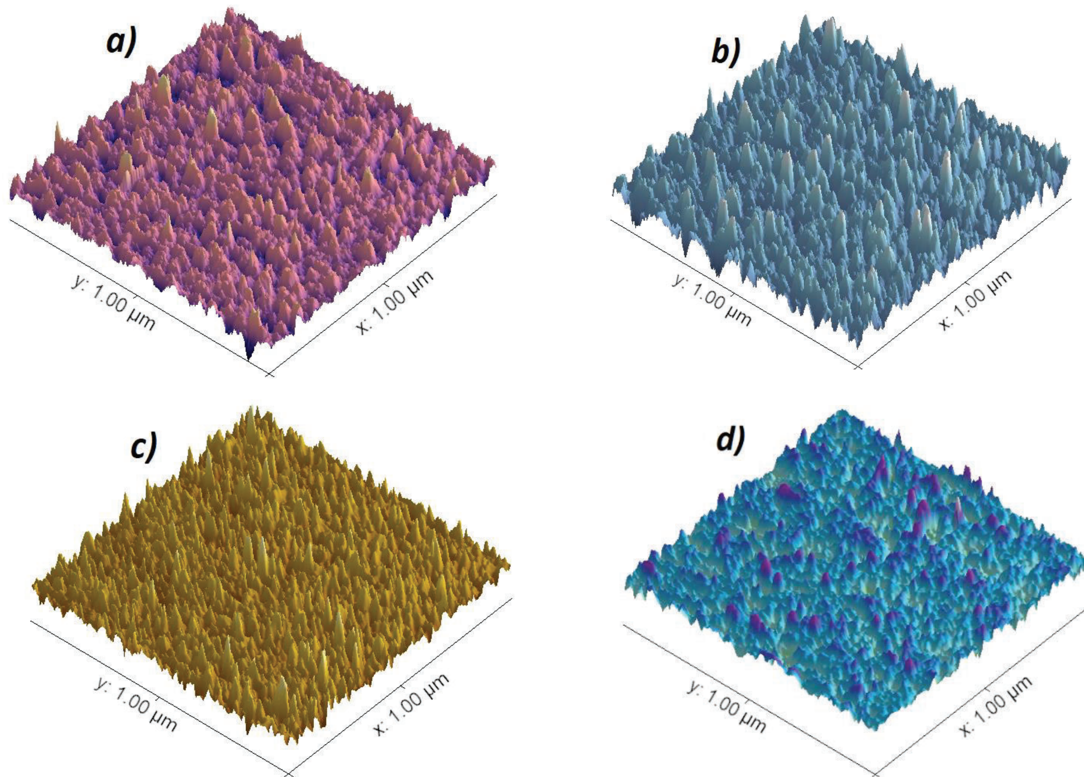

Figure 5. 3D AFM images of AlN thin films for: a) #1; b) #2; c) #3; d) #4

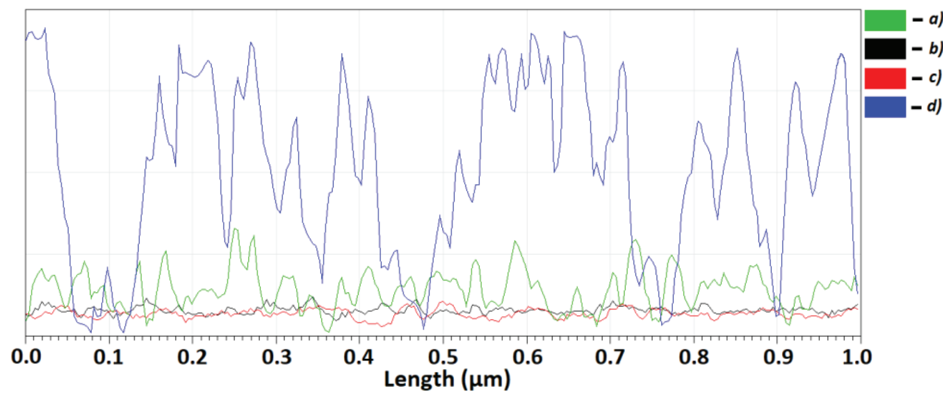

Figure 6. Comparison of surface roughness profiles for images presented in Figure 5.

8.6 Secondary-ion mass spectrometry results

The SIMS profiles are given in Figure 7 for AlN- (a) and H- (b) ions. When processing SIMS data in order to securely establish the presence of AlN one can directly search for AlN^- ion. The reason for this is that this ion is situated at ~41u on the mass spectrum, it is well defined and separated from other ions which are likely to exist in the analyzed samples, this fact eliminates any ambiguity. AlN^- distribution are presented for all samples obtained within this study.

All sample have a visible abrupt transition from AlN layer into substrate with the exception of the one which has undergone the annealing procedure. The annealed sample appears to have

lost the interface between the layer and the substrate suggestion that some sort of fusion has taken place. The fact that melting point of Si (~1400 °C) is close to the temperature values utilized in the vacuum chamber (1350°C) makes such fusion possible, it will be described in more detail, however, in the discussion of ERDA and NRA results.

The direct calculation of thickness through SIMS is complicated by the fact that it is necessary to know the density in order to produce accurate values. But given that the amount of cycles were different for the various batches of samples, namely 600 (150sccm, 0.15s), 700 (100sccm, 0.12s), and 1200(20sccm, 0.06s), it can be seen that SIMS data on thickness ratios are in excellent agreement with the GPC measurements (Figure 4).

The hydrogen (H-) profile shows similar tendencies as AlN profile. One can observe a slight increase in intensity at the interface level, however whether this increase is genuine or a result of matrix effects is difficult to establish [71].

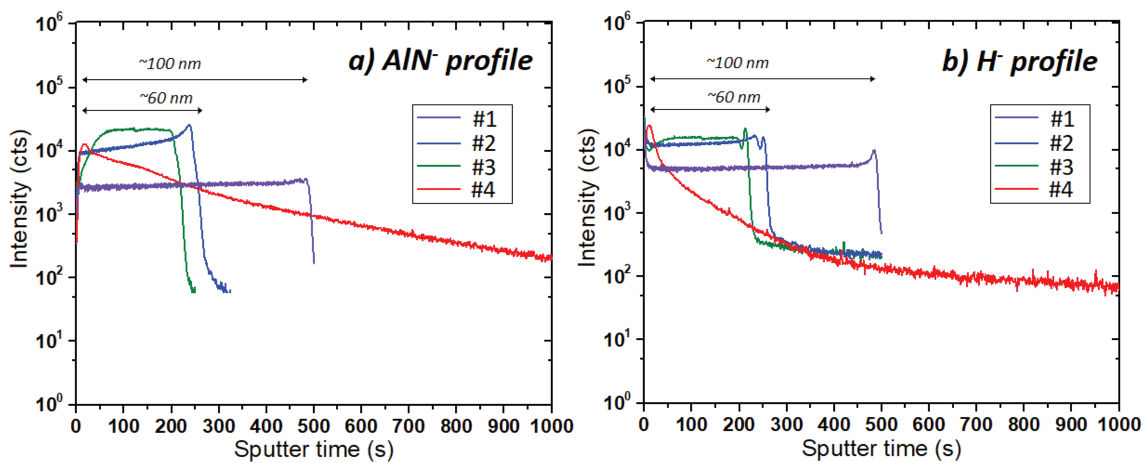

Figure 7. SIMS profiles for: a) AlN^- ions; b) H^- ions

8.7 Nuclear reaction analysis results

Figure 8 demonstrates NRA spectra for all the samples. Values at 6400 keV, which is slightly above the surface resonance energy (6385 keV), could be misleading due to H_2O accumulation. The longer a sample is exposed to air the more H_2O will be present at the surface region. Hence, the values at 6500 keV provide more realistic picture on hydrogen concentration, which varies from ~3 to ~5 at.%. The beam energy was increased up to 7000 keV during NRA measurement by the step of 100 keV, which after calculating stopping power in SRIM software was estimated to be ~35 nm. It should be noted that these values are approximate, since calculating stopping

power for materials with uncertain elemental concentration is a tricky matter. As can be seen from the spectrum, only 2 samples have concentrations larger than 0 at.% at the 6600 keV, which is well anticipated, considering that only 2 out of 4 samples have the layer thickness exceeding 70nm, those sample are the 20sccm; 0.06s TMA sample (purple) which had the most cycles during the deposition (1200) and the annealed sample (red) which has apparently fused into the substrate and by so doing extended itself beyond its initial thickness value (55.8 nm). Despite that stepping in this particular NRA measurement is rather rough, it serves its main purpose well, that purpose being corroboration of the results provided by ERDA below.

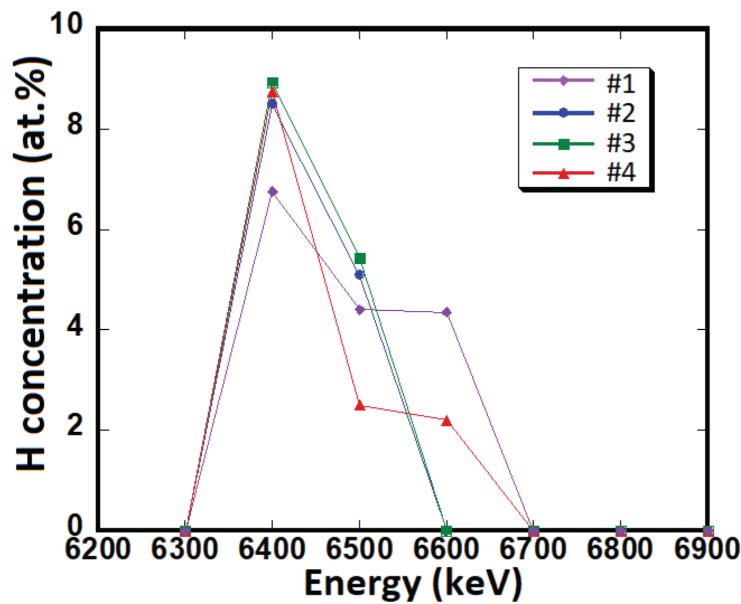

Figure 8. Hydrogen depth profile within the AlN layers according to NRA (100keV ≈ 35nm)

In this section, a comparison for hydrogen concentration values extracted from both NRA and ERDA analyses (see Table 2) is also provided. As can be noticed, there is a good agreement between the values and the deviations across the two techniques are within the expectations.

Table 2. Hydrogen concentration in obtained AlN according to NRA and ERDA

#Sample	NRA (surface)	NRA(bulk)	ERDA(average)
20sccm; 0.06s TMA	6.72%	4.41%	4.20%
100sccm; 0.12s TMA	8.51%	5.09%	4.62%
150sccm; 0.15s TMA	8.94%	5.43%	4.71%
100sccm; 0.12s TMA annealed	8.75%	2.49%	2.23%

8.8 Elastic recoil detection analysis results

ERDA spectra in Figure 9 are provided for illustrative reasons and in order to emphasize a few peculiar phenomena. The first one is that according to the spectra all samples appear to be heavily oxidized. As has been stated in the introduction section, oxidization of amorphous AlN upon exposure to air is a notorious and widely reported issue [72-28]. Another thing worth noticing is the lack of mass resolution which results in elements which are close to each other in mass appear as a single curve, as is the case with aluminum (atomic weight ≈ 27) and silicon (atomic weight ≈ 28) in the spectra (Figure 9 b, c). However, at closer inspection the delineation between these elements can be noticed as demonstrated in 3x magnified segments of the curves presented in corresponding circles. In this ERDA measurement a standard silicon detector was used. More advanced type of detector as for instance gas ionization chamber [68] would most likely provide superior mass resolution. In ERDA spectra for the AlN deposited on LSAT substrate (Figure 9 a) the situation is slightly different - since in this scenario Al is a constituent element of both the layer and the substrate there would be no delineation, instead however, one can clearly observe the transition from AlN films to the LSAT substrate by the change in intensity, what is more - intensity of Al counts appears to be much higher in the film than in substrate.

For the annealed sample (Figure 9 d) the delineation between Si and Al is no longer distinguishable, which perfectly correlates with what what could be observed in the SIMS spectrum. High temperature appears to cause diffusion of AlN layer into the substrate removing the interface between the two. Even though the concentration of Al atoms is still gradually decreasing deeper into the sample, this change is no longer sufficient to result in a visible transition on the spectrum.

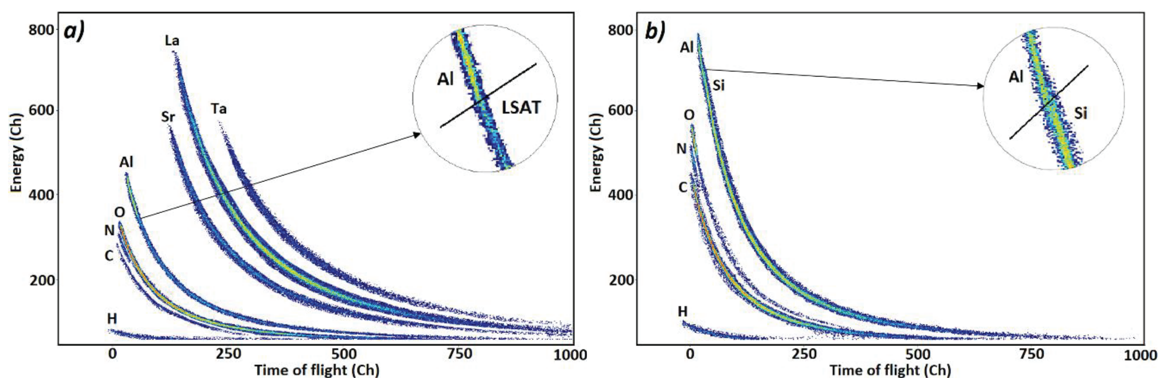

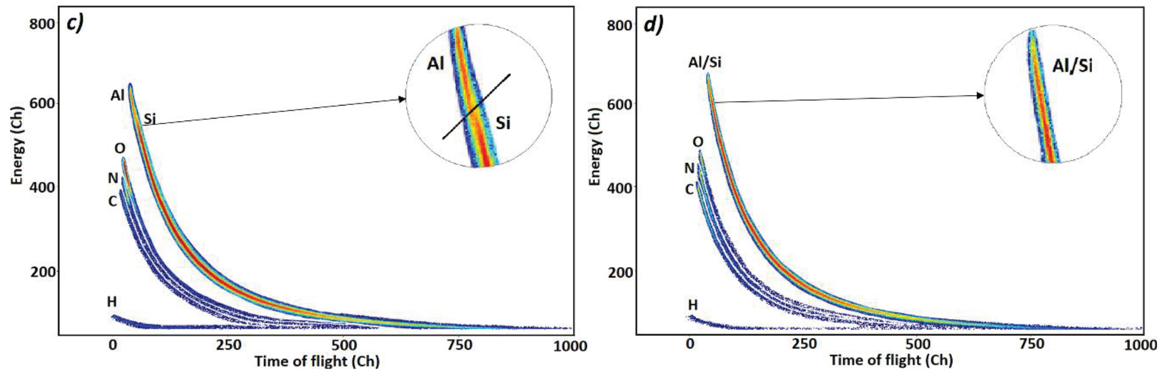

Figure 9. ERDA spectra for: a) #1; b) #2; c) #3; d) #4

The depth profiles extracted form the ERDA data are shown in Figure 10. The substrate peaks for SiC and LSAT were excluded from the spectra since they have little to none bearing to the discussion of the results. The Si peak, however, for annealed and as-deposited samples were integrated in ordrer to provide a comparison and draw the reader's attention to an interesting phenomenon occurring at 1350 °C between AlN layer and the Si substrate. As has been mentioned earlier, due to the lack of mass resolution of the used detector and disappearance of the interface between the film and the substrate – one can no longer see the delineation between Al and Si ions for the annealed sample (Figure 9 d). For this reason, it is rendered extremely difficult to separate Al from the Si signal in the software, which is why its distribution in Figure 10d might not be as precise as it is for other elements. Nevertheless, judging by the distribuiton pattern to extracted from ERDA data, one can conclude that there seem to be a rather drastic difference between annealed and as-deposited samples. First of all, the depth profile of the annealed sample confirms the idea of 'fusion' and, as expected, there is no abrupt transition from the layer into the substrate, instead, one can observe a gradual decrease in intensity of all elements. Effect provided by annealing seems to be rather considerable as the AlN layer-related ions are still detected at the depth which exceeds the thickness of the initial layer by a factor of three (55nm vs 180nm+). It should be emphasized here, that data acquired from ERDA measurement perfectly correlates with what could be observed in the SIMS profile (see Figure 7 a,b). The other aspect worth of attention is the significant reduction in oxygen concentration and increase in that of nitrogen, which confirms that aggressive annealing of AlN layer in nitrogen atmosphere has indeed produced a favorable effect on the overall quality of the film. With that being said, such treatment can be viable in terms alleviation of the persistent AlN oxidization issue. However, one might want to consider using a more heat-resistant substrate (SiC, HOPG etc.) to avoid the said fusion, in the

cases where preservation of well-defined interface between the substrate and the layer is preferential.

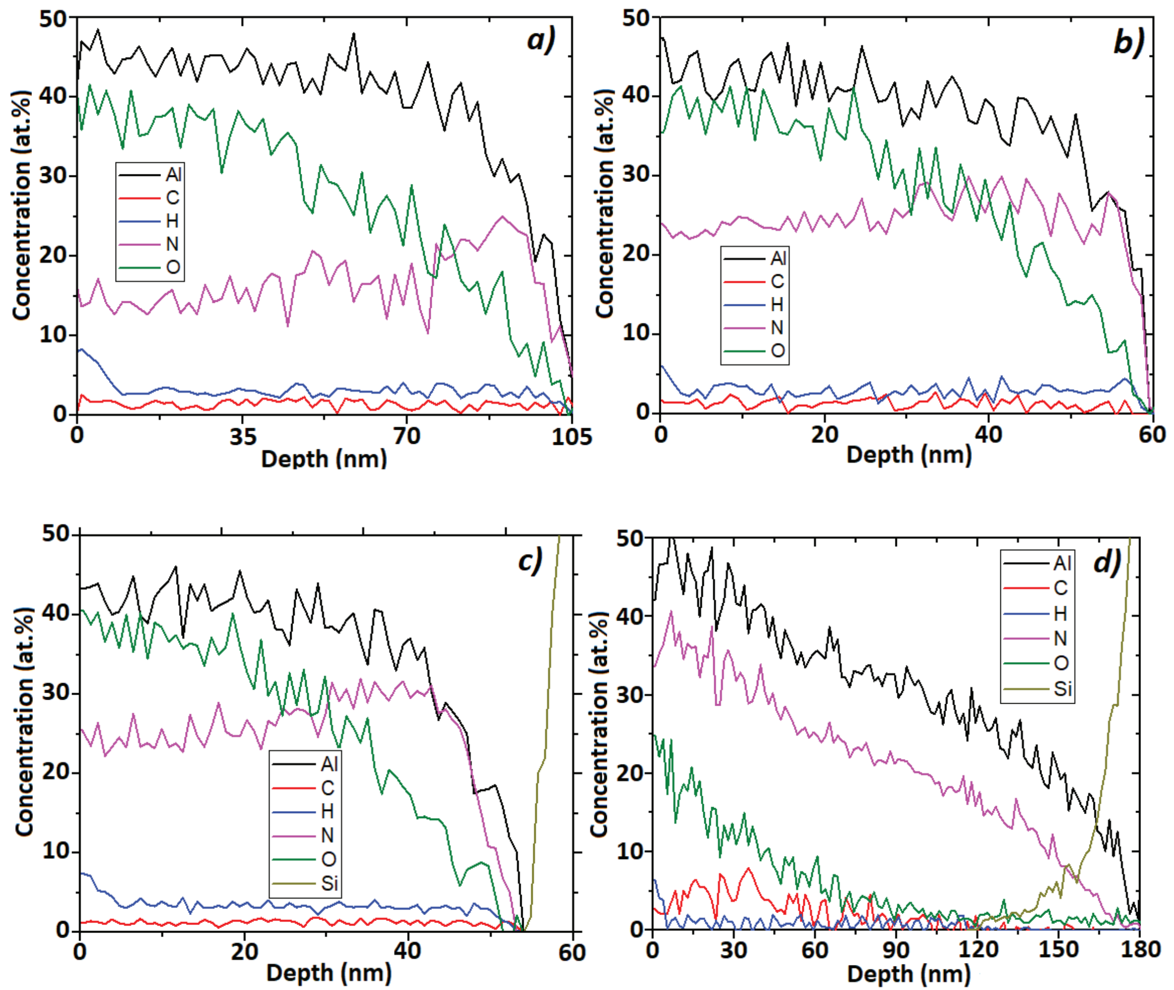

Figure 10. Elemental distribution in AlN samples according to ERDA: a) #1; b) #2; c) #3; d) #4

The approximate elemental concentration according to ERDA are given in Table 3. As we can see, the carbon concentration is low (within 1-2%) with only the annealed sample exhibiting an increased amount, which must have been a result of some sort of contamination which took place in the chamber during annealing process. Other than carbon, concentration values are in good agreement with the values reported by a similar study [79]. In that study, authors suggest that one of the possible reasons of carbon occurrence is an unwanted reaction between nitrogen atoms and CH-groups during plasma introduction which results in appearance of C-N bonds; the other possible reason is incomplete removal of TMA organic ligands from Al atoms which are adsorbed by the substrate. This latter speculation also partially explains the presence of hydrogen, with it being a constituent element of the said ligands. The other part of the hydrogen amount is

likely to occur from the nitrogen precursor introduction stage. N_2/H_2 gas mixture may cause incorporation of amine groups (N-H) [80]. The increased hydrogen concentration at the surface comes from H_2O accumulation, as was already established in the NRA section. On the whole, uniform depth profiles of both carbon and hydrogen indicate that these contaminations take place due to series of unwanted but altogether unavoidable side reactions occurring throughout the entire deposition process. However, it should be stated that concentration of these so-called PE-ALD defects is within reasonable bounds. The thermal ALD, in general, results in far greater amounts of carbon and hydrogen concentrations

Table 3. Approximate concentrations of elements within the layers extracted from the ERDA depth profiles.

Element / Sample	Al	C	H	N	O
a)	41,3%	1.7%	4.2%	18.3%	34.5%
b)	34.9%	1.4%	4.6%	26.9%	32.2%
c)	35.4%	1.3%	4.7%	29.1%	29.5%
d)	44.2%	4.1%	2.2%	34.7%	14.8%

8.9 Conclusion of the study

In this work several batches of AlN samples by plasma-enhanced atomic layer deposition were deposited with the main goal being investigation of the amount of hydrogen impurities within the deposited samples. The recipe parameters were different for each deposition in order to establish whether alteration in N_2/H_2 flux and TMA pulse time would lead to any changes in the resulting layers. GPC measurements revealed that increase in those parameters indeed leads to a more improved growth rate with the change being most drastic between 20 and 100 sccm/0.06 and 0.12s (N_2H_2/TMA). The optimal saturation, however, is reached at around 150sccm/0.15s (N_2H_2/TMA) which is confirmed by SIMS analysis, in which one can observe an increase in intensity of AlN^- ion for the samples exposed to more intensive precursors dosing.

To achieve the goal in detecting and quantifying hydrogen, deposited samples have been thoroughly analysed with the use of such technique as: elastic recoil detection analysis (ERDA); nuclear reaction analysis (NRA), secondary-ion mass spectrometry (SIMS). Generally, it can be said, that the results harvested from all these methods are in good agreement with one another. The layers obtained within the scope of this study have demonstrated low amounts of hydrogen

contamination (3-5 at. %), especially when compared to thermal variation of ALD, which puts PE-ALD in a more favourable position, at the very least in terms of minimizing hydrogen impurities.

Aside from investigation of hydrogen, an interesting phenomenon, which takes place during high temperature treatment of AlN on Si, has been demonstrated. Apparently, such temperature treatment (at 1350 °C for 1 hour) causes a fusion of the initial layer into the substrate. Other than that, such treatment seems to be a viable option when it comes to post-processing of the obtained films prone to oxidation, as the chemical composition of the deposited films was considerably improved upon annealing, drastically reducing the concertation of oxygen and increasing that of nitrogen. Thus, the results presented in this study can be important for optimization of the AlN ALD technology as well as for post-processing of the obtained layers.

Conclusion

This work was aimed at enhancing the understanding of AlN ALD process and exploring alternative solutions to conventional deposition recipes. The major contribution of this dissertation lies in the fact that these alternative solutions prove to be superior whether in terms of cost-efficiency or chemical reactivity. The task at hand was undertaken through a series of experiments which were followed by rigorous interpretation of the obtained data. These experiments were consistently published as individual articles in impacted journals as well as in WoS indexed conferences during my PhD study. The dissertation was presented as a compilation of these articles which are organized into corresponding chapters. A detailed overview of all the research presented in the dissertation is provided in the discussion below. The discussion begins with Chapter 3, as Chapters 1 and 2 are introductory and do not contain any experimental results.

Thus, Chapter 3 was entirely dedicated to the study of silicon substrates - the most popular substrates utilized in a variety of thin films deposition techniques. The substrates were subjected to various post-processing procedures, such as annealing and etching by argon, to investigate the change in the surface features under harsh environments. To achieve that purpose, AFM technique was utilized and was followed by stereometric analysis of the surface characteristics. The information on the chemical composition and as well as chemical bonds was provided by XPS. Results of that study demonstrated that the Si substrates had a native oxide layer which is thickened by the annealing procedure. Etching by argon, on the other hand, results in the removal of the said oxide layer. Stereomteric analysis provided thorough and detailed picture on the surface microstructure before and after the processing of the substrates. Thus, these results are important in terms of understanding the chemistry which take place at the interface level during the precursor introduction.

In the Chapters 4 and 5, new approaches for the deposition of AlN were suggested. In the Chapter 4, hydrazine (N_2H_4) and ammonia (NH_3) were used as a nitrogen precursor. Hydrazine is considered a rather unconventional precursor for deposition of AlN, which is why, is it of interest to test its viability as a nitrogen precursor and provide comparison with a more common ammonia. By the results of this study it was discovered that hydrazine demonstrates superior reactivity in comparison to ammonia, which leads to better values of growth rate and improved chemical composition in terms of purity. Additionally, lower dissociation energy of hydrazine molecule allows for lower deposition temperatures, which also is an important factor in ensuring the better quality of the layer. Furthermore, the results provided by ERDA showed that the hydrogen contamination in the resulted layers was as

high as 30% for both precursors. Research presented in Chapter 5 was intended to resolve several important issues which the usage of hydrazine entails. Despite the generally positive results, the usage of hydrazine poses certain difficulties. Aside from being a rather expensive compound, hydrazine is also known for its explosiveness, which is why, it requires extreme caution during handling. In this regard, a new, previously untested precursor was introduced - hydrazinium chloride (N_2H_5Cl). Hydrazinium chloride is basically a chlorine containing salt of hydrazine, but unlike pure hydrazine it is relatively cheap and easier to handle. The results obtained within that study showed that hydrazine chloride is indeed a viable precursor choice for the deposition of AlN thin films. The presence of Al-N bonds was detected by XPS. According to XPS the obtained layers also appeared to be heavily oxidized. After consulting the literature, it was found out that the oxidization issue of AlN is widely reported and requires post-processing. Hence, the high-temperature annealing at 1350 °C in nitrogen atmosphere was performed for the obtained layers. Such treatment, indeed, has produced a favourable effect on the layers. The concentration of Al-N bonds was significantly increased upon treatment, which can be explained by two factors described in Chapter 5:

1) It is known that the intensity of oxidization increases towards the surface. High-temperature induces recombination of the atoms, which results in a more uniform concentration profiles.

2) Annealing in nitrogen environment causes existing Al-O bonds to break and form Al-N bond instead.

Annealing also seems to have caused crystallization of the films according to AFM and XRD. Unfortunately, during this study there was no possibility to investigate hydrogen concentration, as this sort of analysis requires advanced equipment utilizing high-energy primary ions. However, one may speculate that its amount should be in decent agreement with the results reported in Chapter 4, where hydrazine was used, due to the fact that N_2H_5Cl dissociates into hydrazine in the chamber, therefore the chemistry inside the chamber should bear some resemblance. It is also worth to emphasize that no amount of chlorine was detected in the resulting layers even by extremely sensitive SIMS analysis. That indicates that chlorine is completely removed from the chamber during the purge stage in the form of hydrogen chloride (HCl) into which hydrazine chloride decomposes. It is an important observation because, according to the literature, AlN thin films obtained by other chlorine containing precursors (e.g. $AlCl_3$) suffer from some amounts of chlorine impurity.

Chapter 6 contains short communication which describes AlN thin films obtained by PE-ALD. A heavy focus of this research was put into detection of hydrogen by common and available techniques which do not require particle accelerator, such as FTIR and SIMS. As a

result of this study it was discovered that the obtained films indeed have some hydrogen impurities, though seemingly less than was reported for thermal ALD. Even though both methods lack the possibility of quantification, they provide enough information to warrant further investigation with the use of more advanced techniques. Furthermore, it was discovered by FTIR that hydrogen seems to have formed bonds with carbon, as a small peak was observed at ~1500cm-1 which is attributed to C-H bond.

Chapter 7 reports on AlN deposited on HOPG substrate. There are no records in the literature of HOPG being utilized as a substrate for AlN thin films. Nevertheless, this substrate might a promising option due to its extremely high-melting point 3550 °C, which unlocks the possibility of annealing under very high-temperatures. In comparison, Si substrates have melting point of only 1,410 °C. Another benefit of HOPG is its laminated (layered) nature, which allows transferring of the deposited films if necessary. The obtained layers were characterized by AFM, XPS and SIMS. AFM demonstrated that the layers are uniform and have low values of surface roughness (~35 Å). XPS revealed the presence of Al-N bond whereas SIMS detected the presence of AlN^+ ion. Thus, HOPG was determined to be a viable substrate choice for the deposition of AlN thin films by ALD.

The aim of the study described in Chapter 8 was to investigate the hydrogen contamination of AlN thin films deposited by PE-ALD. According to the literature, hydrogen impurity in AlN thin films is common and its presence can be detrimental to the mechanical or electrical properties of the film. Additionally, it was shown in Chapter 4 that the amount of hydrogen in AlN obtained by thermal ALD was 22-26 at.%. Which is why, the hydrogen phenomenon is concerning and its investigation is important. According to the results of this study, thin films deposited with the use of plasma module (PE-ALD) have demonstrated far superior quality, at least in terms of hydrogen contamination. According to ERDA and NRA data, the quantity of hydrogen constituted only 3-5 at.%. However, similarly to the films obtained using thermal ALD, PE-ALD films were not immune to oxidization. Thus, the high-temperature annealing (1350 °C) in N_2 atmosphere was performed once again, and once again led to a drastic decrease in the amount of oxygen. IBA methods have also revealed an interesting phenomenon which appears to have occurred as a result of the annealing - a so-called of fusion of the AlN into the Si substrate. Given that the annealing temperature was quite close to the melting point of Si substrate (1410 °C), such fusion is not entirely unexpected. As was explained in Chapter 8, the choice of a substrate did not seem to produce much of an effect on the resulting layer, at least from the point of view of chemical composition analysis. The impact of deposition regimes, on the other hand, was noticeable

and variation in these regimes was established to have influence not only on the growth rate of the film, but on the density of Al-N bonds as well. In this regard, the optimal parameters for PE-ALD of AlN were determined in this study. The optimal parameters were found to be the following: flux intensity of N_2/H_2 gas mixture 150 sccm, TMA pulse time 0.15 sec and the deposition temperature 300 °C.

As results clearly suggest, each approach has its advantages as well as shortcomings. However, almost in each scenario AlN thin films deposited using ALD have demonstrated acute proneness to oxidization upon exposure to air. This issue, however, is by no means exclusive to the films obtained within the scope of this work. The same discovery has been also made by many other researchers in the field. All thing considered, this notorious oxidization problem seems to be unavoidable in most scenarios and calls for appropriate post-processing measures. One such measure was proposed here, which is high-temperature annealing in nitrogen atmosphere at 1350 °C for about 1 hour (Chapters 5 and 8). Upon such processing, the overall quality of the layers was significantly improved, resulting in massive decrease of the amount of oxygen. Annealing also seems to have induced crystallization of the AlN according to XRD and AFM data.

In conclusion, it should be stated once again that the main novelty of this dissertation consists in the implementation of previously untested precursors. However, different substrates and deposition regimes, as they were described in the aims of the dissertation (deposition temperature, precursor exposure time etc.), were also tested. All the research presented above is a good evidence to the fact that optimization of ALD technology in terms of obtaining high-quality AlN thin films is not a simple task, and many challenges arise along the way. Many of these challenges have been highlighted in this dissertation, and a viable solution, through which the inadequacies of the resulted layers can be at least partially remedied, has been proposed. Overall, each of the described approaches for deposition of AlN films has demonstrated its utility in certain aspects, and the summation of all the data presented here is a comprehensive and valuable contribution into the understanding of ALD AlN process.

Finally, as has been mentioned earlier, the heaviest focus of this dissertation was put into characterization of the samples in terms of chemical composition. That being said, there is still much work to be done on the topic. For instance, it may be worthwhile to obtain more thorough data on the optical properties, as well as to explore the electric behaviour by depositing Ohmic contacts or to look for other effective methods of post processing. All of this, however, would be enough to fit another dissertation's volume and therefore is considered to be the implications for future research.

References

[1] B.C. Mallick, C.-T. Hsieh, K.-M. Yin, Y.A. Gandomi, K.-T. Huang, Review—On Atomic Layer Deposition: Current Progress and Future Challenges, ECS J. Solid State Sci. Technol. 8 (2019) N55–N78. doi:10.1149/2.0201903jss.

[2] E. Ahvenniemi, et al. Review Article: Recommended reading list of early publications on atomic layer deposition—Outcome of the "Virtual Project on the History of ALD," J. Vac. Sci. Technol. A Vacuum, Surfaces, Film. 35 (2017) 010801. doi:10.1116/1.4971389.

[3] J.R. van Ommen, A. Goulas, Atomic layer deposition on particulate materials, Mater. Today Chem. 14 (2019) 100183. doi:10.1016/j.mtchem.2019.08.002.

[4] D. Muñoz-Rojas, T. Maindron, A. Esteve, F. Piallat, J.C.S. Kools, J.M. Decams, Speeding up the unique assets of atomic layer deposition, Mater. Today Chem. 12 (2019) 96–120. doi:10.1016/j.mtchem.2018.11.013.

[5] T. Gougousi, Atomic layer deposition of high-k dielectrics on III–V semiconductor surfaces, Prog. Cryst. Growth Charact. Mater. 62 (2016) 1–21. doi:10.1016/j.pcrysgrow.2016.11.001.

[6] H. Kim, H.B.R. Lee, W.J. Maeng, Applications of atomic layer deposition to nanofabrication and emerging nanodevices, Thin Solid Films. 517 (2009) 2563–2580. doi:10.1016/j.tsf.2008.09.007.

[7] H. Kim, Characteristics and applications of plasma enhanced-atomic layer deposition, Thin Solid Films. 519 (2011) 6639–6644. doi:10.1016/j.tsf.2011.01.404.

[8] S.E. Potts, W. Keuning, E. Langereis, G. Dingemans, M.C.M. van de Sanden, W.M.M. Kessels, Low Temperature Plasma-Enhanced Atomic Layer Deposition of Metal Oxide Thin Films, J. Electrochem. Soc. 157 (2010) P66. doi:10.1149/1.3428705.

[9] M. Leskelä, J. Niinistö, M. Ritala, Comprehensive Materials Processing, 4.05 - Atomic Layer Deposition, Elsevier (2014), 101-123. doi: 10.1016/B978-0-08-096532-1.00401-5.

[10] E. Yarar, V. Hrkac, C. Zamponi, A. Piorra, L. Kienle, E. Quandt, Low temperature aluminum nitride thin films for sensory applications, AIP Adv. 6 (2016). doi:10.1063/1.4959895.

[11] H.J. Yun, H. Kim, B.J. Choi, Nucleation and growth behavior of aluminum nitride film using thermal atomic layer deposition, Ceram. Int. 46 (2020) 13372–13376. doi:10.1016/j.ceramint.2020.02.118.

[12] A.M. Alsaad, Q.M. Al-Bataineh, I.A. Qattan, A.A. Ahmad, A. Ababneh, Z. Albataineh, I.A. Aljarrah, A. Telfah, Measurement and ab initio Investigation of Structural, Electronic, Optical, and Mechanical Properties of Sputtered Aluminum Nitride Thin Films, Front. Phys. 8 (2020). doi:10.3389/fphy.2020.00115.

[13] Z. Chen, Z. Zhu, K. Härkönen, E. Salmi, Batch processing of aluminum nitride by atomic layer deposition from AlCl 3 and NH 3 , J. Vac. Sci. Technol. A. 37 (2019) 020925. doi:10.1116/1.5079509.

[14] A. Ullah, Q. Wang, I. Ahmad, M. Usman, Irradiation effects on Nd and W doped Aluminum Nitride thin films, Phys. B Condens. Matter. 586 (2020) 412086. doi:10.1016/j.physb.2020.412086.

[15] Y. Bian, M. Liu, G. Ke, Y. Chen, J. DiBattista, E. Chan, Y. Yang, Aluminum nitride thin film growth and applications for heat dissipation, Surf. Coatings Technol. 267 (2015) 65–69. doi:10.1016/j.surfcoat.2014.11.060.

[16] A. Ullah, M. Usman, W. Qingyu, I. Ahmad, M. Maqbool, Structural, electrical and optical characterizations of yttrium doped aluminum nitride thin films before and after ions irradiation, Opt. Mater. (Amst). 116 (2021) 111097. doi:10.1016/j.optmat.2021.111097.

[17] S. Mertin, B. Heinz, O. Rattunde, G. Christmann, M.A. Dubois, S. Nicolay, P. Muralt, Piezoelectric and structural properties of c-axis textured aluminium scandium nitride thin films up to high scandium content, Surf. Coatings Technol. 343 (2018) 2–6. doi:10.1016/j.surfcoat.2018.01.046.

[18] C. Fei, X. Liu, B. Zhu, D. Li, X. Yang, Y. Yang, Q. Zhou, AlN piezoelectric thin films for energy harvesting and acoustic devices, Nano Energy. 51 (2018) 146–161. doi:10.1016/j.nanoen.2018.06.062.

[19] J. Liu, Y. Yuan, Z. Ren, Q. Tan, J. Xiong, High-temperature dielectric properties of aluminum nitride ceramic for wireless passive sensing applications, Sensors (Switzerland). 15 (2015) 22660–22671. doi:10.3390/s150922660.

[20] G. Piazza, V. Felmetsger, P. Muralt, R.H. Olsson, R. Ruby, Piezoelectric aluminum nitride thin fi lms for microelectromechanical systems, MRS Bull. 37 (2012) 1051–1061. doi:10.1557/mrs.2012.268.

[21] A. Afsari, M.J. Sarraf, Design of a hydrogen sulfide gas sensor based on a photonic crystal cavity using graphene, Superlattices Microstruct. 138 (2020) 106362. doi:10.1016/j.spmi.2019.106362.

[22] S.S. Varghese, S. Lonkar, K.K. Singh, S. Swaminathan, A. Abdala, Recent advances in graphene based gas sensors, Sensors Actuators, B Chem. 218 (2015) 160–183. doi:10.1016/j.snb.2015.04.062.

[23] F. Yang, J. Zhu, X. Zou, X. Pang, R. Yang, S. Chen, Y. Fang, T. Shao, X. Luo, L. Zhang, Three-dimensional TiO2/SiO2 composite aerogel films via atomic layer deposition with enhanced H2S gas sensing performance, Ceram. Int. 44 (2018) 1078–1085. doi:10.1016/j.ceramint.2017.10.052.

[24] A. Bratov, N. Abramova, A. Ipatov, Recent trends in potentiometric sensor arrays-A review, Anal. Chim. Acta. 678 (2010) 149–159. doi:10.1016/j.aca.2010.08.035.

[25] W. Ren, S. Mura, J.M.K. Irudayaraj, Modified graphene oxide sensors for ultra-sensitive detection of nitrate ions in water, Talanta. 143 (2015) 234–239. doi:10.1016/j.talanta.2015.05.073.

[26] S. Zhuiykov, K. Kalantar-Zadeh, Development of antifouling of electrochemical solid-state dissolved oxygen sensors based on nanostructured Cu 0.4Ru 3.4O 7 + RuO 2 sensing electrodes, Electrochim. Acta. 73 (2012) 105–111. doi:10.1016/j.electacta.2011.11.018.

[27] Y. Xu, L. Zheng, C. Yang, W. Zheng, X. Liu, J. Zhang, Chemiresistive sensors based on core-shell ZnO@TiO2 nanorods designed by atomic layer deposition for n-butanol detection, Sensors Actuators, B Chem. 310 (2020) 127846. doi:10.1016/j.snb.2020.127846.

[28] S. Zhuiykov, E. Kats, Atomically thin two-dimensional materials for functional electrodes of electrochemical devices: A review, Ionics (Kiel). 19 (2013) 825–865. doi:10.1007/s11581-012-0837-2.

[29] H. Xu, M.K. Akbari, S. Kumar, F. Verpoort, S. Zhuiykov, Atomic layer deposition – state-of-the-art approach to nanoscale hetero-interfacial engineering of chemical sensors electrodes: A review, Sensors Actuators, B Chem. 331 (2021) 129403. doi:10.1016/j.snb.2020.129403.

[30] S.M. George, Atomic layer deposition: An overview, Chem. Rev. 110 (2010) 111–131. doi:10.1021/cr900056b.

[31] S. Hashemi Astaneh, L.P. Faverani, C. Sukotjo, C.G. Takoudis, Atomic layer deposition on dental materials: Processing conditions and surface functionalization to improve physical, chemical, and clinical properties - A review, Acta Biomater. 121 (2021) 103–118. doi:10.1016/j.actbio.2020.11.024.

[32] K. Cao, J. Cai, B. Shan, R. Chen, Surface functionalization on nanoparticles via atomic layer deposition, Sci. Bull. 65 (2020) 678–688. doi:10.1016/j.scib.2020.01.016.

[33] C. Auth, et al. A 22nm high performance and low-power CMOS technology featuring fully-depleted tri-gate transistors, self-aligned contacts and high density MIM capacitors (2012) Digest of Technical Papers - Symposium on VLSI Technology, art. no. 6242496, pp. 131-132.

[34] R.W. Johnson, A. Hultqvist, S.F. Bent, A brief review of atomic layer deposition: From fundamentals to applications, Mater. Today. 17 (2014) 236–246. doi:10.1016/j.mattod.2014.04.026.

[35] R.K. Choudhary, P. Mishra, A. Biswas, A.C. Bidaye, Structural and Optical Properties of Aluminum Nitride Thin Films Deposited by Pulsed DC Magnetron Sputtering, ISRN Mater. Sci. 2013 (2013) 1–5. doi:10.1155/2013/759462.

[36] A. Ullah, Q. Wang, I. Ahmad, M. Usman, Irradiation effects on Nd and W doped Aluminum Nitride thin films, Phys. B Condens. Matter. 586 (2020) 412086. doi:10.1016/j.physb.2020.412086.

[37] Y. Bian, M. Liu, G. Ke, Y. Chen, J. DiBattista, E. Chan, Y. Yang, Aluminum nitride thin film growth and applications for heat dissipation, Surf. Coatings Technol. 267 (2015) 65–69. doi:10.1016/j.surfcoat.2014.11.060.

[38] A. Ullah, M. Usman, W. Qingyu, I. Ahmad, M. Maqbool, Structural, electrical and optical characterizations of yttrium doped aluminum nitride thin films before and after ions irradiation, Opt. Mater. (Amst). 116 (2021) 111097. doi:10.1016/j.optmat.2021.111097.

[39] X. He, Q. Wen, Z. Lu, Z. Shang, Z. Wen, A micro-electromechanical systems based vibration energy harvester with aluminum nitride piezoelectric thin film deposited by pulsed direct-current magnetron sputtering, Appl. Energy. 228 (2018) 881–890. doi:10.1016/j.apenergy.2018.07.001.

[40] Y. Wu, C.H. Jia, W.F. Zhang, Growth of conductive and insulative highly-orientated aluminum nitride thin films using laser molecular beam epitaxy, Diam. Relat. Mater. 25 (2012) 139–143. doi:10.1016/j.diamond.2012.02.022.

[41] A. Shah, J. Ahmad, I. Ahmad, M. Mehmood, A. Mahmood, M.A. Rasheed, Copper ion implanted aluminum nitride dilute magnetic semiconductors (DMS) prepared by molecular beam epitaxy, Appl. Surf. Sci. 317 (2014) 262–268. doi:10.1016/j.apsusc.2014.08.112.

[42] K. Järrendahl, S.A. Smith, T. Zheleva, R.S. Kern, R.F. Davis, Growth of highly (0001)-oriented aluminum nitride thin films with smooth surfaces on silicon carbide by gas-source molecular beam epitaxy, Vacuum. 49 (1998) 189–191. doi:10.1016/s0042-207x(97)00177-2.

[43] S. Karmann, H.P.D. Schenk, U. Kaiser, A. Fissel, W. Richter, Growth of columnar aluminum nitride layers on Si(111) by molecular beam epitaxy, Mater. Sci. Eng. B. 50 (1997) 228–232. doi:10.1016/S0921-5107(97)00168-2.

[44] J.H. Edgar, D.T. Smith, C.R. Eddy, C.A. Carosella, B.D. Sartwell, c-Boron-aluminum nitride alloys prepared by ion-beam assisted deposition, Thin Solid Films. 298 (1997) 33–38. doi:10.1016/S0040-6090(96)08884-0.

[45] H.Y. Chen, S. Han, C.H. Cheng, H.C. Shih, Effect of argon ion beam voltages on the microstructure of aluminum nitride films prepared at room temperature by a dual ion beam sputtering system, Appl. Surf. Sci. 228 (2004) 128–134. doi:10.1016/j.apsusc.2004.01.039.

[46] T. Šikola, J. Spousta, R. Češka, J. Zlámal, L. Dittrichová, A. Nebojsa, K. Navrátil, D. Rafaja, J. Zemek, V. Peřina, Deposition of metal nitrides by IBAD, Surf. Coatings Technol. 108–109 (1998) 284–291. doi:10.1016/S0257-8972(98)00654-9.

[47] S. Six, J.W. Gerlach, B. Rauschenbach, Ion beam assisted pulsed laser deposition of epitaxial aluminum nitride thin films on sapphire substrates, Surf. Coatings Technol. 142–144 (2001) 397–401. doi:10.1016/S0257-8972(01)01133-1.

[48] K. Antonova, L. Duta, A. Szekeres, G.E. Stan, I.N. Mihailescu, M. Anastasescu, H. Stroescu, M. Gartner, Influence of laser pulse frequency on the microstructure of aluminum

nitride thin films synthesized by pulsed laser deposition, Appl. Surf. Sci. 394 (2017) 197–204. doi:10.1016/j.apsusc.2016.10.114.

[49] L. Duta, G.E. Stan, H. Stroescu, M. Gartner, M. Anastasescu, Z. Fogarassy, N. Mihailescu, A. Szekeres, S. Bakalova, I.N. Mihailescu, Multi-stage pulsed laser deposition of aluminum nitride at different temperatures, Appl. Surf. Sci. 374 (2016) 143–150. doi:10.1016/j.apsusc.2015.10.093.

[50] M. Chubarov, F. Mercier, S. Lay, F. Charlot, A. Crisci, S. Coindeau, T. Encinas, G. Ferro, R. Reboud, R. Boichot, Growth of aluminum nitride on flat and patterned Si (111) by high temperature halide CVD, Thin Solid Films. 623 (2017) 65–71. doi:10.1016/j.tsf.2016.11.045.

[51] B. Armas, M. De Icaza Herrera, F. Sibieude, Deposition of aluminium nitride coatings using a cold wall CVD reactor, Surf. Coatings Technol. 123 (2000) 199–203. doi:10.1016/S0257-8972(99)00510-1.

[52] E. Österlund, S. Suihkonen, G. Ross, A. Torkkeli, H. Kuisma, M. Paulasto-Kröckel, Metalorganic chemical vapor deposition of aluminum nitride on vertical surfaces, J. Cryst. Growth. 531 (2020) 125345. doi:10.1016/j.jcrysgro.2019.125345.

[53] O.S. Joo, K.D. Jung, S.H. Cho, J.H. Kyoung, C.K. Ahn, S.C. Choi, Y. Dong, H. Yun, S.H. Han, MOCVD of aluminum nitride thin films with a new type of single-source precursor: AlCl3:tBuNH2, Chem. Vap. Depos. 8 (2002) 273–276. doi:10.1002/1521-3862(20021203)8:6<273::AID-CVDE273>3.0.CO;2-O.

[54] T. Nguyen, N. Adjeroud, S. Glinsek, Y. Fleming, J. Guillot, P. Grysan, J. Polesel-Maris, A film-texture driven piezoelectricity of AlN thin films grown at low temperatures by plasma-enhanced atomic layer deposition, APL Mater. 8 (2020). doi:10.1063/5.0011331.

[55] M. Alevli, C. Ozgit, I. Donmez, N. Biyikli, The influence of N2/H2 and ammonia N source materials on optical and structural properties of AlN films grown by plasma enhanced atomic layer deposition, J. Cryst. Growth. 335 (2011) 51–57. doi:10.1016/j.jcrysgro.2011.09.003.

[56] V. Rontu, P. Sippola, M. Broas, G. Ross, T. Sajavaara, H. Lipsanen, M. Paulasto-Kröckel, S. Franssila, Atomic layer deposition of AlN from AlCl 3 using NH 3 and Ar/NH 3 plasma , J. Vac. Sci. Technol. A Vacuum, Surfaces, Film. 36 (2018) 021508. doi:10.1116/1.5003381.

[57] Y.J. Lee, S.W. Kang, Growth of aluminum nitride thin films prepared by plasma-enhanced atomic layer deposition, Thin Solid Films. 446 (2004) 227–231. doi:10.1016/j.tsf.2003.10.004.

[58] V. Rontu, P. Sippola, M. Broas, G. Ross, T. Sajavaara, H. Lipsanen, M. Paulasto-Kröckel, S. Franssila, Atomic layer deposition of AlN from AlCl 3 using NH 3 and Ar/NH 3 plasma , J. Vac. Sci. Technol. A Vacuum, Surfaces, Film. 36 (2018) 021508. doi:10.1116/1.5003381.

[59] C.T.M. Ribeiro, A.R. Zanatta, F. Alvarez, X-ray photoelectron spectroscopy of amorphous AlN alloys prepared by reactive rf sputtering, J. Non. Cryst. Solids. 299–302 (2002) 323–327. doi:10.1016/S0022-3093(01)01190-5.

[60] M.H. Cho, Y.S. Kang, H.Y. Kim, P.S. Lee, J.Y. Lee, Enhancement of the chemical stability of hydrogenated aluminum nitride thin films by nitrogen plasma treatment, Electrochem. Solid-State Lett. 4 (2001) 135–137. doi:10.1149/1.1339241.

[61] X. Wu, A. Seyeux, I. Vickridge, S. Voyshnis, P. Marcus, ToF-SIMS and ERDA study of hydrogen and deuterium in nickel-base alloys oxidized in water, Corros. Sci. 140 (2018) 151–158. doi:10.1016/j.corsci.2018.06.006.

[62] R. Dallaev, N. Papěž, D. Sobola, S. Ramazanov, P. Sedlák, Investigation of structure of AlN thin films using Fourier-transform infrared spectroscopy, Procedia Struct. Integr. 23 (2019) 601–606. doi:10.1016/j.prostr.2020.01.152.

[63] N.P. Barradas, J. Likonen, E. Alves, L.C. Alves, P. Coad, A. Hakola, A. Widdowson, Integration of SIMS into a general purpose IBA data analysis code, AIP Conf. Proc. 1336 (2011) 281–285. doi:10.1063/1.3586104.

[64] A. Založnik, P. Pelicon, Z. Rupnik, I. Čadež, S. Markelj, In situ hydrogen isotope detection by ion beam methods ERDA and NRA, Nucl. Instruments Methods Phys. Res. Sect. B Beam Interact. with Mater. Atoms. 371 (2016) 167–173. doi:10.1016/j.nimb.2015.11.004.

[65] F. Jambon, L. Marchetti, M. Sennour, F. Jomard, J. Chêne, SIMS and TEM investigation of hydrogen trapping on implantation defects in a nickel-based superalloy, J. Nucl. Mater. 466 (2015) 120–133. doi:10.1016/j.jnucmat.2015.07.045.

[66] J. Jokinen, P. Haussalo, J. Keinonen, M. Ritala, D. Riihelä, M. Leskelä, Analysis of A1N thin films by combining TOF-ERDA and NRB techniques, Thin Solid Films. 289 (1996) 159–165. doi:10.1016/S0040-6090(96)08927-4.

[67] K. Arstila, J. Julin, M.I. Laitinen, J. Aalto, T. Konu, S. Kärkkäinen, S. Rahkonen, M. Raunio, J. Itkonen, J.P. Santanen, T. Tuovinen, T. Sajavaara, Potku - New analysis software for heavy ion elastic recoil detection analysis, Nucl. Instruments Methods Phys. Res. Sect. B Beam Interact. with Mater. Atoms. 331 (2014) 34–41. doi:10.1016/j.nimb.2014.02.016.

[68] P. Ström, P. Petersson, M. Rubel, G. Possnert, A combined segmented anode gas ionization chamber and time-of-flight detector for heavy ion elastic recoil detection analysis, Rev. Sci. Instrum. 87 (2016). doi:10.1063/1.4963709.

[69] H. Miyake, G. Nishio, S. Suzuki, K. Hiramatsu, H. Fukuyama, J. Kaur, N. Kuwano, Annealing of an AlN buffer layer in N2-CO for growth of a high-quality AlN film on sapphire, Appl. Phys. Express. 9 (2016). doi:10.7567/APEX.9.025501.

[70] R. Dallaev, D. Sobola, P. Tofel, Ľ. Škvarenina, P. Sedlák, Aluminum Nitride Nanofilms by Atomic Layer Deposition Using Alternative Precursors Hydrazinium Chloride and Triisobutylaluminum (2020). Coatings, 10(10). https://doi.org/10.3390/coatings10100954

[71] C.W. Magee, E.M. Botnick, Hydrogen Depth Profiling Using Sims - Problems and Their Solutions., J. Vac. Sci. Technol. 19 (1981) 47–52. doi:10.1116/1.571015.

[72] T. Matsumae, Y. Kurashima, E. Higurashi, K. Nishizono, T. Amano, H. Takagi, Room temperature bonding of aluminum nitride ceramic and semiconductor substrate, Ceram. Int. 46 (2020) 25956–25963. doi:10.1016/j.ceramint.2020.07.083.

[73] J. Zhang, Q. Zhang, H. Yang, H. Wu, J. Zhou, L. Hu, Bipolar resistive switching properties of AlN films deposited by plasma-enhanced atomic layer deposition, Appl. Surf. Sci. 315 (2014) 110–115. doi:10.1016/j.apsusc.2014.07.117.

[74] V. Rontu, P. Sippola, M. Broas, G. Ross, T. Sajavaara, H. Lipsanen, M. Paulasto-Kröckel, S. Franssila, Atomic layer deposition of AlN from AlCl 3 using NH 3 and Ar/NH 3 plasma , J. Vac. Sci. Technol. A Vacuum, Surfaces, Film. 36 (2018) 021508. doi:10.1116/1.5003381.

[75] H. Kim, N. Do, S. Chul, H. Ju, B. Joon, Improved interfacial properties of thermal atomic layer deposited AlN on GaN, Vacuum. 159 (2019) 379–381. doi:10.1016/j.vacuum.2018.10.067.

[76] N. Sharma, S. Ilango, S. Dash, A.K. Tyagi, X-ray photoelectron spectroscopy studies on AlN thin films grown by ion beam sputtering in reactive assistance of N+/N2+ ions: Substrate temperature induced compositional variations, Thin Solid Films. 636 (2017) 626–633. doi:10.1016/j.tsf.2017.07.006.

[77] A.E. Murillo, L. Melo-Máximo, B. García-Farrera, O. Salas Martínez, D.V. Melo-Máximo, J. Oliva-Ramírez, K. García, L. Huerta, J. Oseguera, Development of AlN thin films for breast cancer acoustic biosensors, J. Mater. Res. Technol. 8 (2019) 350–358. doi:10.1016/j.jmrt.2018.02.007.

[78] R. Dallaev, D. Sobola, P. Tofel, Ľ. Škvarenina, P. Sedlák, Aluminum Nitride Nanofilms by Atomic Layer Deposition Using Alternative Precursors Hydrazinium Chloride and Triisobutylaluminum (2020). Coatings, 10(10). https://doi.org/10.3390/coatings10100954

[79] A.P. Perros, H. Hakola, T. Sajavaara, T. Huhtio, H. Lipsanen, Influence of plasma chemistry on impurity incorporation in AlN prepared by plasma enhanced atomic layer deposition, J. Phys. D. Appl. Phys. 46 (2013). doi:10.1088/0022-3727/46/50/505502.

[80] A.J.M. Mackus, S.B.S. Heil, E. Langereis, H.C.M. Knoops, M.C.M. van de Sanden, W.M.M. Kessels, Optical emission spectroscopy as a tool for studying, optimizing, and monitoring plasma-assisted atomic layer deposition processes, J. Vac. Sci. Technol. A Vacuum, Surfaces, Film. 28 (2010) 77–87. doi:10.1116/1.3256227.

Author's publications

Impacted publications

(Publication are in chronological order; IF is given according to WoS as of 4.3.2021)

[A1] KASPAR P., SOBOLA D., ČÁSTKOVÁ K., DALLAEV R., ŠŤASTNÁ E., SEDLÁK P., KNÁPEK A., TRČKA T., HOLCMAN V. **Case Study of Polyvinylidene Fluoride Doping by Carbon Nanotubes**, *Materials, MDPI,* 2021 Volume 14, Issue 6, pp. 1-11. ISSN: 1996-1944. DOI:10.3390/ma14061428 **(IF: 3.067)**

[A2] PAPEŽ N., DALLAEV R., KASPAR P., SOBOLA D., ŠKARVADA P., ŢĂLU S., RAMAZANOV Sh., NEBOJSA A. **Characterization of GaAs Solar Cells under Supercontinuum Long-Time Illumination.** *Materials, MDPI,* 2021 Volume 14, Issue 2, pp. 1-13. ISSN: 1996-1944. DOI: 10.3390/ma14020461 (**IF: 3.067)**

[A3] KASPAR, P.; SOBOLA, D.; KNÁPEK, A.; BURDA, D.; ORUDZHEV, F.; DALLAEV, R.; TOFEL, P.; TRČKA, T.; GRMELA, L.; HADAS, Z.; ČÁSTKOVÁ, K. **Characterization of Polyvinylidene Fluoride (PVDF) Electrospun Fibers Doped by Carbon Flakes**. *Polymers, MDPI, 2020* Volume 12, Issue 12, pp. 1-15. ISSN: 2073-4360. DOI: 10.3390/polym12122766 (**IF: 3.426)**

[A4] DALLAEV, R.; SOBOLA, D.; TOFEL, P.; ŠKVARENINA, Ľ.; SEDLÁK, P. Aluminum Nitride Nanofilms by **Atomic Layer Deposition Using Alternative Precursors Hydrazinium Chloride and Triisobutylaluminum**. *Coatings, MDPI,* 2020, Volume 10, Issue 10, pp. 1-14. ISSN: 2079-6412. DOI: 10.3390/coatings10100954 (**IF: 2.436)**

[A5] KNÁPEK, A.; DALLAEV, R.; BURDA, D.; SOBOLA, D.; ALLAHAM, M.; HORÁČEK, M.; KASPAR, P.; MATĚJKA, M.; MOUSA, M**. Field emission properties of polymer graphite tips prepared by membrane electrochemical etching**. *Nanomaterials,* 2020, Volume 1, Issue 1, pp. 1-12. ISSN: 2079-4991. DOI: 10.3390/nano10071294 (**IF: 4.324)**

[A6] PAPEŽ, N.; GAJDOŠ, A.; SOBOLA, D.; DALLAEV, R.; ŠKARVADA, P.; MACKŮ, R.; GRMELA, L. **Effect of gamma radiation on properties and performance of GaAs based solar cells**. *Applied Surface Science,* 2020, Volume 527, Issue 146766, pp. 135-146. ISSN: 0169-4332. DOI: 10.1016/j.apsusc.2020.146766 (**IF: 6.182)**

[A7] PAPEŽ, N.; GAJDOŠ, A.; DALLAEV, R.; SOBOLA, D.; SEDLÁK, P.; MOTÚZ, R.; NEBOJSA, A.; GRMELA, L. **Performance analysis of GaAs based solar cells under gamma irradiation**. *Applied Surface Science,* 2020, Issue 510, pp. 265-272. ISSN: 0169-4332. DOI: 10.1016/j.apsusc.2020.145329 **(IF: 6.182)**

[A8] RAMAZANOV, S.; SOBOLA, D.; ORUDZHEV, F.; KNÁPEK, A.; POLČÁK, J.; POTOČEK, M.; KASPAR, P.; DALLAEV, R. **Surface Modification and**

Enhancement of Ferromagnetism in BiFeO3 Nanofilms Deposited on HOPG. *Nanomaterials,* 2020, Volume. 10, Issue 10, pp. 1-17. ISSN: 2079-4991. DOI: 10.3390/nano10101990 **(IF: 4.324)**

[A9] STACH, S.; ŢĂLU, S.; DALLAEV, R.; ARMAN, A.; SOBOLA, D.; SALERNO, M. **Evaluation of the Topographical Surface Changes of Silicon Wafers after Annealing and Plasma Cleaning**. *Silicon,* 2019, Volume 11, Issue 1, pp. 1-8. ISSN: 1876-990X. DOI: 10.1007/s12633-019-00351-x (**IF: 1.499)**

[A10] SOBOLA, D.; PAPEŽ, N.; DALLAEV, R.; RAMAZANOV, S.; HEMZAL, D.; HOLCMAN, V. **Characterization of nanoblisters on HOPG surface.** In *Journal of ELECTRICAL ENGINEERING. Journal of Electrical Engineering.* FEI STU Bratislava: De Gruyter OPEN, 2019. pp. 132-136. ISSN: 1335-3632. DOI: 10.2478/jee-2019-0055 (**IF: 0.686)**

[A11] KASPAR, P.; SOBOLA, D.; DALLAEV, R.; RAMAZANOV, S.; NEBOJSA, A.; REZAEE, S.; GRMELA, L. **Characterization of Fe2O3 thin film on highly oriented pyrolytic graphite by AFM, Ellipsometry and XPS.** *Applied Surface Science,* 2019, Volume. 493, Issue 1, pp. 673-678. ISSN: 0169-4332. DOI: 10.1016/j.apsusc.2019.07.058 **(IF: 6.182)**

[A12] ŢĂLU, S.; YADAV, R.; ŠIK, O.; SOBOLA, D.; DALLAEV, R.; SOLAYMANI, S.; MAN, O. **How topographical surface parameters are correlated with CdTe monocrystal surface oxidation**. *MATERIALS SCIENCE IN SEMICONDUCTOR PROCESSING,* 2018, Issue 85, pp. 15-23. ISSN: 1369-8001. DOI: 10.1016/j.mssp.2018.05.030 (**IF: 3.085)**

[A13] ABDULAGATOV A.I., RAMAZANOV SH.M., DALLAEV R.S., MURLIEV E.K., PALCHAEV D.K., RABADANOV M.KH., ABDULAGATOV I.M. **Atomic Layer Deposition of AlN Using Tris(diethylamido)aluminum with Ammonia or Hydrazine.** *Russian Microelectronics,* 2018, Volume. 47, Issue 2, pp. 118-130. ISSN: 1063-7397. DOI: 10.1134/S1063739718020026 (**IF: 0.384)**

Conference proceedings indexed in WoS/Scopus databases

[B1] DALLAEV, R. **Structural characterization of AlN thin films obtained on silicon surface by PE-ALD**. In *Proceedings of the 26th Conference STUDENT EEICT 2020.* 2020. pp. 197-202. ISBN: 978-80-214-5868-0.

[B2] DALLAEV, R.; PAPEŽ, N.; SOBOLA, D.; RAMAZANOV, S.; SEDLÁK, P**. Investigation of structure of AlN thin films using Fourier-transform infrared spectroscopy.** In *Procedia Structural Integrity. Procedia Structural Integrity.* Elsevier, 2020. pp. 601-606. ISSN: 2452-3216. DOI: 10.1016/j.prostr.2020.01.152

[B4] PAPEŽ, N.; DALLAEV, R.; SOBOLA, D.; MACKŮ, R.; ŠKARVADA, P. **Microstructural investigation of defects in photovoltaic cells by the electron beam-**

induced current method. In *Procedia Structural Integrity. Procedia Structural Integrity.* Elsevier, 2020. pp. 595-600. ISSN: 2452-3216. DOI: 10.1016/j.prostr.2020.01.151

[B5] ŢĂLU, Ş.; SOBOLA, D.; PAPEŽ, N.; DALLAEV, R.; SEDLÁK, P. **Efficient processing of data acquired using microscopy techniques.** In *DEStech Transactions on Social Science, Education and Human Science.* Lancaster, Pennsylvania 17602 U.S.A.: DEStech Publications, Inc., 2018. pp. 202-207. ISBN: 978-1-60595-566-7. ISSN: 2475-0042. DOI: 10.12783/dtssehs/amse2018/24838

[B6] ŢĂLU, S.; SOBOLA, D.; SOLAYMANI, S.; DALLAEV, R.; BRÜSTLOVÁ, J. **Scale-dependent Choice of Scanning Rate for AFM Measurements.** In *DEStech Transactions on Computer Science and Engineering.* 2018. pp. 453-459. ISBN: 978-1-60595-065-5. ISSN: 2475-8841. DOI: 10.12783/dtcse/cnai2018/24197

Otherwise indexed conference proceedings

[C1] ŢĂLU, S.; SOBOLA, D.; DALLAEV, R. **Micro-courses for education to scanning probe microscop**y. In *Proceedings of the 1st International Scientific Conference "Modern Management Trends and the Digital Economy: from Regional Development to Global Economic Growth".* Atlantis Press, 2019. pp. 546-549. ISBN: 978-94-6252-721-8. ISSN: 2352-5428. DOI: 10.2991/mtde-19.2019.109

[C2] ŞTEFAN ŢĂLU, RASHID DALLAEV, DINARA SOBOLA. **Evaluation of Surface Characteristics of Highly Oriented Pyrolitic Graphite**. In *2018 2nd International Conference on Advances in Management Science and Engineering (AMSE 2018).* 2018. pp. 150-154. ISBN: 978-1-60595-566-7. DOI: 10.12783/dtssehs/amse2018/24828

[C3] ŢĂLU, S.; DALLAEV, R.; SOBOLA, D.; ŠKVARENINA, Ľ. **Scanning Probe Microscopy of Organisms in Activated Sludge.** In *2017 2nd International Conference on Applied Mechanics and Mechatronics Engineering (AMME 2017). DEStech Transactions on Engineering and Technology Research.* Lancaster, Pennsylvania 17602 U.S.A.: DEStech Publications, Inc., 2018. pp. 129-135. ISBN: 978-1-60595-521-6. ISSN: 2475-885X. DOI: 10.12783/dtetr/amme2017/19495

[C4] ŢĂLU, S.; DALLAEV, R.; SOBOLA, D. **Surface Appearance of Highly Oriented Pyrolitic Graphite.** *DEStech Transactions on Computer Science and Engineering,* 2018 International Conference on Computer, Electronic Information and Communications (CEIC 2018) DOI**:** 10.12783/dtcse/ceic2018/24574

List of abbreviations

ALD – atomic layer deposition

ALE - atomic layer epitaxy

CVD - chemical vapor deposition

PE-ALD - plasma-enhanced atomic layer deposition

CMOS - complementary metal-oxide semiconductor

IC - integrated circuit

NP - nanoparticles

SE - sensing electrodes

MS - magnetron sputtering

MBE - molecular beam epitaxy

IBAD - ion beam assisted deposition

PLD - pulsed laser deposition

AFM - atomic force microscopy

XPS - X-ray photoelectron spectroscopy

HOPG - highly oriented pyrolytic graphite

ERDA - elastic recoil detection analysis

NRA - nuclear reaction analysis

SIMS - secondary ion mass spectrometry

FTIR - Fourier-transform infrared spectroscopy

TMA - trimethylaluminum

RBS - Rutherford backscattering spectrometry

NRA - nuclear resonance analysis

List of figures

Figure 1. Scheme of an ALD process

Figure 2. Illustration of the AlN wurtzite structure, where the (a) m plane, (b) a plane, and (c) c plane

Figure 3. Schematic illustration of a transistor structure with (a) the conventional planar design; (b) the tri-gate design

Figure 4. GPC as a function of: a) temperature of deposition; b) pulse time of N_2/H_2, c) pulse time of TMA

Figure 5. 3D AFM images of AlN thin films for: a) #1; b) #2; c) #3; d) #4

Figure 6. Comparison of surface roughness profiles for images presented in Figure 5

Figure 7. SIMS profiles for: a) AlN^- ions; b) H^- ions

Figure 8. Hydrogen depth profile within the AlN layers according to NRA (100keV $\approx$ 35nm)

Figure 9. ERDA spectra for: a) #1; b) #2; c) #3; d) #4

Figure 10. Elemental distribution in AlN samples according to ERDA: a) #1; b) #2; c) #3; d) #4

Curriculum vitae

PERSONAL INFORMATION

Mgr. et Mgr. Rashid Dallaev

+420 777 828 938

rashiddallaev@yahoo.com

Web: https://www.vutbr.cz/lide/rashid-dallaev-206711

WORK EXPERIENCE

01/07/2011–31/12/2011
Dagestan State University, Russia, Makhachkala
Laboratory assistant, dealing with:
-atomic force microscopy
-chemical treatment of the samples

01/01/2021-present
Brno University of Technology (BUT), Czech Republic, Brno
An employee at Faculty of electrical engineering and communication (FEEC), Department of Physics

2018-present
Central European Institute of Technology (CEITEC). Czech Republic, Brno
Active user of ALD, SIMS, XPS, AFM equipment in CEITEC lab

EDUCATION AND TRAINING

01/09/2008–31/08/2013
1st master degree
Dagestan State University, Makhachkala (Russia)
Study program: Organic chemistry

01/09/2013–31/08/2015
2nd master degree
Dagestan State University, Makhachkala (Russia)
Study program: Analytical chemistry

01/09/2015–2017
C.Sc. student
Dagestan State University, Faculty of Physics, Department of Physics of Condensed State, Makhachkala (Russia)
Study program: Solid state physics

01/09/2017–2021
PhD. student
Brno University of Technology, Faculty of Electrical Engineering and Communication (FEEC)
Study program: Electrical engineering and communication technology (2017-2020) ---------------------- > Microelectronics and technology (2021)

LANGUAGES PROFICIENCY

Mother tongue(s) Russian

Other language(s)

	UNDERSTANDING		SPEAKING		WRITING
	Listening	Reading	Spoken interaction	Spoken production	
English	C2	C2	C2	C2	C2
Czech	B2	C1	B1	B1	B1

Levels: A1 and A2: Basic user - B1 and B2: Independent user - C1 and C2: Proficient user
Common European Framework of Reference for Languages

EXPERIENCES ABROAD

15/09/2019–22/09/2019 **Germany (Dresden)**

ECASIA 2019 conference

20/10/2020–25/11/2020 **Sweden (Uppsala)**

35-day internship in Sweden at Uppsala Univeristy, Tandem Lab. Measuring hydrogen content in AlN samples obtained using ALD in CEITEC by ion-beam solid interaction methods such (ERDA, RBS, NRA etc.)

OTHER ACHIEVEMENTS

Conferences — Local EEICT conference organized by BUT

1st place award (2021)

Three times 2nd place award (2018, 2019, 2020)

SCIENTIFIC IDs

Scopus https://www.scopus.com/authid/detail.uri?authorId=57201461813

Publons https://publons.com/researcher/3405724/rashid-dallaev/

ResearchGate https://www.researchgate.net/profile/Rashid-Dallaev

ORCID iD 0000-0002-6823-5725